T.R.

GEBZE TECHNICAL UNIVERSITY

GRADUATE SCHOOL OF NANOTECHNOLOGY

PREPARATION AND CHARACTERIZATION OF HIGHLY ACTIVE RUTHENIUM NICKEL BIMETALLIC NANOCATALYST FOR DEHYDROGENATION OF AMMONIA BORANE

CEYHUN YILDIRIM

A THESIS SUBMITTED FOR THE DEGREE OF

MASTER OF SCIENCE

IN

DEPARTMENT OF NANOSCIENCE AND NANOENGINEERING

GEBZE

2020

T.R.

GEBZE TECHNICAL UNIVERSITY

INSTITUTE OF NANOTECHNOLOGY

PREPARATION AND CHARACTERIZATION OF HIGHLY ACTIVE RUTHENIUM NICKEL BIMETALLIC NANOCATALYST FOR DEHYDROGENATION OF AMMONIA BORANE

CEYHUN YILDIRIM

A THESIS SUBMITTED FOR THE DEGREE OF

MASTER OF SCIENCE

IN

DEPARTMENT OF NANOSCIENCE AND NANOENGINEERING

THESIS SUPERVISOR

PROF. DR. OSMAN ÖZTÜRK

THESIS SECOND SUPERVISOR

ASSOC. PROF. DR. ERCAN ÖZDEMİR

GEBZE

2020

T.C.

GEBZE TEKNİK ÜNİVERSİTESİ

NANOTEKNOLOJİ ENSTİTÜSÜ

AMONYAK BORANIN DEHİDROJENİZASYONU İÇİN YÜKSEK ETKİNLİKLİ RUTENYUM NİKEL İKİLİ-METALİK NANOKATALİZÖRLERİN HAZIRLANMASI VE KARAKTERİZASYONU

CEYHUN YILDIRIM

YÜKSEK LİSANS TEZİ

NANOBİLİM VE NANOMÜHENDİSLİK ANABİLİM DALI

TEZ DANIŞMANI

PROF. DR. OSMAN ÖZTÜRK

TEZ İKİNCİ DANIŞMANI

DOÇ. DR. ERCAN ÖZDEMİR

GEBZE

2020

GEBZE TEKNİK ÜNİVERSİTESİ	YÜKSEK LİSANS JÜRİ ONAY FORMU

GTÜ Nanoteknoloji Enstitüsü Yönetim Kurulu'nun 28/01/2020 tarih ve 2020/02 sayılı kararıyla oluşturulan jüri tarafından 04/02/2020 tarihinde tez savunma sınavı yapılan Ceyhun Yıldırım'ın tez çalışması Nanobilim ve Nanomühendislik Anabilim Dalında YÜKSEK LİSANS tezi olarak kabul edilmiştir.

JÜRİ

ÜYE (TEZ DANIŞMANI)	:	Prof. Dr. Osman ÖZTÜRK
ÜYE (II. TEZ DANIŞMANI)	:	Doç. Dr. Ercan ÖZDEMİR
ÜYE	:	Prof. Dr. Ferda HACIVELİOĞLU
ÜYE	:	Dr. Öğr. Üyesi Oğuz Kaan ÖZDEMİR
ÜYE	:	Dr. Öğr. Üyesi İsrafil KÜÇÜK

ONAY

Gebze Teknik Üniversitesi Nanoteknoloji Enstitüsü Yönetim Kurulu'nun

...../...../..... tarih ve ...../..... sayılı kararı.

SUMMARY

The aim of this study was to synthesize a novel, cost effective, highly active bimetallic nanocatalyst for the dehydrogenation of ammonia borane (AB) and optimizing the operating conditions of hydrolysis reaction. The most important advantages of these catalyst are the low price and availability of the activated carbon used as the support material, positive interactions between metals and support and synergetic effect between nickel and ruthenium. A series of catalyst synthesized on different supporting materials with various stoichiometries and loadings in DI-water, ethanol, methanol, 0.1 M NaOH and, purged DI-water. The reducing agent was sodium borohydride (SBH-$NaBH_4$) and washed with 4M NH_3, 0.1 M NaOH, DI-water and finally dried in a vacuum oven under vacuum at 40 °C. Four different catalyst synthesis methods were applied and their impact on the catalytic activity investigated. X-ray diffraction (XRD), scanning electron microscopy (SEM), energy dispersive x-ray spectroscopy (EDX), x-ray photoelectron spectroscopy (XPS), zeta potential measurement techniques were applied to characterize the catalysts. At the end of the optimization tests Ru_1Ni_1/AC found as most effective catalyst with a turnover frequency (TOF) value of 440 mol H_2 mol Ru^{-1} min^{-1} and the activation energy (E_a) of 60.8 ± 1.6 kJ/mol.

Keywords: Ammonia borane, ruthenium, activated carbon, nanocatalyst, dehydrogenation, hydrogen storage.

ÖZET

Bu tez çalışmasında amonyak borandan (AB) hidroliz reaksiyonu ile hidrojen elde edilmesi için yenilikçi, ucuz ve yüksek katalitik etkinliğe sahip nanokatalizör geliştirilmesi ve optimum çalışma koşullarının belirlenmesi amaçlanmıştır. Katalizör sisteminin bütün iyi özellikleri aktif karbonun fiyatı, ulaşılabilirliği ve kolay eldesi ile birlikte metallerin birbirleri ve aktif karbon arasındaki olumlu etkileşimden kaynaklanmaktadır. Bu doğrultuda, farklı destek malzemeleri üzerinde, farklı metal ve yükleme-bileşim oranlarıyla ve sodyum borhidrür (SBH-$NaBH_4$) ile metaller indirgenerek katalizör sistemleri de-iyonize su, etanol, metanol, azotla doyurulmuş su, 0.1 M NaOH çözeltisi ortamlarında sentezlenmiş ve ardından 4 M NH_3, 0.1 M NaOH ve de-iyonize su ile yıkanarak vakumlu etüvde 40 °C'de vakum altında kurutulmuştur. Çalışma dahilinde katalizör sentezlemek için dört farklı sentez yöntemi kullanılmış ve bu yöntemlerin katalitik aktivite üzerindeki etkileri incelenmiştir. Malzeme karakterizasyonu için x-ışınları kırınımı (XRD), taramalı elektron mikroskobu (SEM), enerji yayılımlı x-ışını analizi (EDS), x-ışınları ışılelektron tayfı (XPS), zeta potansiyel ölçüm yöntemleri kullanılmıştır. Çalışmaların sonunda en aktif katalizör olarak Ru_1Ni_1/AC, 440 mol H_2 mol^{-1} Ru dk^{-1} TOF değeri ve (E_a) 60.8 ± 1.6 kJ/mol aktivasyon enerjisi ile bulunmuştur.

Keywords: Amonyak boran, hidrojen depolama, aktif karbon, rutenyum, nanokatalizör, dehidrojenasyon.

ACKNOWLEDGEMENT

I would like to thank to both of my supervisors Prof. Dr. Osman Öztürk and Assoc. Prof Dr. Ercan Özdemir for all advises and guidance, intimacy, and satisfying scientific answers to my questions.

Thanks to Adem Şen and Ahmet Nazım due to the helps during the characterization on SEM-EDX, XRD, Zeta Potential devices.

I want to thank all the people (I don't want to disclose them by mentioning their names) in front of the Institute of Nanotechnology for drinking coffee together and scientific conversation. Thanks to İlker Öztoprak due to his helps during the XPS fitting and patient answer to my continuous questions.

I owe a debt of gratitude to the members of a worker family, my mother Fatma Yıldırım, my father Ekrem Yıldırım and my brother Erdost Yıldırım for years who supported me without any economic expectations.

Finally, I want to thank women who are mostly invisible workers of science.

TABLE of CONTENTS

LIST of ABBREVIATIONS and ACRONYMS

Abbreviations and Acronyms		**Explanations**
Å	:	Angstrom (10^{-10} m)
µL	:	Microliter (10^{-6}L)
µm	:	Micrometer (10^{-6} m)
λ	:	Wavelength of the electromagnetic radiation
AB	:	Ammonia borane
AC	:	Activated carbon
ACCT	:	Adhesive conductive carbon tape
Bm	:	Biomass
CB	:	Carbon black
CBM	:	Carbon-based-materials
CNF	:	Carbon nanofiber
CNT	:	Carbon nanotube
E_a	:	Activation energy
EDS	:	Energy dispersive x-ray spectroscopy
eV	:	Electron volt
FCC	:	Face centered cubic
GHG	:	Greenhouse gas
HC	:	Hydrocarbon
HCP	:	Hexagonal closed package
I	:	Intensity
IEP	:	Isoelectric point
kV	:	Kilovolt
M	:	Molar (mol/L)
MCM-48	:	Mobile composition of matter, no:48
mL	:	Milliliter (10^{-3} L)
mM	:	Millimolar (mmol/L, 10^{-3}M)

MWCNT	:	Multi-walled carbon nanotube
nm	:	Nanometer (10^{-9} m)
OBM	:	Oxide-based-materials
PZC	:	Point of zero charge
RNAC	:	Ruthenium Nickel Catalyst Supported on Activated Carbon
RNAC_NN	:	Ru:Ni (1:1) RNAC Synthesized in 0.1 M NaOH Aqueous Solution and Washed with 0.1 M NaOH Aqueous Solution
RNAC_NW	:	Ru:Ni (1:1) RNAC Synthesized in 0.1 M NaOH Aqueous Solution and Washed with DI-Water
RNAC_WN	:	Ru:Ni (1:1) RNAC Synthesized in DI-Water and Washed with 0.1 M NaOH Aqueous Solution
RNAC_WW	:	Ru:Ni (1:1) RNAC Synthesized in DI-Water and Washed DI-Water
rxn	:	Reaction
SBH	:	Sodium borohydride
SEM	:	Scanning electron microscopy
SFE	:	Surface free energy
T	:	Treated
TEM	:	Transmission electron microscopy
TOF	:	Turnover frequency [mol H_2 x mol^{-1} (metal) x min^{-1}]
TON	:	Total turnover number [mol H_2 x mol^{-1} (metal)]
UT	:	Untreated
XPS	:	X-ray photoelectron spectroscopy
XRD	:	X-ray diffraction

LIST of FIGURES

LIST of TABLES

1. INTRODUCTION

1.1. Energy Consumption and Carbon Emission

From learning of the usage of fire up to now, energy is one of the indispensable elements of humankind. At least we need energy for cooking and warming throughout human existence. Energy means life and also, modern societies cannot continue without energy.

There is a big issue with production of energy. Fossil fuels and potential fossil fuels, firewood, have been used to produce energy throughout history. Energy have been obtained by the combustion reaction of those fuels. Issue come up from byproducts of this burning reaction. Byproducts are NO_x, SO_x, CO_x and they create greenhouse gas (GHG) effect. GHG cause global warming. Global warming is one of the biggest problems of modern societies.

Since invention of steam machines, in 18^{th} century, coal consumption had increased. After invention of internal combustion engine and became popular, petroleum consumption had increased. Petroleum was followed by natural gas and finally, nowadays, “hydrogen economy” is talked and researched. From coal to hydrogen we can observe that there is a hydrogen enrichment in the fuel (Figure 1.1).

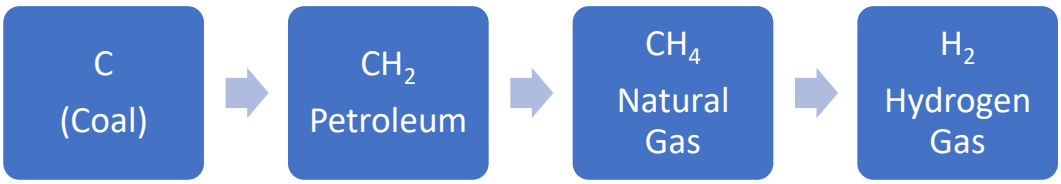

Figure 1.1: Timeline of fuels.

Combustion reactions of fuels that given in Figure 1.1, are given in the following equations (Eq.1.1, Eq.1.2, Eq.1.3, Eq.1.4).

$$C + ½\, O_2 \rightarrow CO_2 + Heat \quad (1.1)$$

$$CH_2 + 3/2\, O_2 \rightarrow CO_2 + H_2O + Heat \quad (1.2)$$

$$CH_4 + 2O_2 \rightarrow CO_2 + 2H_2O + Heat \quad (1.3)$$

$$H_2 + O_2 \rightarrow H_2O + Heat \quad (1.4)$$

As seen in equations above, all combustion reactions, out of (Eq. 1.4), form carbon dioxide, depending on impurities in those fuels, NO_x, SO_x can also be released. These gases are named as GHGs. They absorb heat which comes from the sun and this causes increasing of the temperature of the earth crust, namely global warming. Fossil fuels have a big share of usage, at about 85.99%, as primary energy source. Hydropower and nuclear power are following fossil fuels with shares of 6.79% and 4.44% respectively [1]. Renewability of hydropower is a matter of debate. As a result of deforestation and using fossil fuels 9.86 x 10^{12} kg/year carbon are released to atmosphere as CO_2. The plants have a capacity of absorption 2 x 10^{12} kg carbon per year by the help of photosynthesis and the same amount is valid for algae. Excess carbon gathers in the atmosphere. This amount, at about 5 x 10^{12} kg/year, corresponds annual increase of 0.4% of the CO_2 concentration in the atmosphere due to human activities. In spite of no significant change in the CO_2 emission between 2011-2016, there is a big increase, 2.1%, from 2016 to 2017 [2–6].

Renewable energy sources give us a chance to overcome carbon emission problem and so global warming. Hydrogen is one of the clean energy sources. Like all of other fuels or energy sources, hydrogen is an energy carrier. Fuels carry us energy of the sun. Fossil fuels store energy of the sun by the help of photosynthesis and nutrition of the animals by plants while organisms were alive, and the period of fossilization occurs by existence of sun power.

As seen in Figure 1.2 the world energy consumption was 5 x 10^{12} kWh/year in 1860, but nowadays it was increased to 1.6 x 10^{14} kWh/year in 2017. It will be repetition, but 86% of this consumption supplied by fossil fuels [2,7].

Hydrogen is one of the cleanest energy carriers and fuel cells can convert its chemical potential energy to electricity directly with a by-product, it is only water. Finding a safe, volume and mass effective, low cost hydrogen storage method is a big issue for transition to “hydrogen economy”. AB is an assertive material for solid and portable hydrogen storage which is safe, mass and volume effective, cheap and stable in aqueous media.

AB can release hydrogen via its thermolysis and hydrolysis reactions. Hydrolysis reaction occurs in the presence of suitable catalysts. This study focused on finding a suitable catalyst for hydrolysis reaction of ammonia borane. History of hydrogen, its production, hydrogen storage materials and methods, and catalysis are explained briefly in the following chapters.

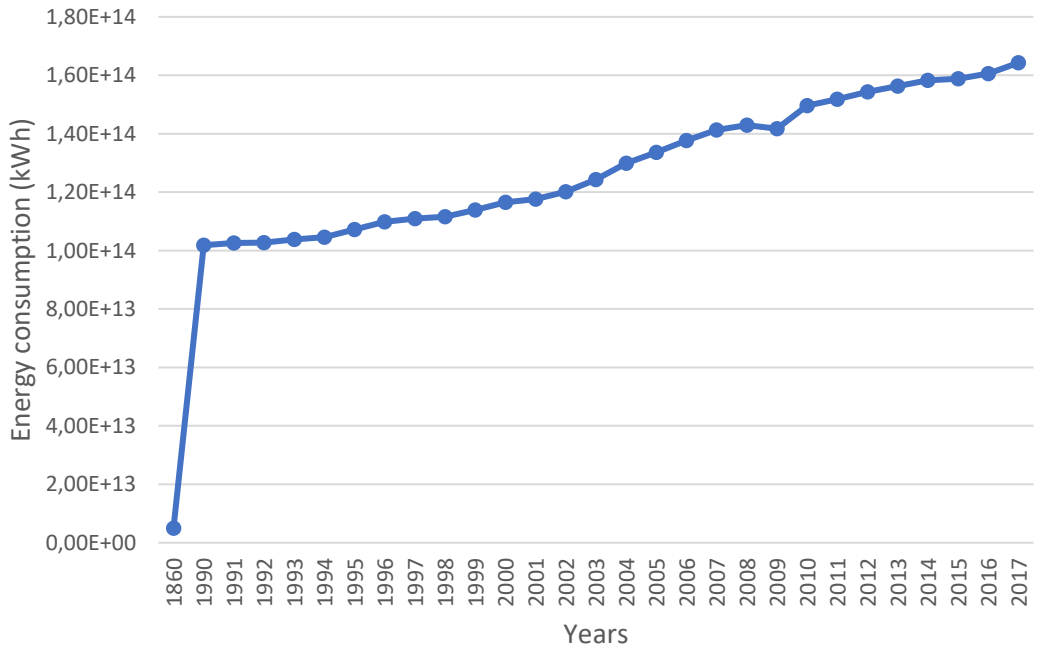

Figure 1.2: Changes in world energy consumption from 1860 to the period of 1990-2017.

1.2. History of Hydrogen

One of the ancient philosophers, Aristotle (384 B.C-322B.C) had claimed that there have been four basic elements. They were fire, water, earth and air [8]. The

properties of these four elements were shown in Figure 1.3. Fire is dry and hot; water is wet and cold; earth is cold and dry; and finally air is wet and hot [9].

Jan Baptista van Helmont (1580-1644) was against the belief of many alchemists. Alchemists had believed that metals could be destroyed by dissolving in acids, but Helmont showed them they were wrong. He solved determined amount of silver in acid and then recover the silver with first amount by reacting the solution with copper. He had probably noticed that there was a gas releasing during the reaction. Based on this observation he discovered that air was not an element and there was another air with different properties. He called it as Greek word “chaos” which means “empty space”; and its spelling in Dutch Language is “gas” [10–13].

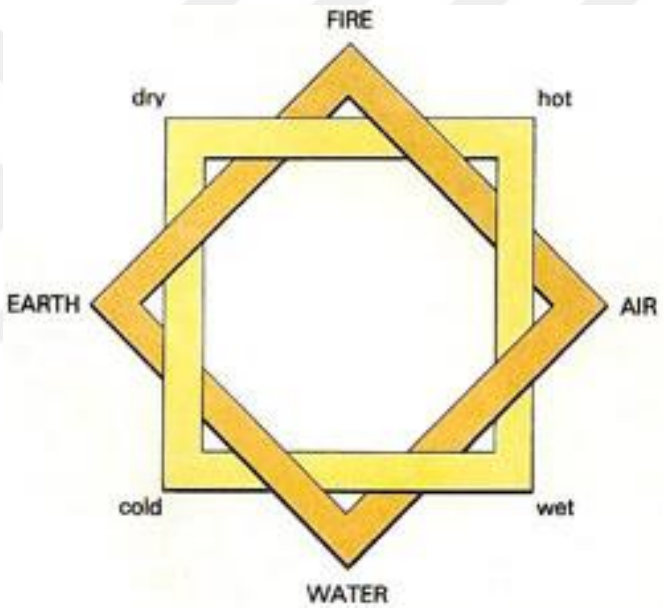

Figure 1.3: Four basic elements of Aristotle.

Henry Cavendish discovered that there was a different type of air, this new realized one was “inflammable air”. He obtained “inflammable air” by reacting zinc with acid. Then he burnt “inflammable air” and he saw that water was formed as a result of burning reaction. By this way he ensured that water is consist of hydrogen and oxygen [14].

When the French Academy of Science had entrusted Antoine Laurent Lavoisier (1743-1794) to filling flight balloons, he turned to production of “flammable air” by the cheapest way. He heated a rifle barrel till it became white-hot and then passed

water through the barrel. While water passing through the rifle barrel “oxygen principle” (at that times, sometimes term of “principle” had been used instead of “element”) oxidized the iron and “flammable principle” was liberated [15–21].

Lavoisier, Guyton de Morveau (1737-1816), Claude-Louis Berthollet (1748-1822) and Antoine François de Fourcroy (1755-1809) published a work, with the name of “Méthode de Nomenclature Chimique” (Chemical Nomenclature Methods). They proposed term of oxygen for life air. “Oxy” means acidic and “gene” for genesis from the Greek words, so oxygen means that “acid creator”. Lavoisier et al. supposed that oxygen is the reason of acidity. They proposed the term of “hydrogen” for “flammable air”. “Hydor” means water former, again in Greek words, because it forms water with hydrogen. “Bad air” is nitrogen, Sulfuric acid for vitriol acid, carbonic acid instead of air acid and oxide for calc were proposed by them. Marie Anne Pierette Paulze, Lavoisier’s wife, supported him during his studies by translating his reference sources from English to French, taking his experimental notes, propagandizing his doctrine, designing their house for hosting Lavoisier’s scientist visitors, imprinting schemes of devices on copper plates in fact she had 13 imprints in Lavoisier’s one of the most famous works “Traité…” and signed as Paulze Lavoisier [10,15,17,19,22,23].

Lavoisier and Pierre Laplace had developed “ice calorimeter” (Figure 1.4) and then measured combustion heat of hydrogen in 1783-1784. Amount of ice melted was approximately equal to 9.7×10^7 J/kgH_2 and this value was not too far from the exact value of 1.2×10^8 J/kgH_2.

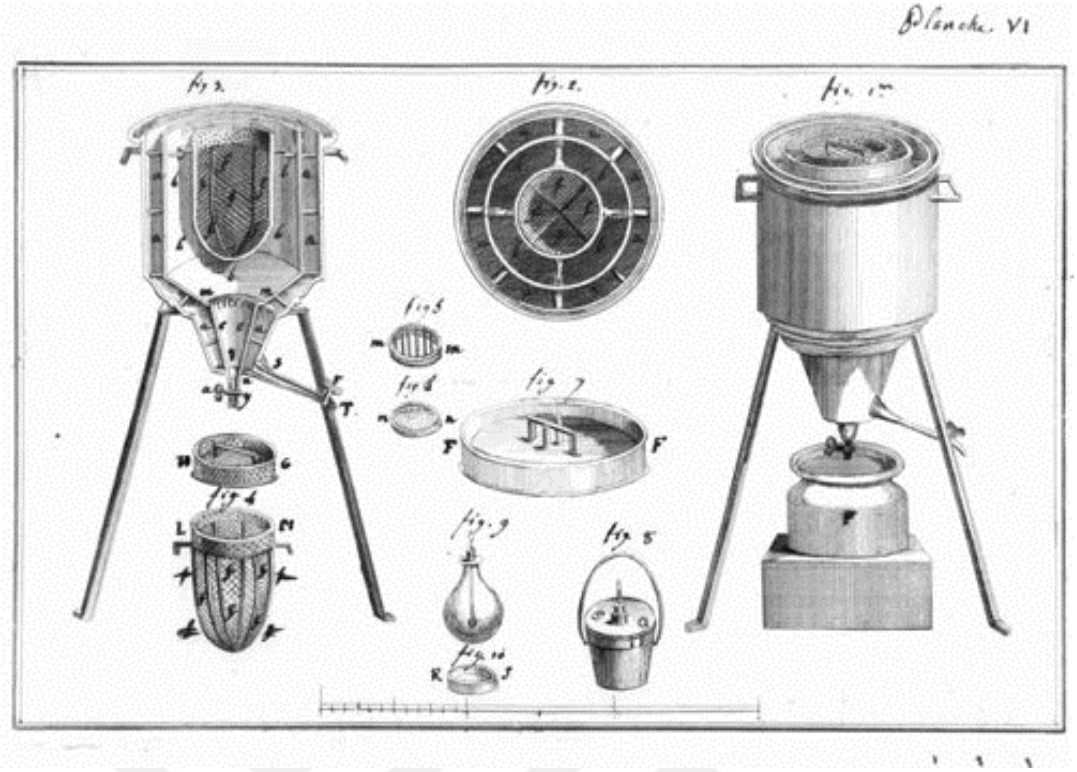

Figure 1.4: Schematic view of Laplace and Lavoisier's ice calorimeter.

In 1800, William Nicholson (1753-1815) heard about invention of Italian scientist Alessandro Volta's (1745-1827) electric battery and undertook to build his own battery. Then Nicholson and Sir Anthony Carlisle (1768-1840) saw that bubbles occurred when poles of battery were submerged to the water. These bubbles were hydrogen and oxygen, and this method would be named as electrolysis. They produced hydrogen by passing electrical current through water [10,24–26].

The first mass produced hydrogen device was "Döbereiner Platinum Lighter" (it was also called as Döbereiner's Hydrogen Lighter) which was invented by Johann Wolfgang Döbereiner (1780-1849) in 1823. It was sold about 20.000 pieces. Hydrogen gas which had produced by the reaction of zinc metal with sulfuric acid, flowed into a cancellous platinum. As a result of catalytic reaction between hydrogen and platinum, cancellous platinum became so hot and ignited hydrogen. Figure 1.5 gives a schematic view of lighter [10,27,28].

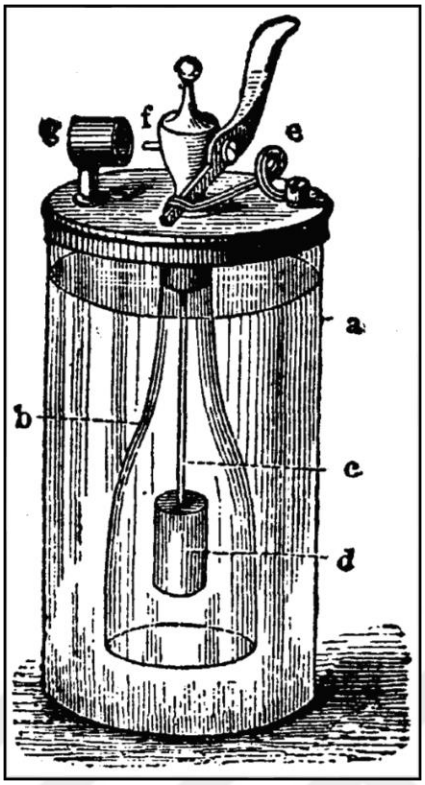

Figure 1.5: Döbereiner Platinum Lighter A) Glass cylinder B) Open Bottle C) Platinum wire D) Zinc E) Stopcock F) Nozzle G) Platinum sponge.

Sir William Grove (1811-1896) invent “gas voltaic battery” based on electrolysis in 1839. He built an experimental setup which generated electricity by reacting hydrogen and oxygen to form water without burning on platinum plates (Figure 1.6). He just reversed the electrolysis reaction. He used generated electricity for electrolysis of water again. This invention is pioneer of modern fuel cells [29,30].

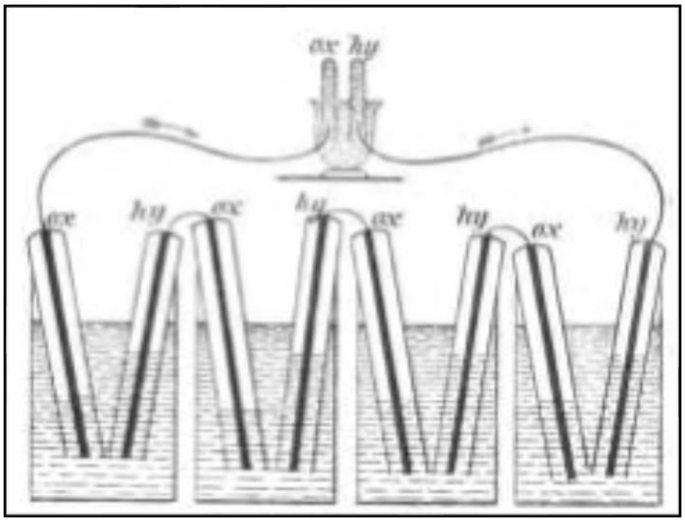

Figure 1.6: Gas voltaic battery invented by Grove in 1839. Sulfuric acid was used as electrolyte. Platinum plates were in contact with oxygen (ox) and hydrogen (hy) in glass tubes. Generated electricity was used to electrolyze water, in the upper glass.

After the discovery of palladium metal by English Chemist William Hyde Wollastone (1766-1828) in 1802 [31], Scottish Chemist Thomas Graham (1805-1869) showed that palladium can absorb large amounts of hydrogen by the way of forming metal hydride. When hydrogen was not considered to be a metal, this phenomenon named as occlusion of hydrogen by T. Graham. He was awarded the Keith Prize of the Royal Society of Edinburgh for this discovery in 1834 [32,33]. Nowadays, metal hydrides are one of the most studied methods for hydrogen storage.

Famous French Author Jules Verne (1828-1905) predicted that hydrogen would substitute of coal and he mentioned about it in his famous work L'ile Mystériouse (The Mysterious Island) in 1874. He suggested water as a fuel by attributing discussions on phlogiston and electrolysis of water. He expressed that hydrogen has much more energy density than coal by the help of his fictitious character engineer Cyrus Smith [34,35].

In 1898, English Chemist James Dewar (1842-1923) succeeded to obtain liquefied hydrogen by using liquid nitrogen under 180 atm pressure [36,37]. He was also invented Dewar flask under favor of this invention he is known as father of modern thermoses [38].

In 1909, Fritz Haber (1868-1934) who is the German Chemist, developed a catalyzed method for producing ammonia from elemental hydrogen and nitrogen and he received the Nobel Prize upon this development. War gas of phosgene (COCl)

was invented by Fritz Haber and thousands of soldiers died because of this gas during the World War I and this invention made contradictive his Nobel Prize. His wife Clara, who could not bear to pangs of conscience, pricked herself by Haber's gun [39–45].

In 1952, the first hydrogen bomb (also called as thermos nuclear bomb) was ignited by the USA and, it was thousand times more powerful than the dropped one in Hiroshima [46].

Prof. T. Nejat Veziroğlu organized The Hydrogen Economy Miami Energy Conference (THEME) in 1974 and a small group of scientists including Veziroğlu got together under the name of "Hydrogen Romantics". International Association for Hydrogen Energy was formed as a result of THEME and Hydrogen Romantics [26,47].

In 2014 National Hydrogen Association was formed in Turkey [48].

Energy consumption, CO_2 emissions, history of hydrogen was glanced, and the queued subject is "hydrogen production". The methods which used for producing hydrogen will be touched briefly.

2. HYDROGEN PRODUCTION

Hydrogen is the most abundant element in universe and probably on the earth, however hydrogen can be found in usable form, namely molecular hydrogen (H_2), inadequate amount. It can be found in the form of hydrocarbons or water as compounds with carbon or oxygen. Molar abundance percentage of hydrogen in dry air is only 5.3 x 10^{-7}, this amount is far from answering energy need of modern societies [49].

There are several methods to produce hydrogen, some of them ground on fossil sources and some of them renewable sources (Figure 2.1).

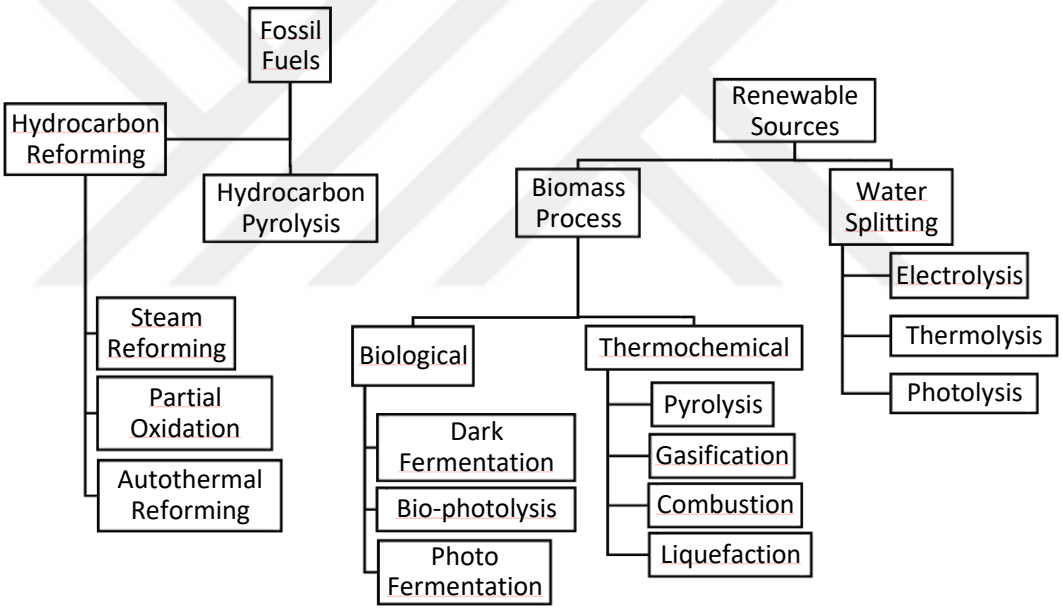

Figure 2.1: Categorical view of hydrogen production methods.

2.1. Hydrogen Production from Fossil Fuels

Fossil fuels can be sources for hydrogen production by several different methods, which include pyrolysis and hydrocarbon reforming. These two methods are most studied, commonly used and commercialized methods. About 96% of hydrogen, produced from fossil fuels and, if it is looked closer, it can be seen that 48% of produced hydrogen comes from natural gas, 30% comes from heavy oils and

naphtha, and finally 18% comes from coal. As seen in these data, fossil fuels are still dominant sources for producing hydrogen.

2.1.1. Hydrocarbon Pyrolysis

In hydrocarbon pyrolysis (HP) method, source of hydrogen is only hydrocarbons. HP is a well-known way to produce hydrogen. Light hydrocarbons (LHCs) which has a boiling point between 50-200 °C, are converted to carbon and hydrogen directly however conversion mechanism of heavy hydrocarbons (HHCs) which have boiling temperatures above 350 °C, consists of two steps - hydrogasification and cracking of methane. Thermal decomposition of LHCs occurs by following the (Eq. 2.1.). Hydrogasification and cracking of methane steps and overall reaction for HHCs occurs by following (Eq. 2.2.), (Eq. 2.3.) and (Eq. 2.4.) respectively.

Therm. Decomp. of LHCs: $$C_nH_m \rightarrow nC + \frac{1}{2}mH_2 \quad (2.1)$$

Hydrogasification: $$CH_{1.6} + 1.2H_2 \rightarrow CH_4 \quad (2.2)$$

Cracking of methane: $$CH_4 \rightarrow C + 2H_2 \quad (2.3)$$

Overall reaction for HHCs: $$CH_{1.6} \rightarrow C + 0.8H_2 \quad (2.4)$$

This reaction needs high temperatures at about 980 °C, atmospheric pressure, water-free and air-free environment. The energy necessity is 37.6 kJ/mol H_2 therefore a determined amount of produced H_2 is burned for corresponding this requirement.

2.1.2. Hydrocarbon Reforming

In hydrocarbon reforming (HR) methods hydrogen comes from hydrocarbons and steam, more precisely water. There are three methods under this title as

reformation processes, namely steam reforming method (SRM), partial oxidation method (POM), and autothermal reforming method (ARM). SRM is endothermic reaction, POM is exothermic, and ARM is combination of both of endothermic and exothermic reactions. A typical HR plant must consist desulphurization unit, reforming and cleaning sections and the operation units, for example pumps, expander, heat exchangers, combustors, coolers, etc. [50,51].

2.1.2.1. Steam Reforming Method

SRM is based on a catalytic transformation of hydrocarbons and steam to hydrogen. SRM consists of syngas ($CO + H_2$) generation, water-gas shift and gas purification steps. Fossil sources are usually light hydrocarbons which have high H/C ratio. If feedstock involves sulfur compounds it is necessity to apply a desulfurization process to get rid of sulfur and to avoid poisoning of catalyst by sulfur. SRM requires high temperatures at about 900 °C thus it enables to use non-precious metal catalysts such as nickel. High temperatures, relatively high pressures and H/C ratio about 3.5 avoid coking formation on catalyst surface and provide high purity of hydrogen in syngas generation step. After syngas generation, the gas mixture is fed into a water-gas shift reactor to react CO with steam and generate additional hydrogen. As a final step, there are two choices as CO_2-removal and methanation to produce methane or pressure swing adsorption to produce high-purity hydrogen. The reactions for syngas generation (Eq. 2.5.), water-gas shift (WGS) (Eq. 2.6.) and methanation (Eq. 2.7.) is given in following equations.

Syngas generation: $$C_nH_m + nH_2O \rightarrow nCO + (n + \frac{1}{2}m)\, H_2 \quad (2.5)$$

WGS: $$CO + H_2O \rightarrow CO_2 + H_2 \quad (2.6)$$

Methanation: $$CO + 3H_2 \rightarrow CH_4 + H_2O \quad (2.7)$$

In SRM, energy requirement for hydrogen production is 63.3 kJ/mol H_2 and it can be supplied by nearly 35% of natural gas which used in process. Nickel-based catalysts are commonly used in SRM [50,52–55].

2.1.2.2. Partial Oxidation Method

Hydrocarbons and steam are the sources of hydrogen in POM. HCs, steam and oxygen converted to hydrogen and carbon oxides. There are two types of mechanisms in POM as catalytic and non-catalytic ones. Fossil sources lie between methane, naphtha and coal. Sulfur removing is applied as first step before partial oxidation of HCs with pure oxygen to produce syngas. After syngas generation, water-gas shift and methanation steps are applied. This method is the most suitable one for hydrogen production from HHCs. A big part of produced hydrogen comes from steam due to lower H/C ratios of HHCs, for example, in the partial oxidation of coal all produced hydrogen comes from steam. The catalytic type of POM occurs at about 950 °C and non-catalytic one occurs up to 1350 °C. Catalytic and non-catalytic reformation reactions (Eq. 2.8. and Eq. 2.9. respectively) are below, and water-gas shift and methanation reactions are the same with WGS and methanation reactions of SRM [50,51,55].

Catalytic reformation rxn: $C_nH_m + ½\ nO_2 \rightarrow nCO + ½\ mH_2$ (2.8)

Non-catalytic ref. rxn: $C_nH_m + nH_2O \rightarrow nCO + (n+ ½\ m)\ H_2$ (2.9)

2.1.2.3. Autothermal Reforming Method

ATR is a combination of exothermic partial oxidation and endothermic steam reforming processes. The heat is supplied by exothermic partial oxidation and hydrogen production increased by steam reforming. Oxygen or air and, steam are blown into the reforming unit to start reforming and oxidation simultaneously by following (Eq. 2.10.) [50,51,56].

$$C_nH_m + ½\ nH_2O + ¼\ nO_2 \rightarrow nCO + (½\ n + ½\ m)\ H_2 \quad (2.10)$$

2.2. Renewable Sources

Methods which expressed up to here, are based on fossil fuels, however they have major share in hydrogen production. Those methods are time-limited due to the limitations of fossil fuels. Also, those methods cause greenhouse gases emission like burning reactions of fossil fuels. Hydrogen production from renewable sources can be compiled under two titles according to sources. These are biomass and water. It is expected that renewable sources will override fossil ones.

2.2.1. Water Splitting

Water splitting is based on production of hydrogen from its eponym, water. The source is one of the most abundant and recyclable so endless raw material on earth. 71% of earth crust is covered by water and it is suggested that volume of the liquid water is about 1.39×10^9 km^3 [50,57–59].

2.2.1.1. Electrolysis

Electrolysis is a well-known and most effective method for hydrogen production from water. The reaction is endothermic, and the energy requirement supplied by electricity. If electricity is generated by renewable sources such as wind, solar power, etc. electrolysis is a green way for hydrogen generation. Overall reaction of electrolysis is given in Eq. 2.11.

$$H_2O \rightarrow H_2 + ½\ O_2 \quad (2.11)$$

Some devices were developed for electrolysis to reduce energy requirement per mole of hydrogen by using catalysts and/or high temperatures. Alkaline electrolyzer cells (AEC), proton exchange membrane electrolyzer cells (PEMEC), solid

oxide electrolyzer cells (SOEC) are the types of electrolysis devices. Reactions according to electrolyzer types are given below [50,58–61]:

- AEC and SOEC

Anode: $4OH^- \rightarrow O_2 + 2H_2O + 4e^-$ (2.12)

Cathode $2H_2O + 2e^- \rightarrow 2OH^- + H_2$ (2.13)

- PEMEC

Anode: $2H_2O \rightarrow O_2 + 4H^+ + 4e^-$ (2.14)

Cathode: $4H^+ + 4e^- \rightarrow 2H_2$ (2.15)

Electrolysis provides extremely pure hydrogen, but operation costs of these plants are very high due to high consumption of electricity. AECs need 53.4 kWh of energy per kilogram of hydrogen.

2.2.1.2. Thermolysis

Water splitting by thermolysis or thermochemical way is based on heating water up to temperatures which allow decomposition of water to oxygen and hydrogen. Decomposition of water starts after surpassing of 2500 °C, however the temperature can be lowered by changing reaction medium and the compounds can be fully recycled at the end of the hydrogen generation process. Sulfur-iodine, cerium-chlorine, iron-chlorine, vanadium-chlorine, copper-sulphate and copper-chlorine cycles were tested in the previous studies. All cycles necessitate high temperatures at about 850 °C out of copper- chlorine cycle. In copper-chlorine cycle operating temperature is up to 530 °C and efficiency is about 43%. Reactions and required temperatures for copper-chlorine cycle steps are given below (Eq.2.16-2.19) [50,58,62,63].

T<100 °C -electrolysis, Step1: $2CuCl_{(aq)} + 2HCl_{(aq)} \rightarrow H_{2(g)} + 2CuCl_{2(aq)}$ (2.16)

T<100 °C, Step2: $CuCl_{2(aq)} \rightarrow CuCl_{2(s)}$ (2.17)

T=400 °C, Step3: $2CuCl_{2(s)} + H_2O_{(g)} \rightarrow Cu_2OCl_{2(s)} + 2HCl_{(g)}$ (2.18)

T=500 °C, Step4: $Cu_2OCl_{2(s)} \rightarrow 2CuCl_{(l)} + ½\ O_{2(g)}$ (2.19)

Even the temperature requirement is lowered to 530 °C, this value is still high. This necessity should be lowered to levels which can be answered by solar energy.

2.2.1.3. Photolysis

Photolysis or photo-electrolysis is based on the interaction between the light and a semiconductor material. When a photon which has enough energy to overcome bandgap of semiconductor material interacts with semiconductor, an electron and hole pair is created. They are separated by the help of potential difference between semiconductor and electrolyte. The holes remain at the anode side where water split into H^+ and electrons move through an external circuit to cathode side. Created protons move through the electrolyte to the cathode side for combining with electrons which come to cathode side by the help of external circuit and they create H_2.

There are two types of photolysis system, the first one just generates hydrogen and the other one generates electricity. However, the efficiency of photolysis is too low at about 0.06% and hydrogen generation costs are relatively high with the price of 10.36 $/kg$H_2$ [50,58,61,64].

2.3. Biomass Process

Biomass (Bm) is a renewable source for hydrogen production. All product types of animals and plants which we generally named as wastes are the sources of

biomass. Plant based products store energy of sunlight by the help of photosynthesis. CO_2 emission is occurred while processing of biomass at amount of stored energy. Biomass process methods can be gathered under two titles as thermochemical and biological processing. We start with the thermochemical processing.

2.3.1. Thermochemical Processes

Thermochemical ways for processing of biomasses consists 4 different methods. Biomass pyrolysis and biomass gasification are preferable methods than liquefaction and combustion. Biomasses transformed into hydrogen and hydrogen-rich fuels by thermochemical processes.

2.3.1.1. Biomass Pyrolysis

Biomass sources can be transformed to liquid oils, coal and gaseous compounds by heating raw materials up to temperature range of 380-530 °C under pressure range of 1-5 bar. This method requires oxygen-free media except partial combustion reaction where required heat for reactions produced. Biomass type, temperature, catalyst type, pressure can affect hydrogen production and its cost. Related reactions (Eq. 2.20 - 2.22) are given below:

$$\text{Pyrolysis of Bm} \rightarrow H_2 + CO + CO_2 + \text{hydrocarbon gases} + \text{tar} + \text{coal} \quad (2.20)$$

$$C_nH_m + nH_2O \rightarrow nCO + (n + ½\ m)\ H_2 \quad (2.21)$$

$$CO + H_2O \rightarrow CO_2 + H_2 \quad (2.22)$$

Produced syngas is threated again to obtain hydrogen by the way of steam reforming and for more hydrogen production water-gas shift [50,65].

2.3.1.2. Biomass Gasification

Gasification is one of the thermochemical processes for transforming biomass to the syngas. This method has a wide operation condition range. It works at the temperature range between 500 and 1400 °C and pressure range from atmospheric to 33 bars according to plant scale. The reactions of biomass gasification with air and steam are shown in Eq. 2.23 and Eq. 2.24 respectively. Biomass type, steam or air to biomass ratio, particle size of raw materials, catalyst type, temperature and pressure can affect hydrogen yield [50,61,62,65].

$$Bm + air \rightarrow H_2 + CO + CO_2 + N_2 + HC\ gases + tar + coal + H_2O \quad (2.23)$$

$$Bm + steam \rightarrow H_2 + CO + CO_2 + N_2 + HC\ gases + tar + coal \quad (2.24)$$

2.3.2. Biological Process

Dark-fermentation, bio-photolysis and photo-fermentation are the main methods in biological process for hydrogen generation. Due to opportunity of waste minimization, interest on biological processes is increasing. Some microorganisms i.e. bacteria and algae, and enzymes are used in biological processes.

2.3.2.1. Bio-Photolysis

Bio-photolysis is based on photosynthesis reaction of plants and algae. Photosynthesis mechanism has been modified to produce hydrogen gas instead of carbon-based compounds. Light is absorbed by systems of photosynthesis and liberates electrons. Liberated electrons of water by photons are used in CO_2 reduction or hydrogen generation. In the green plant cells, only CO_2 reduction occurs

due to absence of an enzyme which is used for hydrogen generation. On the other hand, microalgae can produce hydrogen because they have hydrogenase enzymes which green plants don't have.

However, the rate of hydrogen generation rate is lower than the CO_2 reduction rate. Small amount of oxygen blocks the activity of hydrogenase, as a result, hydrogen generation reduces. Some types of microalgae, which can be classified as "green algae", can start producing hydrogen after a period in anaerobic and dark media [66,67].

2.3.2.2. Dark Fermentation

Fermentation is a biochemical process which occurred in oxygenic or oxygen-free media by some microorganisms. Organic feed materials are transformed to alcohols, acetone and hydrogen by microbial processes and, they produced at minimum amount of produced CO_2 in the reaction.

Dark fermentation take place under anaerobic (oxygen-free) and dark conditions. Anaerobic bacteria are the living machines which transform raw materials to alcohols, acetone and hydrogen. Eq. 2.25 and Eq. 2.26 show the transformation reaction of glucose to acetic and butyric acids (respectively) and hydrogen.

$$C_6H_{12}O_6 + 2H_2O \rightarrow 2CH_3COOH + 4H_2 + 2CO_2 \quad (2.25)$$

$$C_6H_{12}O_6 + 2H_2O \rightarrow CH_3CH_2CH_2COOH + 2H_2 + 2CO_2 \quad (2.26)$$

Given examples above belong to fermentation of glucose. But it is relatively expensive and fermentation of glucose at big amount is not readily available. It can be extracted from agricultural wastes, on the other hand starch or cellulose can be used as raw materials thus the process can get cheaper [50,66,68,69].

2.3.2.3. Photo-Fermentation

Photo-fermentation, as the name suggests, takes place in a light environment in the presence of nitrogen. Under favor of the existence of nitrogenase enzyme, some photosynthetic bacteria can convert organic acids to hydrogen and carbon dioxide. Eq. 2.27 shows the transformation reaction of acetic acid to hydrogen and carbon dioxide by photosynthetic bacteria under light [50].

$$CH_3COOH + 2H_2O + \text{light energy} \rightarrow 4H_2 + 2CO_2 \quad (2.27)$$

Production rate and hydrogen yield are directly proportional to intensity of the light. In industrial scale coloration of water in the pool is a major problem due to preclusion of penetration of daylight into deeper levels of the pool and this situation causes toxic material production and known as “coloration”.

Researchers developed a hybrid system to overcome coloration issue. Dark-fermentation and photo-fermentation methods work together in this hybrid system [50].

3. HYDROGEN STORAGE AND TRANSPORTATION

Storage and transportation are also big issues in the field of hydrogen economy. It can be transferred by pipelines, trucks, ships and barges. Pipeline length reach to 4542 km in the world (2608 km in U.S., 1598 km in Europe and 337 km in rest of the world) in 2018. Pipeline length was 2220 km in the world in 2008. Hydrogen transferring tubes can operate at pressure range of 10 to 20 bar. The energy density of hydrogen is 36% of the natural gas in same amount and pressure. Due to volumetric energy and viscosity differences the transportation power per energy is 2.2 times higher than natural gas [70–72].

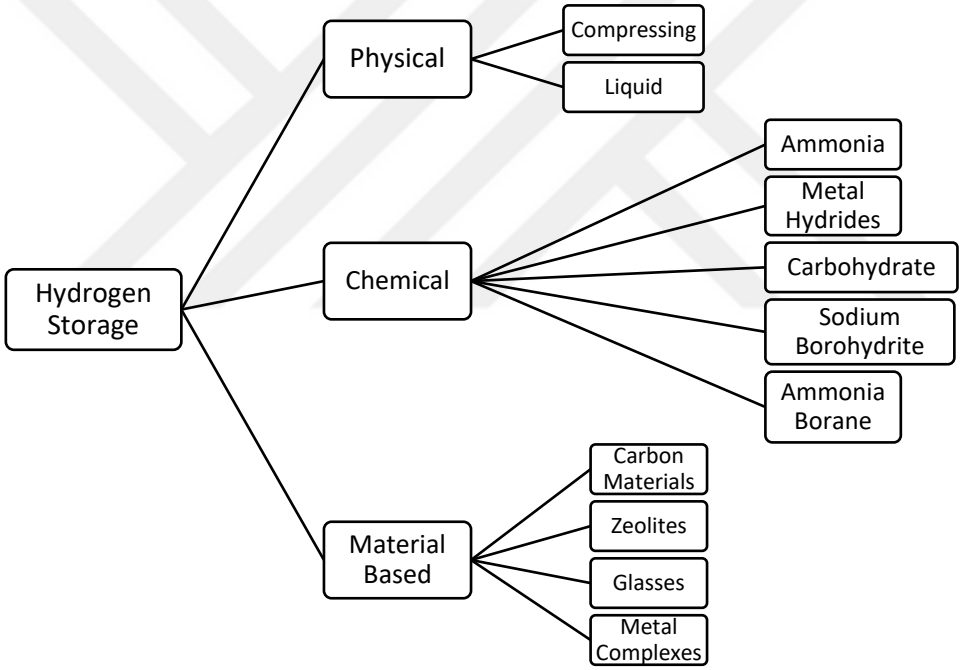

Figure 3.1: Hydrogen Storage Methods.

Figure 3.1 shows the methods for hydrogen storage. There are three main topics under hydrogen storage and now we are starting to scrutinize these topics.

3.1. Physical Hydrogen Storage

Under this title two topics will be focused, as compressed and liquid hydrogen storage.

3.1.1. Compressed Storage

Storing hydrogen in high-pressure tanks is the most commonly used method which can be seen even in the laboratories or, as propane cylinder in the kitchens, LPG storage tanks on the cars. This is most commonly used technique because it is well-known way.

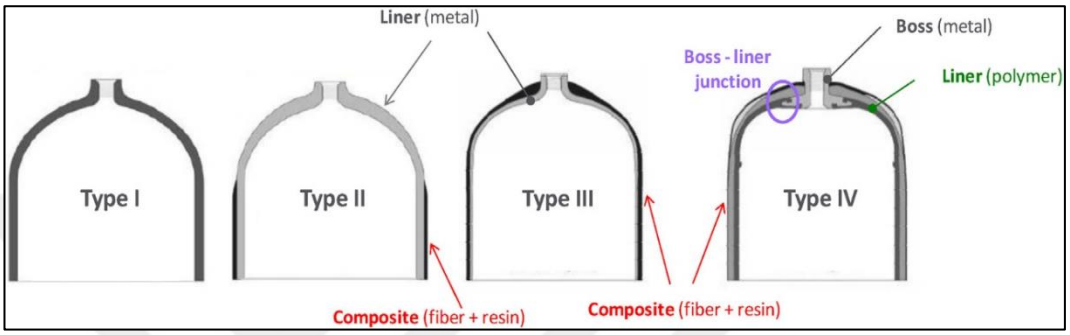

Figure 3.2: 4 Types of high-pressure hydrogen tanks.

Basically, there are four types of pressure tanks, they are shown in Figure 3.2 [73]. Commonly metallic parts made of aluminum 6061 or 7060 and inox or chrome molybdenum steels; if they are composite, polymer parts are polyethylene or polyamide-based polymers and reinforcements are aramid, glass or carbon fibers. The 4th type tanks can operate under the pressure up to 1000 bars. Preferability of types is changing according to cost effectiveness, resistance to pressure and weight performance [73–75].

3.1.2. Liquid Hydrogen Storage

Cryogenic vessels are used for about 40 years to store or transport medical and industrial gases. They can be seen around big hospitals for storage of oxygen. Liquid hydrogen storage is usually used for stationary applications at customers' area or transportation of hydrogen by trucks or devoted ships. This method requires cryogenic systems at temperature of 20 K. While compressed hydrogen tanks have a capacity of 0.03 kg L^{-1}, liquid hydrogen tanks can store 0.07 kg L^{-1}. These tanks need good isolation to keep the low temperatures. And also, ductility and toughness

decreasing due to low temperatures and hydrogen embrittlement are big issues for liquid hydrogen storage tanks and studies are continuing on development of new materials for tanks [73,74].

3.2. Material-Based Hydrogen Storage

Liquid and compressed hydrogen storage systems have some disadvantages and risks such as low temperature requirement (high energy consumption to liquify the gas and isolation problems of tanks) for cryogenic systems, low weight capacity per volume or mass for compressed tanks and, flaming or explosion risks for both methods. These disadvantages and risks make cryogenic and compressed hydrogen storage unfavorable for mobile applications.

Safety and storage effectiveness are most important criteria for mobile applications. To answer these expectations carbon-based materials, zeolite, glass, metal complexes were developed for hydrogen storage.

Before start to explain material-based hydrogen storage, it should be better to describe adsorption mechanism. This process, namely adsorption, occurs on the surface of storage material. Hydrogen molecules interact with the atoms at the surface of the storage material, and the distance between molecules and the surface atoms decreases. This mechanism has an ability of reducing the operating pressure and cost of the storage material. The major drawback for adsorption-based hydrogen storage (material-based) requirement of high pressures and low temperatures together. The interaction between surface atoms and hydrogen molecules is based on weak intermolecular interactions, therefore adsorption occurs only at low temperatures. Now we can scrutinize materials for hydrogen storage [76].

3.2.1. Carbon-Based Materials

Hydrogen molecules hold on to surface of carbon through Van der Waals interactions which has a bonding energy of 6 kj mol^{-1}. There are different types of

carbon structures (fullerene, carbon nanotubes, graphene) and they will be explained in coming sections.

3.2.1.1. Fullerenes

Fullerenes are pentagonal and hexagonal structures of carbon which comes together to form a spherical shape. Fullerenes are used to trap hydrogen in their central space. Alkali metal doping affects the electronegativity of the fullerene thus, this changes the capacity of hydrogen storage.

Lithium (Li) and potassium (K) doped fullerenes (C_{60}) were studied to see the effect of doping metal and electronegativity on hydrogen storage performance. It was seen that K-doped fullerenes are not stable but Li-doped ones are. However, lithium is expensive, and its abundance is limited on the earth so, this reduces the commercialization chance of this type of matter.

3.2.1.2. Carbon Nanotubes

Carbon nanotubes (CNTs) have hollow cylinder structure which have a diameter at about 2 nm. They can store hydrogen through their microscopic pores. There are two types of CNTs as single and multiwall carbon nanotubes. CNTs can be modified by doping transition and alkali metal atoms to change the electronegativity of the matter namely, attraction ability or hydrogen storage capacity.

A study on Li-doped and K-doped CNTs shows that the storage capacity can be increased 20 wt.% and 14 wt.% respectively. However, K-doped CNTs are unstable while Li-doped ones showing stable behavior. On the other hand, in despite of stability Li is expensive and its abundance is limited as we said shortly before. And Li-doped CNTs requires high temperatures (200-400 °C) for maximum adsorption and desorption performance. These values are high for mobile applications.

3.2.1.3. Graphene

Graphene is composed of arranging hexagonal carbon units in two dimensions. It is a layered structure and hydrogen is stored between these layers. Storage capacity of graphene can be changed by tuning of the distance between layers of graphene, sheet curvature or by functionalization. Temperature must be about 450 °C for desorption of hydrogen. This method or matter is cheaper, safer and, easier than CNTs.

3.2.2. Zeolites

Zeolites have sieve-like porous structure. Under high pressure and temperatures about 300 °C, zeolites enable to involve hydrogen gas. This property and their sieve-like structure are used in filtering impurities in gases or liquids and storing. Hydrogen gas is sent into zeolites under high pressure and temperature and then it is cooled to room temperature, thus hydrogen is trapped in the matter. They are thermally stable, cheap and compositionally adjustable.

We will investigate porous materials such as metal-organic frameworks, covalent-organic frameworks etc. under this title because they are all porous materials and they have ordinate porous.

3.2.2.1. Metal-Organic Frameworks

Metal-organic frameworks (MOFs) are one group of the porous materials which used to store hydrogen. MOFs are porous materials and, their pore sizes are in nanometer scale, due to being nanoporous material they have high surface areas. MOFs have a metallic centers and non-polar organic bridges between metallic centers. Metal-oxide centered MOFs have higher stability even if they emptied or heated. First study on MOF-based hydrogen storage published in 2003 and from that time they have taken growing attention. Rosi et al. stated that metal-hydrides or carbon materials have had some disadvantages for hydrogen storage, and they

started to study on a new alternative material, namely metal-organic frameworks. It is expressed that MOFs are stable, highly porous, have adaptable cavities, large surface area, configurable pore sizes and properties, sufficient thermal stability [70,74,75,77]. Molecular structure of IRMOF-10 as an example given in Figure 3.3 [78].

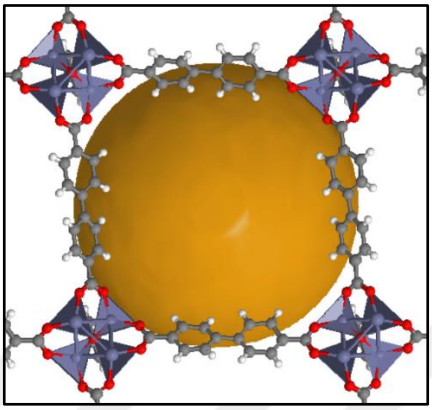

Figure 3.3: An example of metal organic frameworks (IRMOF-10).

3.2.2.2. Covalent Organic Frameworks

This type of material is a little different then MOFs. COFs don't include metal ions to make strong and porous material. Instead of metal ions COFs contain strong C—C, C—O, Si—C, B—O bonds to produce highly porous and less dense materials. COF-102-3 shows the gravimetric storage capacity of 26.7 and 6.5 wt.% under pressure of 100 bar and temperature 77 and 300 K° respectively. However, these pressure values still very high and energy consumption amounts are still insufficient [79–81].

3.2.3. Glasses for Hydrogen Storage

3.2.3.1. Glass Capillary Arrays

Glass capillary arrays are combination of lots of glass capillary tubes to form a mechanically, thermally and chemically stable materials for sample filtration,

collimating, optical beam line splitting and hydrogen storage. The defects in glass such as bubbles, grooves and cracks make them less preferable materials [74,82].

3.2.3.2. Glass Microspheres

Hydrogen is sent into glass microspheres under pressure of 350-700 bar and at 300 °C then rapidly cooled to room temperatures by this way hydrogen has been trapped in glass microspheres. To release hydrogen, microspheres transferred to a low temperature tank and heated up to range of 200-300 °C for controllable releasing [74].

3.2.4. Organometallic Complexes for Hydrogen Storage

Organometallic complexes are combination of transition metal and carbon where transition metals take on a task of increasing hydrogen storage capacity. They have rapid hydrogen adsorption and desorption ability. Electronegativity difference in those molecules cause attracting hydrogen towards electropositive side, namely cation, due to charge polarization mechanism [74].

3.3. Chemical Hydrogen Storage

Chemical hydrogen storage is based on chemical bonding of hydrogen to some elements such as nitrogen, metals, carbon etc. Hydrogen can be released back through some chemical reactions.

3.3.1. Ammonia

Ammonia is one of the most produced chemical materials in the world, and it has been known for approximately for 250 years. Annual production amount of ammonia was higher than 120 million tons in 2006 and the amount reached to 176 million tons. Ammonia can store hydrogen in liquid form even in room temperature

and pressure. Ammonia can be used in solid oxide fuel cells (SOFCs) directly, on the other hand hydrogen must be obtained from ammonia to use as fuel.

Safety is another challenge on usage of ammonia. Ammonia has an explosion risk, it is inflammable and, it is toxic. To avoid toxicity effect, ammonia transformed to metal-amines and inflammableness and explosion risks is decreased. Ammonia can store 17.64 wt.% hydrogen theoretically but, this capacity is decreased when ammonia transformed to metal-amines [83,84].

3.3.2. Carbohydrates

Carbohydrates can be defined by the formula of $C_x(H_2O)_y$, in this formulaic definition x and y can be different however some chemical compounds such as formaldehyde can be adapted to this definition. Thus, carbohydrates should be described with a general stoichiometric formula of $(C_6H_{10}O_5)_n$. These are sugars and, they are one of the most abundant compounds in the world. They can be found in the structure of plant cell-walls on the other hand carbohydrates are the products of photosynthesis reaction.

Glucose and xylose are monosaccharides and they form starch and cellulose by combining with different amounts. Researchers could obtain 12 moles of hydrogen from aqueous solution of ($C_{12}H_{22}O_{11}$) following by the Eq. 3.1.

$$C_{12}H_{22}O_{11(aq)} + 7H_2O_{(l)} \rightarrow C_6H_{12}O_{6(aq)} + 12H_{2(g)} + 6CO_{2(g)} \quad (3.1)$$

Carbohydrates can be stocked in powder or liquid form. They are non-toxic, need low temperatures and pressures. However, as seen in Eq. 3.1 carbohydrates release carbon dioxide as by-product [74,85,86].

3.3.3. Metal Hydrides

Metal hydrides are solid state hydrogen storage materials which generally consist of rare earth metals and transition metal as a root. These types of materials

have crystal structure and, hydrogen settle into vacancies of the crystals. Metal hydrides require different temperature and pressure regimes. Hydrogen storage in metal hydrides is recyclable, much safer and has higher volumetric and gravimetric (up to 14 wt.%) storage capacity than cryogenic or pressure-based storage systems.

Despite of all these advantages highest capacity metal hydrides needs dehydrogenation temperature up to 500 °C. Contact with skin or eyes causes irritation in addition, they react with moist of air, unfavorable to handle, give rise to absorption of impurities into reaction tanks while releasing hydrogen and this last issue causes reduction on lifetime of tanks. Formation reactions of metal hydrides are given below, in Eq. 3.2, Eq. 3.3 [74,87–89].

$$\mathrm{M} + \frac{x}{2}\,\mathrm{H_2} \leftrightarrow \mathrm{MH}_x \tag{3.2}$$

$$M + \frac{x}{2}H_2O + \frac{x}{2}e^- \leftrightarrow MH_x + \frac{x}{2}OH^- \tag{3.3}$$

3.3.4. Sodium Borohydride

Sodium borohydride (SBH) is examined under title of metal hydrates by some researchers but we prefer to examine as a specific subject because SBH still draw a significant attention. Studies have focused on catalyst synthesis for generation of hydrogen from SBH. Monometallic Ru, Pt, Rh etc., bimetallic RuCo, PtCo, AgCu etc. and also non-noble metal based catalysts were produced and tested[90–94].

SBH has a gravimetric storage capacity of 10.8 wt.% but its hydrogen releasing reaction occurs in aqueous or alcoholic media. 4 moles of hydrogen are released per mol of SBH in aqueous media. While two moles of hydrogen are coming from SBH, two moles of H_2 come from water. Catalytic dehydrogenation reaction of SBH is given in Eq. 3.4 [94].

$$NaBH_{4(aq)} + H_2O_{(l)} \rightarrow NaBO_{2(aq)} + 4H_{2(g)} \tag{3.4}$$

As seen in Eq. 3.4 sodium metaborate ($NaBO_2$) is the by-product of hydrolysis reaction and, it can deactivate the catalyst by covering the catalyst surface and, because of this phenomenon, controlling of reaction rate becomes more difficult. Aqueous solution of SBH is not stable when pH is lower than 7, to get better stability predetermined amount of NaOH is usually added to solution. On the other hand, if rate of the reaction is wanted to accelerate the pH of the media should be increased. There is a contradiction between storage media of aqueous SBH (before usage) and reaction media [95].

3.3.5. Ammonia Borane

Ammonia borane (NH_3BH_3 – AB) is one of the most famous and attractive materials for hydrogen storage due to its non-toxicity, high gravimetric hydrogen storage capacity, stability of aqueous solution under ambient conditions, and ability of releasing hydrogen in the presence of suitable catalysts. Hydrogen storage capacity of AB is 19.6 wt.%. Hydrogen can be released from AB by solvolysis and thermolysis. Thermolysis reaction is not suitable for mobile applications because it requires high temperatures (above 100 °C).

It has an orthorhombic structure, with the lattice parameters of a=5.395Å, b=4.887Å, c=4.986Å and all angles are 90°. The electronic configurations of atoms in the complex are given below. Structure views of AB is given in Appendix C:.

- ^{1}H: $1s^1$
- ^{5}B: $1s^2\ 2s^2\ 2p^1$ $-3e^-$ → ^{2}He
- ^{7}N: $1s^2\ 2s^2\ 2p^3$ $+3e^-$ → ^{10}Ne

Due to their electronic configurations given above, boron tends to give 3 electrons, nitrogen tends to receive 3 electrons and hydrogen can behave according to the counterparts. By the help of nature of the atoms, hydrogen is partial positive and nitrogen is partial negative for NH_3 side and hydrogen is partial negative, and boron is partially positive ($H^{\delta+}$-$N^{\delta-}$, $H^{\delta-}$-$B^{\delta+}$). Weak hydrogen bonds were built between

oppositely charged hydrogen atoms. BH_3 and NH_3 species build a complex by using bonds originated from partial charges.

Solvolysis reaction occurs in the presence of catalysts. Catalysts vary from noble metal to non-noble metal catalysts and, monometallic or bimetallic systems. Catalytic releasing reaction of hydrogen from AB occurs according to the following equation (Eq. 3.5).

$$NH_3BH_{3\,(aq)} + 2H_2O_{(l)} \rightarrow NH_4^{+}{}_{(aq)} + BO_2^{-}{}_{(aq)} + 3H_{2\,(g)} \qquad (3.5)$$

As can be seen in Eq. 3.5 two moles of produced hydrogen come from water and 1 mol comes from borane side of the AB. AB has high solubility in water up to 0.336 g/mL and this means that 100 mL of saturated aqueous ammonia borane solution can release more than 3 moles of hydrogen gas [96].

There are several catalyst preparation studies on dehydrogenation of ammonia borane and it still draws growing attention. Figure 3.4 shows the published papers on AB and catalyst preparation for dehydrogenation of AB from 1994 to 2018 (data collected from sciencedirect.com).

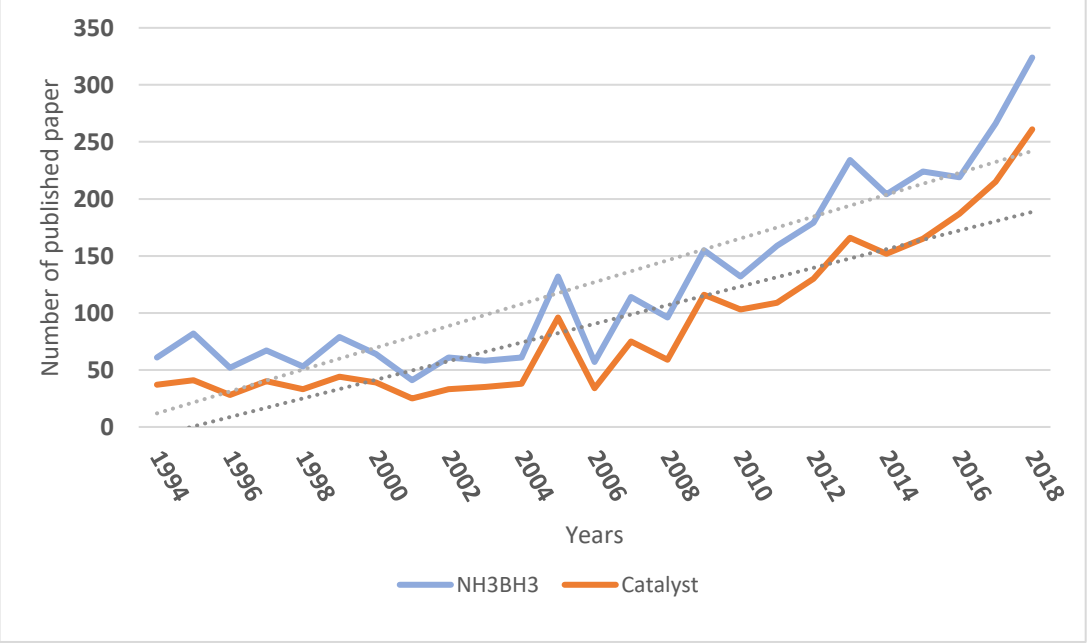

Figure 3.4: Papers on ammonia borane and catalysts for dehydrogenation of AB between 1994-2018.

Precious metals, like Pd, Pt, Ru, Rh, Au, Ag etc. based bimetallic and monometallic catalysts and, non-precious metals, like Co, Cu, Ni, Fe based bimetallic catalysts were studied previously in the literature not only catalyst composition but also, solvent type, catalyst support, catalyst structures were investigated [97–106].

Catalyst activity is stated in TOF (Total Turnover Frequency) value and if it is high, it means that activity of the catalyst is high. TOF calculation will be described in the following sections.

Table 3.1: Monometallic catalysts for dehydrogenation of AB.

Catalyst	**TOF** $[\frac{molH_2}{molRu\ x\ min}]$	**Temp. (°C)**	**Ref.**
Rh/CNTs	706	25	[105]
Ru/CB	429.5	25	[107]
Pt NPs/MIL-101	414	rt	[108]
Ru/Al_2O_3-NFs	327	-	[109]
Ru/TiO_2 (B)	303	-	[110]
Ag/SiO_2-$CoFe_2O_4$	264	25	[111]
Ru/ZrO_2	173	-	[112]
Ru/HfO_2	170	25	[113]
Cu/SiO_2-$CoFe_2O_4$	40	25	[114]
Ni/CNT	26.2	25	[115]
Co/Graphene	13.9	25	[116]
Ni/hBN	4.1	-	[117]
Amorphous Fe	3.1	rt	[118]
Cu/RGO	3.61	-	[119]
Cu NPs	0.2	-	[120]

Table 3.2: Bimetallic catalysts for dehydrogenation of AB.

Catalyst	TOF $[\frac{molH_2}{molRu\ x\ min}]$	Temp. (°C)	Ref.
PtCo@nanoPG	461.7	rt	[121]
Ru@Co/Graphene	344	rt	[122]
Ru@Ni/Graphene	340	25	[123]
Pt-CoCu@SiO_2	272.8	-	[124]
RuCu/Graphene	135	-	[125]
Ni@Ru NPs	114	rt	[126]
$Co_{35}Pd_{65}$/C	22.7	25	[127]
$Co_{35}Pd_{65}$/C (annealed)	35.7	25	[127]
Cu_9Mo	14.9	-	[120]
Cu_9W	3.6	-	[120]
$Cu_{0.95}Cr_{0.05}$	2.0	-	[120]

In Table 3.1 and Table 3.2, it can be seen that supporting materials and, their interactions with catalysts are very important as well as preparing methods. In Table 3.1, 2nd (Ru/CB) and 8th (Ru/HfO_2) catalysts are ruthenium however, Ru/CB catalyst is 2.5 times faster than Ru/HfO_2. Support material-catalyst interactions cause dramatic increase or decrease on the activity of catalysts. On the other hand, data in Table 3.2 claim that post-synthesis treatments and bimetallic composition types effects the activity of catalysts, again. The comparison between $Co_{35}Pd_{65}$/C and $Co_{35}Pd_{65}$/C (annealed) can show the impact of post-synthesis treatment (annealing is a post-synthesis treatment).

To sum up, ammonia borane still draws growing attention of researchers due to its high gravimetric and volumetric hydrogen storage capacity, stability in aqueous solution, high solubility in water and alcohols, high hydrogen releasing rate in the presence of catalyst, non-toxicity and harmless by-products for catalyst. Figure 3.4 demonstrates this growing attention and the Figure 3.5 shows the gravimetric and volumetric hydrogen densities of the different materials [128].

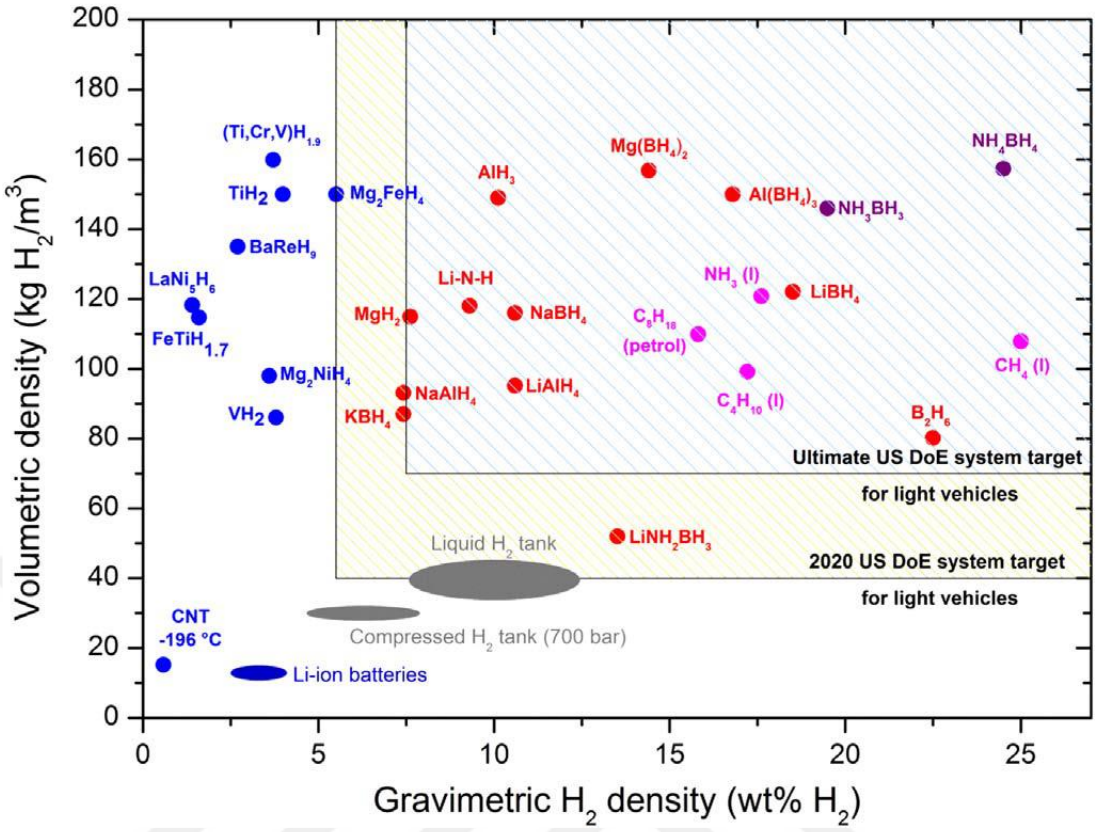

Figure 3.5: A review of hydrogen storage materials (in three phases) according to their volumetric and gravimetric hydrogen density. The area between vertical and horizontal parallel lines states the 2020 targets of The U.S. Department of Energy.

4. CATALYSIS

Catalysis is a phenomenon which means that being accelerated of a chemical reaction by substances named as catalysts. Catalysts do not affect the thermodynamics of a reaction, just change the kinetic of the reaction. Catalysts provide sufficient areas (active sites) for reactants to gather and reacts with. Each reaction has suitable catalysts, which decrease the energy barrier by bringing their surface energies into use. Steps include adsorption of reactants to catalyst surface, reaction between reactants and producing product and finally desorption of product from catalyst surface. After the last step a new group of reactant adsorbs on catalyst surface and the other steps occur respectively. Figure 4.1 shows the energy barrier (E_a) differences between catalyzed and non-catalyzed reactions [129].

It is clearly seen from the Figure 4.1 that bonding of reactants is spontaneous and exothermic reaction which decrease the free energy; 2^{nd} step is a reaction between A and B to produce product (P) and, this step has an energy barrier which must be overcome on the other hand it can be also seen that this energy is not high as much as non-catalytic reaction; lastly, desorption of P is an endothermic step .

- The presence of catalysts proposes alternative pathways for the catalyzed reactions and even if these ways are more complicated, they are energetically more preferable.
- The energy barrier or activation energy of catalyzed reaction is much smaller than non-catalyzed one thereby, catalyzed reaction will be much faster than the other one.
- The total free energy changes of the non-catalytic and catalytic reactions are equal namely, presence of catalyst does not affect the thermodynamic of the reaction. If a reaction is thermodynamically impossible, catalyst cannot change this, even if it is most powerful catalyst.
- Catalysts accelerate the reaction in both direction (forward and backward).

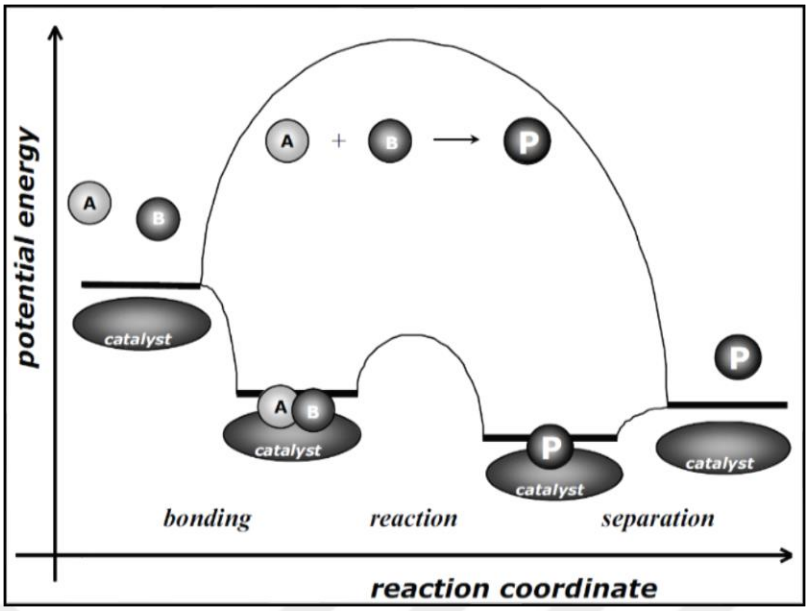

Figure 4.1: The energy barrier changing between catalyzed and non-catalyzed reactions.

- If the catalyst and reactants are not bonded strongly enough, the probability of reaction will be lower.
- If the catalyst and one of the reactants (denote as A) are bonded more strongly than the other reactant (denote as B) as a result, the surface of the catalyst will be mostly covered by the reactant A and reactant B cannot bond to the surface. To see the catalytic effect, both A and B can bond to the catalyst. Not to bond of B or relatively more strong bonding of A prevent or make slower the reaction. This situation known as poisoning of catalyst by A.
- If product (P) is strongly bonded to catalyst, it will be seen the deposition of P on the catalyst surface, and this phenomenon named as poisoning of catalyst by product.

There are three main types of catalysis. These are homogeneous, heterogeneous catalysis and biocatalysis, in addition to these the fourth type of catalysis is nanocatalysis which is a combination of homogeneous and heterogeneous catalysis. The catalysis types will be shortly described in the next sections.

4.1. Biocatalysis

Most people can remember a phrase from biology courses in high school which is “enzyme substrate interactions”. Enzymes are the catalysts of mother nature which make organisms live. Enzymes are proteins and they have unique shapes for bonding to their related substrates. They have active sites according to their shapes and substrates bond to these sites (each substrate identifies their unique active sites on the enzymes) then the reaction occurs to produce product, on the enzyme. Eq. 4.1 shows decomposition of hydrogen peroxide to water and oxygen in the presence of catalyze enzyme [129].

$$2H_2O_2 \rightarrow 2H_2O + O_2 \quad (4.1)$$

Enzymes also catalyze biological reactions such as digestion, building-up DNA molecules, cell division.

4.2. Homogeneous Catalysis

Reactants and catalysts are in the same phases in homogeneous catalysis. Being in the same phase allows an atomic contact between reactants and catalyst thereby all the catalyst becomes surface. This means homogeneous catalysts have high surface area and, high surface area accelerates the reaction rate [129].

Recycling and separation of homogeneous catalyst from the reaction media is difficult and expensive. On the other hand, a part of liquid catalysts is strong acids like sulfuric and hydrofluoric acids. They are very toxic and risky to store. To overcome above-mentioned disadvantages, heterogeneous catalysts were developed [130].

4.3. Heterogeneous Catalysis

In heterogeneous catalysis, reactants and catalyst are in different phases. In heterogeneous catalysis, catalytic reaction occurs only at the catalyst surface. Used material amount to surface area ratio is lower than homogeneous catalyst but they are easily separable and recyclable. Separability and recyclability properties make heterogeneous catalyst most preferable ones for industrial applications.

We use these types of catalyst in our daily life in exhaust systems of internal combustion engine vehicles. Noble metal such as Pt, Rh and Pd are used to convert CO to CO_2 which can be absorbed by green plants to produce oxygen and food. To overcome the low mass to surface area ratio issue, nanocatalysts were developed and nanocatalysts will be glanced in the last title of this section as a catalyst type. Reactions below show the conversion of CO to CO_2 in the presence of heterogeneous catalyst. Eq. 4.2 and 4.3 show adsorption of oxygen and carbon monoxide to active sites (*) of catalysts respectively and Eq. 4.4 is for overall reaction.

$$O_2 + ** \leftrightarrow 2O* \tag{4.2}$$

$$CO + * \leftrightarrow CO* \tag{4.3}$$

$$CO* + O* \leftrightarrow CO_2 + ** \tag{4.4}$$

4.4. Nanocatalysis

To eliminate the disadvantages of both homogeneous and heterogeneous catalysts nanocatalysts were developed. Their sizes are in nanoscale, and they consolidate benefits of other two types.

Nanocatalysts are easily separable from the reaction media, recyclable, they have high surface to mass ratio. These properties make nanocatalysts mostly used and produced catalysts.

To develop a good catalyst, increasing of catalyst's activity is the necessary and not enough condition. In addition, researchers should develop:

- Heat & mass transfer ability,
- To remove impurities from raw materials and catalyst,
- Phase, porosity and surface area,
- Chemical composition of support, bulk, surface and active sites,
- Chemical and mechanical stability of the support, bulk, surface and, active sites.

Catalytic activity can be described by two terms; total turnover frequency total turnover number (TTON or TON- Eq. 4.5), and (TTOF or TOF- Eq. 4.6). The formulas of them are below:

$$TON = \frac{moles\ of\ products}{moles\ of\ catalyst} \tag{4.5}$$

$$TOF = \frac{(moles\ of\ product)}{(moles\ of\ catalyst)x\ time} \tag{4.6}$$

Working mechanisms of catalysts (i.e. catalysts for dehydrogenation of AB) are also based on two important phenomena which named as solid-liquid interface interactions and solid-gas interface interactions. In the catalytic dehydrogenation of ammonia borane, solid catalyst will be dispersed in water (without solvation) and AB must be solved in the water and, its ions become aqueous forms. So, it means that meeting of AB and the catalysts observes a solid-liquid interface on the other hand, production of hydrogen gas and removing it from the solid catalyst surface observes a solid-gas interface. These two phenomena will be discussed briefly (without any complicated formula) for the next two titles, 4.4.1 and 4.4.2.

4.4.1. Solid-Liquid Interfaces

Wetting is a term which we certainly hear in our daily life, and this term is used to characterize the interaction between solid and liquid interfaces. Even if we think on the daily usage of wetting term, we may recognize it is very important for solid-phase catalysts which used in the liquid media. Contact angle (CA) is the parameter which used to determine wetting properties. If catalyst and/or support are not wetted enough it cause reducing of catalysts and reactant interaction and finally it reduces the catalytic activity.

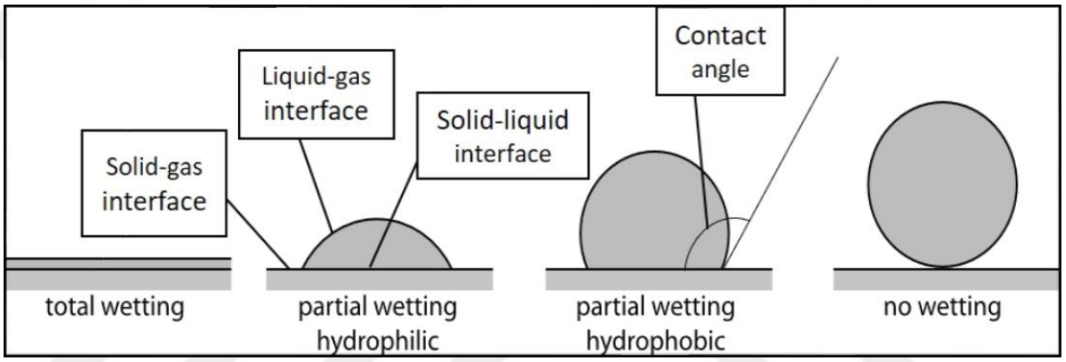

Figure 4.2: Wetting properties according to contact angle (CA). If CA equals 0° it means total wetting and the surface known as super-hydrophilic, if between 0° and 90° it is partial wetting, but it called as hydrophilic, between 90° and 180° it is again partial wetting and called as hydrophobic surface and finally if CA equals 180° there is no wetting and the surface called as super-hydrophobic. (These denominations are valid if the liquid is water. For example, if the liquid is oil these terms become oleophobic and oleophilic).

Wetting is a function of the surface (free) energies (SFE) of solid-gas, solid-liquid and liquid-gas interfaces. SFE is described as the energy required to create a new surface per unit area. It depends on the material identity, and even if it is an energy and energy is a scalar quantity, SFE changes from a surface family to another because of the numbers of unbonded atoms. SFE is originating from reduction of coordination number from bulk structure to surface. We will see an example on FCC structure about changing SFE.

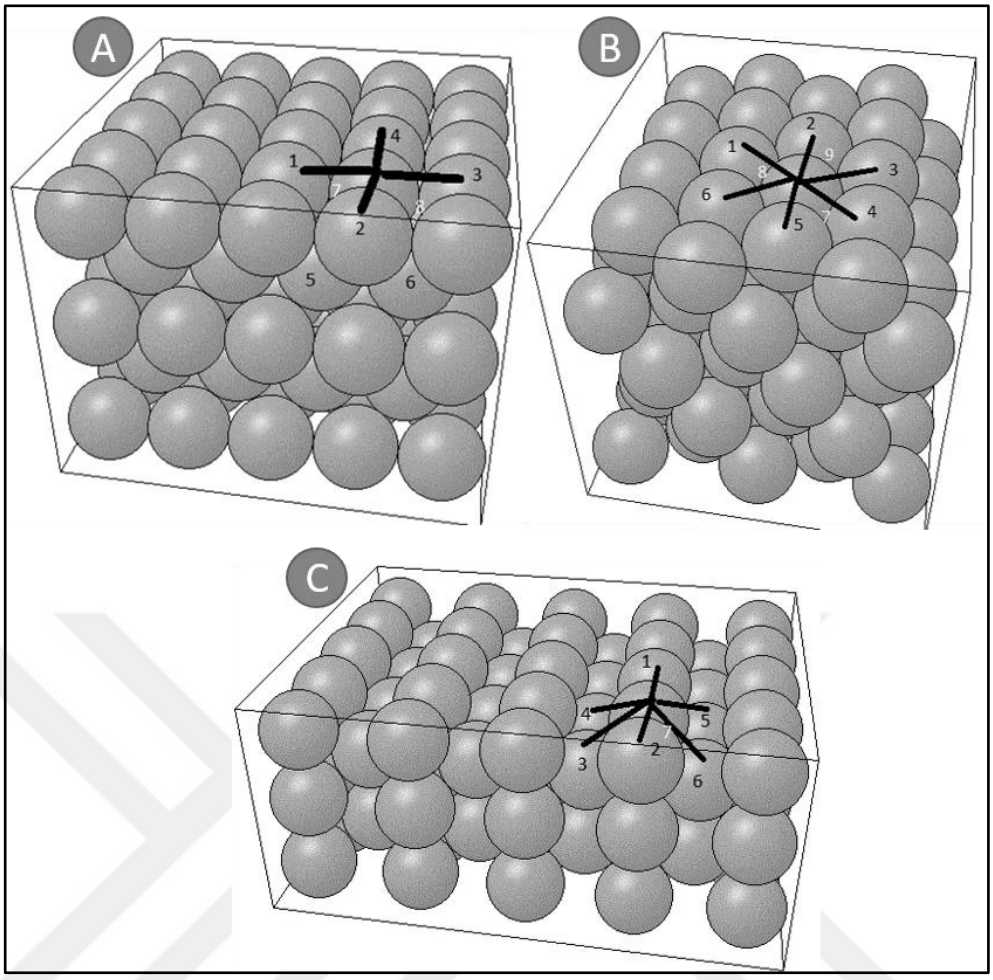

Figure 4.3: Coordination number for face centered cubic (100)(A), (111)(B), (110)(C) surfaces.

As shown in Figure 4.3-A (100) surface has 8 coordination atoms while it has 12 coordination atoms in bulk. The SFE originates from bonding energy of missing 4 atoms for unit cell. If it is wanted to calculate for unit surface area the formula is given in Eq. 4.7:

$$S.F.E = \frac{(CN\ lost)x(\#\ of\ Surf.Atoms)}{Surface\ Area} x(Bond.en.of\ bulk\ atoms) \qquad (4.7)$$

Coordination number lost is 4 for (100), 3 for (111) and 5 for (110) surfaces. Studies for calculating surface free energies of FCC structure shows that (110) surface has more surface free energy than the others.

4.4.2. Solid-Gas Interfaces

While solid-liquid interfaces related with meeting reactants solid gas interfaces related with formation and removing of gaseous products from surface. Mentioned terms are $(H_3N\text{-}BH_3)_{aq}$ and H_2O (or H_3O^+ and OH^-) as reactant and $H_{2(g)}$ as product. Surfaces which have higher energy, tend to bond new atoms even if it is product. So, the amounts of surface free energies must be high enough to let reaction occurs and low enough to remove the product from the surface. This requirement can explain why each reaction has unique catalyst types.

4.5. Catalyst Synthesis Methods Used in This Study

The texture, structure and morphology of the synthesized NPs are dependent on the synthesis methods. The activity of the catalysts is also dependent on the parameters which are affected by the synthesis methods [131–134]. In this study, four different catalyst synthesis methods were employed. They were named as Route A, Route B, Route C and Route D. They will be briefly explained in the next subtitles.

4.5.1. Route A

In Route A procedure, the supporting material was distributed on the bottom of the 25 mL beakers and pre-mixed stock solutions of the metal salts added onto supporting material dropwise until getting it completely wet. Once the addition process ended, the beaker was sealed via perforated tape to let slowly dry for 24h under ambient conditions. Slow drying enables penetration of metal ions into the pores of supporting material and adsorption to the surface. After slow drying, the metal ion impregnated supporting material was put into a vacuum oven to completely dry at 40 °C and 50 mbar vacuum level for 24h (the processes mentioned so far will be called as “P1”). When “P1” ends, required amount of reducing agent (SBH) dissolved in 1 mL water and added directly onto dried supported precursor dropwise. The reduction reaction produces gas and the gas causes foaming due to

gas emission from the reduction reaction and, the supported metal catalyst washed as soon as foaming ended. The supported catalyst washed with 40 mL DI-water in a 50 mL centrifugation tube for 3 times under 9000 rpm and dried at 40 °C, under vacuum (50 mbar) until getting totally dry (the mentioned washing and drying processes hereinafter will be referred as “P2”). Figure 4.4 gives a schematic view of P1 and reduction processes of Route A.

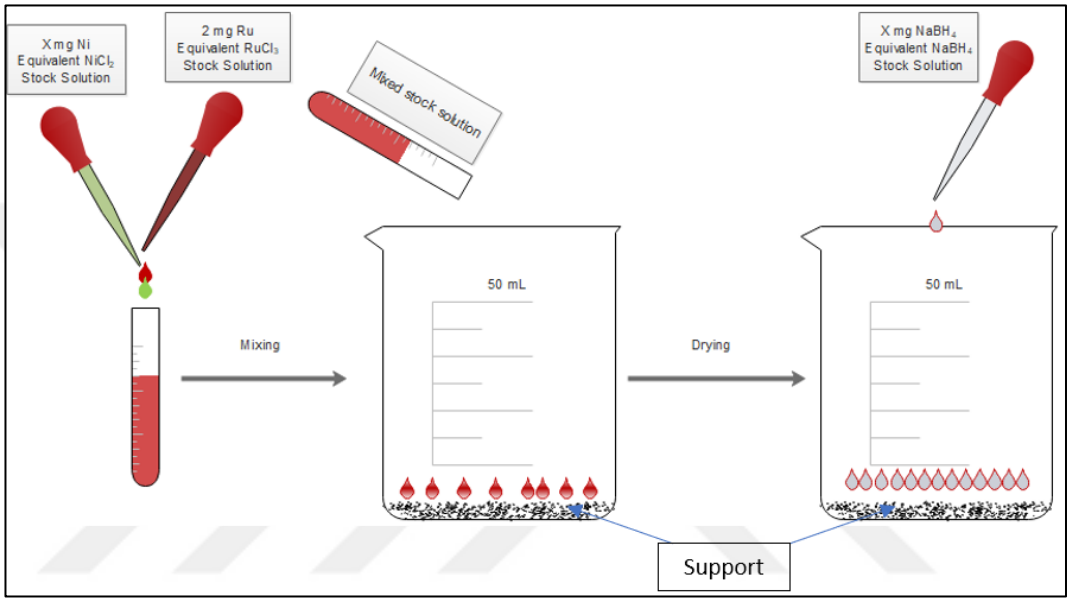

Figure 4.4: Schematic view of Route A.

4.5.2. Route B

“P1” procedure applied without any modification and, after “P1” the dried supported precursor was taken into 10 mL water suspension by stirring it for 15 min. After 15 min, required amount of SBH dissolved in 1 mL of water and added dropwise while the suspension was stirring. It was waited for 1h to complete the reduction reaction and, “P2” applied at the end of 1h. Figure 4.5 gives a schematic view of P1 and reduction processes of Route B.

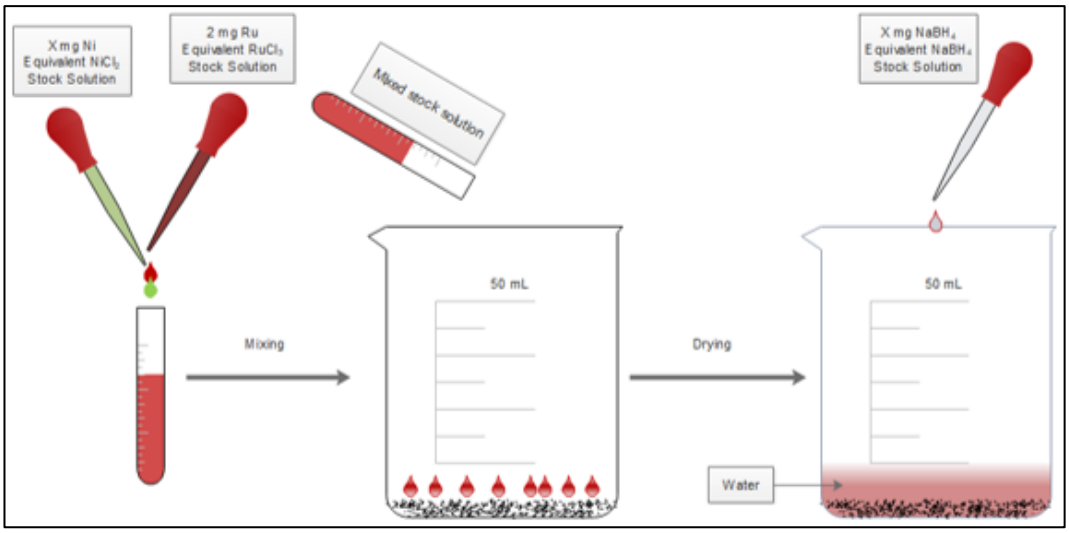

Figure 4.5: Schematic view of Route B.

4.5.3. Route C

The stock solutions of metal salts are diluted in 30 mL of water, sonicated for 2 min and stirred for 15 min to obtain homogenous solution, in a 50 mL beaker. Required amount of supporting material added into the solution while it was stirring and continued to stir on a hotplate for 1h. The required amount of SBH is dissolved in 1mL water and added dropwise into the mixture while it is stirring. When the addition of SBH ended it was waited for 1h to get sure that the reduction reaction completed and the "P2" applied. Figure 4.6 gives a schematic view of Route C, except "P2" process.

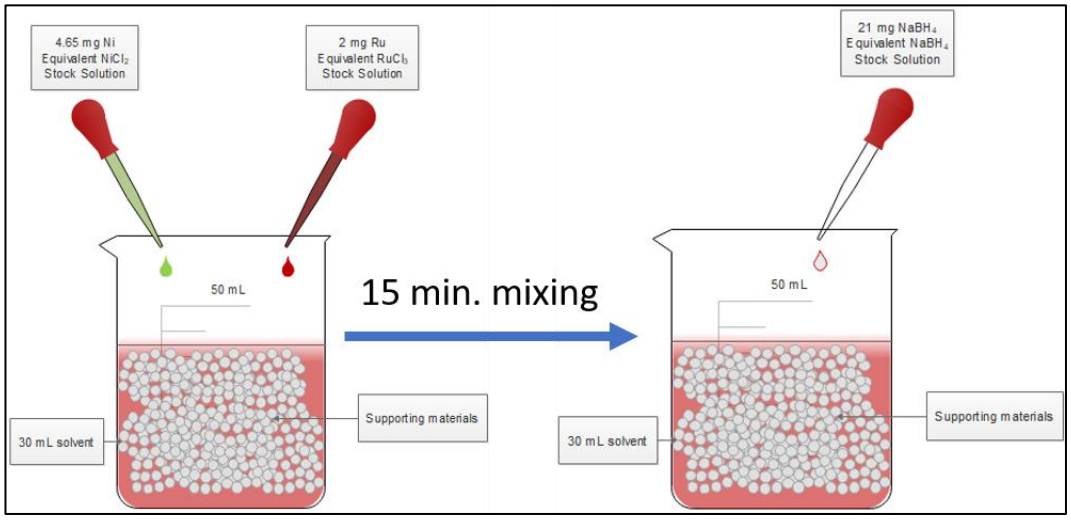

Figure 4.6: Schematic view of Route C.

4.5.4. Route D

All processes of Route D are similar to Route C, except reaction medium. 0.1 M NaOH aqueous solution was used instead of DI-water. Figure 4.7 gives a schematic view of Route D, except “P2” process.

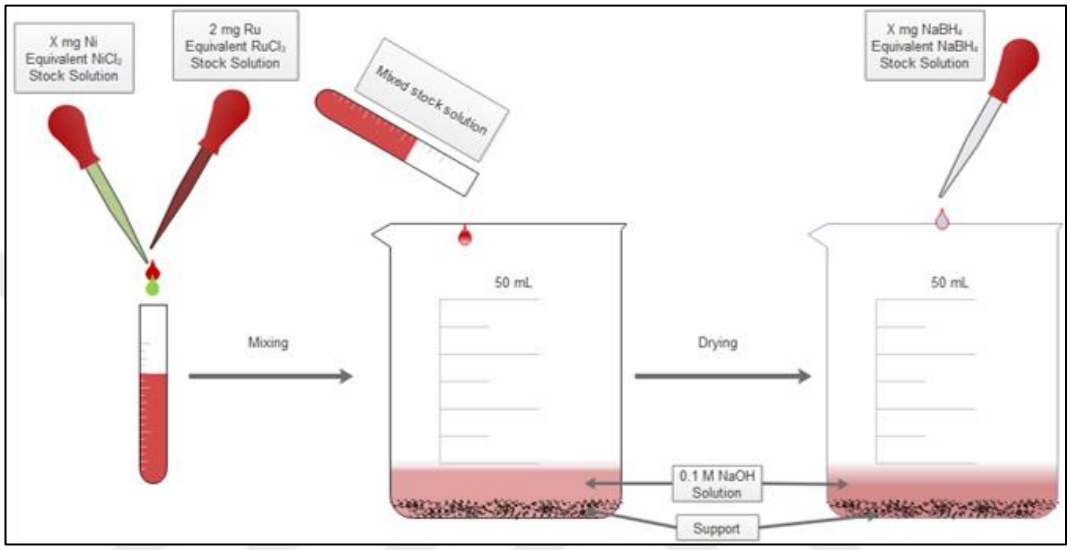

Figure 4.7: Schematic view of Route D.

5. EXPERIMENTAL SECTION

5.1. Materials

Ruthenium(III) chloride hydride ($RuCl_3 \cdot xH_2O$; Alfa Aesar, 99.9 %), nickel(II) nitrate hexahydride ($Ni(NO_3)_2 \cdot 6H_2O$; Alfa Aesar, 98 %) and nickel(II) chloride hexahydride ($NiCl_2 \cdot 6H_2O$; Alfa Aesar, 99.3 %; Sigma-Aldrich, ReagentPlus®), sodium borohydride ($NaBH_4$ Alfa Aesar, 98 %), ammonium sulfate ($(NH_4)_2SO_4$; Merck, 99.5 %), tetrahydrofuran (C_4H_8O; Merck, 99.0% and Sigma-Aldrich, 99.9 %), methanol (CH_3OH; VWR), ethanol (C_2H_5OH; Sigma-Aldrich), diethyl ether ($(C_2H_5)_2O$; Isolab), ammonium hydroxide (Isolab, min.25% ammonia), carbon mesoporous (Sigma-Aldrich, hydrophobic pore surface), carbon nanofiber (Sigma-Aldrich, min.98%, carbon basis, graphitized, platelets-conical- D x L: 100 nm x 20-200 µm) multi-walled carbon nanotube (MWCNT; Sigma-Aldrich, min.90% carbon basis, DxL: 110-170 nm x 5-9 µm), graphite (Sigma-Aldrich, max. 20 µm, synthetic), titanium(IV) oxide pellets (TiO_2; Alfa Aesar), ɣ-aluminum oxide pellets (ɣ-Al_2O_3; Alfa Aesar, 99%), activated carbon (AC) (Alfa Aesar, in powder form and Sigma-Aldrich in pellet form), acetone (C_3H_6O; VWR) were used as received.

In the synthesis of catalyst, analytical balances (Kern ABS 220-4 and Denver Instruments SI-215D), hot plates (VWR VMS-C7 ADVANCED S040, ISOTEX 98-I-B 250, MTOPS MS300HS), micropipette (Transferpette S digital 10-100µL and 100-1000 µL) vacuum oven (MTI DZF-6050), vacuum pump (ZENSEN VPBW-1S), centrifuge (NUVE NF-1200), ultrasonic cleaner (VWR USC 300 THD) were used. Heating and cooling thermostat (LAUDA Proline AP 870), hot plate (IKA RCT CL), gas washing bottle (100 mL) and 4 neck 50 mL glass test reactor (handmade) were employed for catalyst activation tests.

5.2. Synthesis of Catalysts

The activities of the catalysts are strongly dependent on the catalyst synthesis methods. Therefore, it is necessary to systematically analyze all important

preparation parameters. Active metal precursor of catalyst, synthesis method, support material, stoichiometry (if catalyst is not monometallic) and percentage of metal loading on support are the key parameters that can affect the affinity of catalysts. Therefore, in this study catalysts were synthesized by four different methods and tested. They were named as Route A, Route B, Route C and Route D. The synthesis methods were briefly explained in title 4.5 as subtitles.

The catalysts supported on different supports were synthesized by following Route C. In Route C synthesis of catalysts to observe the impact of the supporting material, 2 mg Ru equivalent $RuCl_3 \cdot xH_2O$ and 4.65 mg Ni equivalent of $NiCl_2 \cdot 6H2O$ used as metal precursors and, the mass of supporting material was 93.35 mg. The precursors were mixed in 10mm x 100mm, round bottom glass tube. 20 mg SBH was added dropwise into the slurry as reducing agent. SiO_2, SiO_2-Al_2O_3, Al_2O_3, MCM-48, carbon black, ZrO_2, hematite, TiO_2, MWCNT and CNF were used and tested as catalyst supporting materials.

Route B was followed to synthesize samples for investigating the impact of stoichiometry and, metal loading on the catalytic activity. Used amounts of metals and supporting material are given in Table 6.3, Table 6.4. The most active catalysts were additionally synthesized by following the Route A and Route B to investigate the impact of the synthesis method on catalytic activity. In Route A catalyst synthesis method, 98 mg of supporting material, 1.27 mg Ru equivalent of $RuCl_3 \cdot xH_2O$ and 0.73 mg Ni equivalent of $NiCl_2 \cdot 6H_2O$ used. In order to achieve the Route A and Route B preperation, the water absorption capacities of the oxide-based supports were measured, and the results are listed in Table 5.1.

Table 5.1: Measured water absorption capacities of supporting materials.

Support Materials	**Water Absorption Capacities (µL/g)**
SiO_2	825
Al_2O_3-SiO_2	1200
Al_2O_3	1200
ZrO_2	825
TiO_2	1500
Spherical-Fe_2O_3	1000

5.3. Hydrogen Generation Measurements

All experiments (except activation energy measurement tests) were performed at 25 °C under atmospheric pressure while reaction media was stirring at 700 rpm on a hotplate. The reaction took place in a jacketed 4 neck conical bottom reactor. The set temperature was fixed by using a thermostat. The volume of generated hydrogen was measured by displacement of water from a washing bottle into a graduated cylinder. Experimental setup is shown in Figure 5.1. Once the catalyst was stirred in 9 mL of water for 10 min, 1 mL of 1M ammonia borane was added to the reactor and the reactor cap was closed and sealed immediately. The time for hydrogen generation reaction was recorded per 5 mL of water displacement. Volume of water, molarity of AB was varied during the optimization tests.

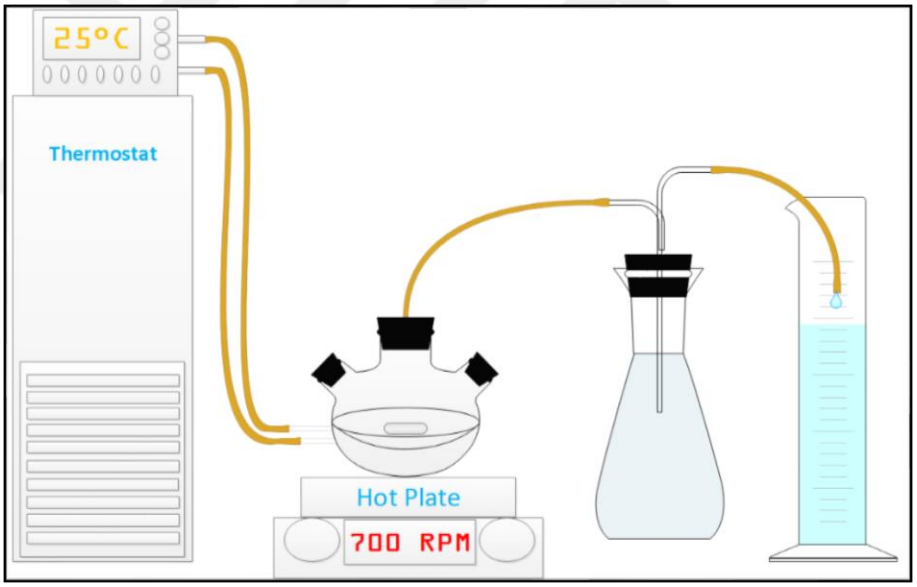

Figure 5.1: Catalytic activity test setup.

5.4. Optimization Tests for Catalytic Hydrolysis Reaction of AB

Two different optimization tests as different Ru:AB molar ratio and different Ru molarity were applied to the catalyst and their impacts were investigated. These optimization tests do not cause any modification on catalyst, they are only about operation conditions for the catalytic hydrolysis reaction.

5.4.1. Optimization of Ru:AB Molar Ratio for Catalytic Hydrolysis of AB

During these tests, the molarity of Ru was changed while the volume of water and the molarity of AB was stabilized. Only the effect of Ru:AB ratio was dominant on the catalytic activity. The tests were applied for seven different ratios from 0.007 to 0.002. The results of these tests are in the section 6.2.1.

5.4.2. Optimization of Ru Molarity for Catalytic Hydrolysis of AB

During these tests the mass of Ru and AB was fixed, and the volume of the water was changed. The optimization tests were carried out for 0.2 to 0.6 mM Ru concentration. The results of this tests are in the section 6.2.2.

5.5. Durability Tests of Ru-Ni/AC for Dehydrogenation of AB

Durability tests were carried out by using most effective catalyst. In the first run, catalyst was tested for 1 mmol AB in 4 mL water. After the reaction completed, 3 mL of water was added to reactor and stirred for 5 min then 1 mmol AB added. This addition procedure was repeated three times. Durability tests also performed in the setup which is shown in Figure 5.1.

6. RESULTS AND DISCUSSIONS

6.1. Catalytic Activity Tests for Hydrolysis of AB

In this section, all significant preparation parameters of Ru–Ni based catalysts were systematically analyzed to obtain a highly efficient catalyst for dehydrogenation of ammonia borane. Catalytic activity tests were performed for each modified catalyst, thereby aiming to obtain the most effective catalyst composition and optimum catalyst operating conditions.

6.1.1. Impact of Supporting Material on Catalytic Activity

It is well known that, specific surface area, adsorption ability, surface charges, wettability, intermolecular & intramolecular bond structures and electronic structure affect the behavior of supporting materials. Catalytic activity is strongly depended on supporting material due to catalyst-support interactions [121,132–134]. Several metal oxides and carbon-based materials were compared as catalyst support. They were alumina (Al_2O_3), silica (SiO_2), alumina-silica (Al_2O_3-SiO_2), spherical hematite (Fe_2O_3), titania (TiO_2), zirconia (ZrO_2), mesoporous silica (MCM48), carbon black, carbon nanofiber, multi-walled carbon nanotube and activated carbon. To examine the effects of the support material on catalytic activity, ruthenium and nickel mole ratio were kept constant as $RuNi_4$ and were tested for dehydrogenation of 1 mmol AB at 25 °C under 700 rpm. 2 mg Ru and 4.65 mg Ni equivalent salt solutions were deposited onto 93.35 mg of catalyst support via Route C. Other catalyst synthesis parameters such as catalyst loading and reducing agent were identical.

The catalytic activity comparisons of catalysts supported on oxide-based-materials (OBM) and carbon-based-materials (CBM) are shown in Figure 6.1 and 6.2, respectively. Also, the most active three catalysts and least active one is shown in Figure 6.3. The results showed that, as compared to carbon-based supporting materials, oxide-based materials, except TiO_2, showed lower catalytic activities. As it can be seen in Figure 6.1, Figure 6.2, Figure 6.3, carbon black, titania and AC

supported $RuNi_4$ are the most active catalysts respectively. Although TiO_2 and AC show almost similar activity, AC was chosen as the support material for further studies due to ease of production and low cost.

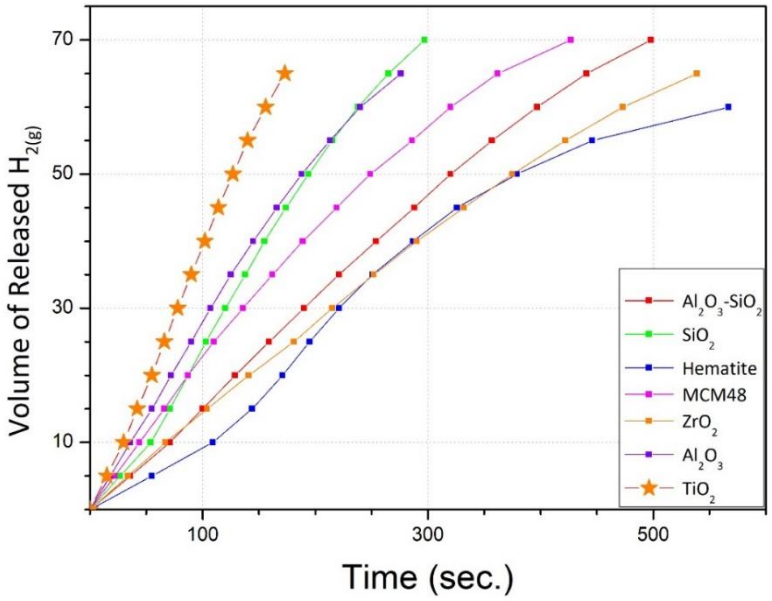

Figure 6.1: Catalytic activity test results of $RuNi_4$/OBM catalysts.

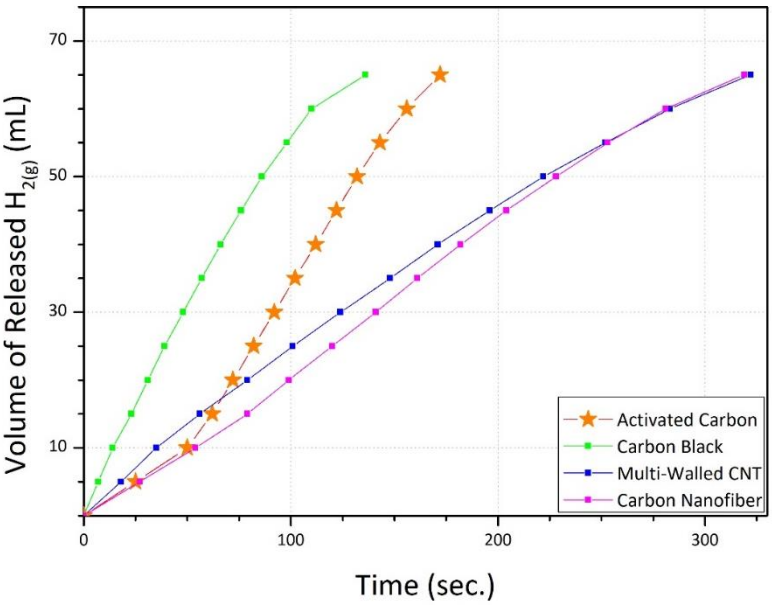

Figure 6.2: Catalytic activity test results of $RuNi_4$/CBM catalysts.

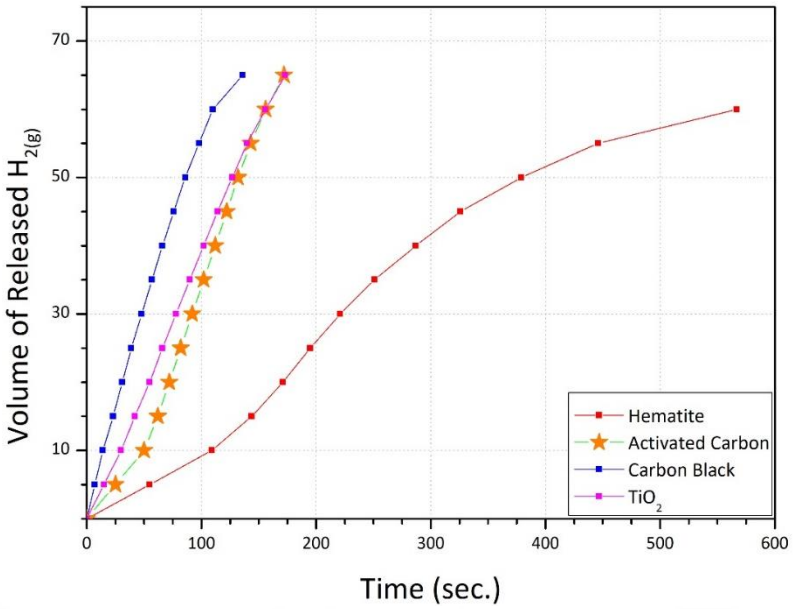

Figure 6.3: Catalytic activity test results of $RuNi_4$ catalysts supported on selected materials.

In order to characterize the electrical condition of the support material surface in the solution, it is necessary to determine the point of zero charge (PZC) point. The PZC can be defined as the pH at which the net surface charge resulting from the adsorption of potential-determining ions H^+ and OH^- is zero. When the solution pH is lower than PZC, the surface of the support particles is positively charged, and opposite is true for pH> PZC. Specific surface area (SSA) (m^2/g) and point zero charge (PZC) values of the used supports are given below in Table 6.1

ACs exhibit slightly different properties according to their raw materials however, they have a mutual property of being porous material [135]. Due to effect of raw materials on properties of AC, two different brands were used and tested. It was mentioned before that the origin of the activated carbon is very important. Activated carbons can be fabricated from different raw materials i.e. coconut shell, rice hull, pistachio shells, apricot stones. Each feedstock causes unique properties. Yeganeh et al. studied on the effect of raw material and some results are shown in Table 6.2.

Iodine number gives a knowledge on adsorption capacity of the material and, metal ion adsorption has a significant effect on the metal-support interaction. On the other hand, surface area of the support is important for catalyst surface area,

distribution and activity. It is shown on the table that there are big differences on iodine number, surface area and pH [136].

Table 6.1: Specific surface area and PZC values of used supports.

Support	SSA (m^2/g)	PZC (pH)	Ref.
Al_2O_3	130	9.0	[137,138]
TiO_2	180	6.6	[138,139]
Fe_2O_3	41	8.6	[140,141]
SiO_2	400-750	2.0	[142,143]
MCM48	1100	7.1	[144,145]
ZrO_2	90-220	3.1	[146,147]
AC	50-1500	4.0-9.0	[148–150]
CB	1000	6.4	[151,152]
CNF	970	2.20-7.70	[153–155]
MWCNT	1600	2.2-11.8	[155,156]

Table 6.2: Effect of raw materials on SSA, iodine number and PZC of AC.

Raw material of activated carbon	Iodine number (mg I/g AC)	Surface Area (m^2/g)	PZC
Residues of Liquorice	413	114	4.20
Rice Hulls	435	158	4.14
Pistachio Shells	953	1184	3.96
Apricot Stones	952	1182	3.98
Almond Shells	830	941	4.09
Walnut Shells	806	892	3.92

Figure 6.4 shows the zeta potential measurement depending to pH, and the IEP. IEP of the used AC calculated as 4.5. Since the catalyst active metals Ru and Ni have a positive charge, the negative support surface is preferred to electrostatic adsorption. As the surface becomes more negatively charged by increasing the pH of the solution, metal ions are strongly adsorbed on the support surface.

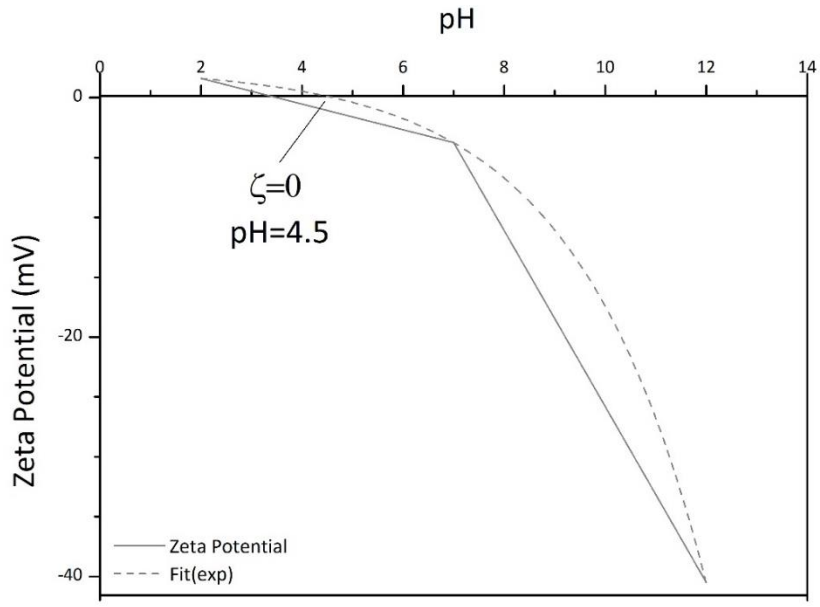

Figure 6.4: Zeta potential measurement of the AC used in the study.

6.1.2. Impact of Post-Treatments of Activated Carbons on Catalytic Activity

Two different AC from Alfa Aesar and Sigma-Aldrich as catalyst support material was tested for dehydrogenation of ammonia borane. ACs were treated with boiling nitric acid for three hours to bind oxygen groups. Untreated and acid washed AC's are called as "UT" and "T", respectively. 2 wt.% metal loading $RuNi_4$/ACx catalysts were synthesized by Route B for investigating the impact of the both AC source and post-treatment efficiency. T-AC (T) (Alfa Aesar), UT-AC (Alfa Aesar) and UT-AC (Sigma Aldrich) supported $RuNi_4$ catalysts were synthesized.

Catalytic activity test results on dehydrogenation of ammonia borane catalyzed by Ru-Ni catalyst supported on ACs demonstrate that ACs obtained from different raw materials have unique support characteristics (Figure 6.5). It can be seen that nitric acid treated activated carbons have lower hydrogen production rates. This can be explained as the decrease on BET surface area due to nitric acid treatment. Also, acid treatment leads to changes in the radical surface groups of AC [157].

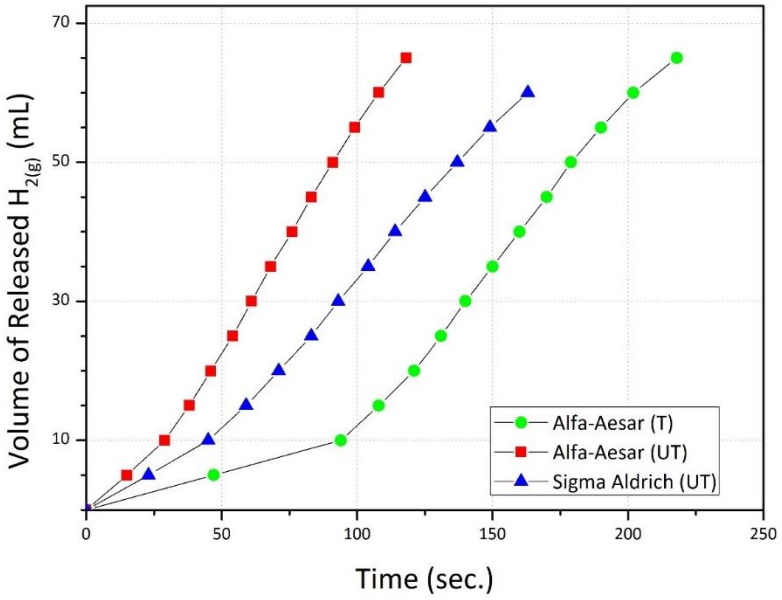

Figure 6.5: Catalytic activity test results according to different type of AC supported Ru_1Ni_4.

6.1.3. Impact of Synthesis Methods on Catalytic Activity

$RuCl_3 \cdot xH_2O$ is mostly used in ruthenium-based catalyst when $NaBH_4$ is used as reducing agent [78,111,121–124]. $Ni(NO_3)_2 \cdot 6H_2O$ and $NiCl_2 \cdot 6H_2O$ are favored nickel precursors [41,42,122,125–129]. Nickel and ruthenium have different reduction potentials (-0.236 eV and +0.60 eV versus SHE respectively) [130] and as it was mentioned in the literature, ammonia borane is not suitable reducing agent for reduction of Ni^{2+}. It can be reduced in the presence of ruthenium particles and due to the difference between their reduction potentials Ru will be firstly reduced species and Ni atoms will be deposited onto reduced Ru nanoparticles. This mechanism causes Ru-core Ni-shell structures [111] and it cannot be changed at room temperatures without changing pH of solution. Metals which have high oxidation tendencies might be removed from the catalyst surface and pass through the solution into ion forms. Unintentionally, it might change (usually reduce) the catalytic activity because of active material loss. Therefore, prepared catalysts were reduced by $NaBH_4$. The tests were conducted for 1 mmol ammonia borane in 10 mL of water over 0.8 mmol (~0.8 mg) Ru containing catalyst. The results of these tests are given below.

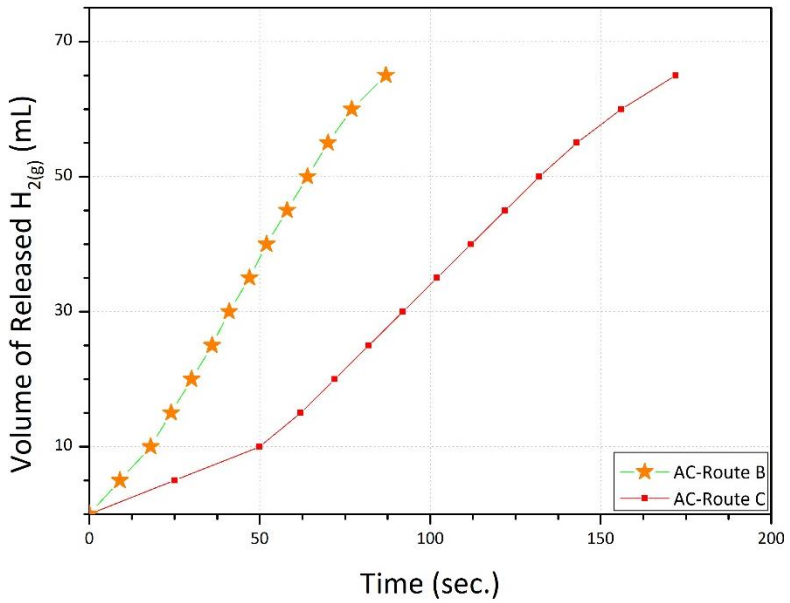

Figure 6.6: Activity test results of $RuNi_4$/AC catalysts synthesized via Route B and Route C.

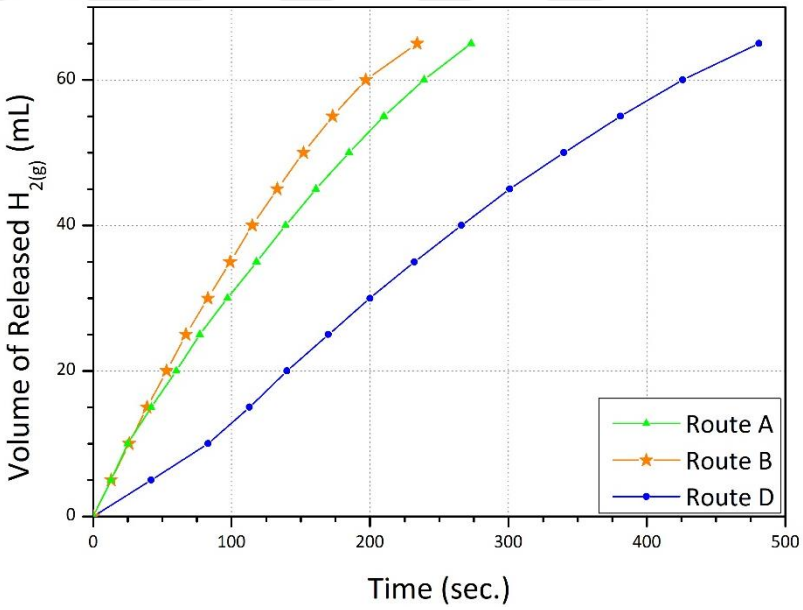

Figure 6.7: Activity test results of Ru_1Ni_1/AC synthesized by Route A, Route B, Route D.

In Figure 6.6 and Figure 6.7., Route A, Route B, Route C and Route D are the synthesis methods which used in this study. As can be clearly seen from the results, Route B predominates the Route A, Route C and Route D. Interaction period between supporting material and metal salt stock solution for the catalysts synthesized by Route B is much longer than Route C, on the other hand the metal ion concentration is almost 10-15 times higher for Route B than Route C. The drying process increases

metal-ion adsorption on the support surface certainly in the Route B, while metal-ions can be reduced anywhere in reaction media (naturally they prefer reducing on support or the other impurities in the reaction media) in Route C. These are the possible reasons behind the activity differences.

For the preparation method Route D, NaOH was used as pH adjusting agent and it cause some additional reactions with SiO_2 which can be naturally found in AC. No further XPS characterization could be applied for samples which synthesized via Route D but, it caused some visible change in the system. During the Route D preparation, large metal particles visible to the naked eye were observed and it is clear that they cause a decrease in the specific surface area. Therefore, catalysts synthesized by Route B and Route C were found to be much more active than that synthesized by Route D (Figure 6.7.)

6.1.4. Impact of Stoichiometry on Catalytic Activity

Thirteen different catalysts with different Ru:Ni stoichiometries were synthesized and tested. The synthesis parameters were tabulated in Table 6.3.

Catalysts with different Ru:Ni mole ratios were synthesized by Route B. The tests were conducted for 1 mmol ammonia borane in 10 mL of water with over 0.8 mmol Ru containing catalyst. Catalytic activity of AC supported Ru_1Ni_0, $Ru_1Ni_{0.3}$, $Ru_1Ni_{0.5}$, $Ru_1Ni_{0,75}$, Ru_1Ni_1, $Ru_1Ni_{1,5}$, Ru_1Ni_2, Ru_1Ni_4, Ru_1Ni_6, Ru_1Ni_8, Ru_1Ni_{10}, Ru_1Ni_{12} and Ru_0Ni_1 were compared for dehydrogenation reaction.

It is clearly seen from Figure 6.8 and Figure 6.9 that presence of nickel accelerates the catalytic activity up to 1:8 (Ru:Ni) ratio. The effect nickel ratio for 1:6 and 1:8 can be expressed as fixing of hydrogen releasing rate, notwithstanding their initial rates were slower than pure supported ruthenium, they generated same amount of hydrogen in shorter period. On the other hand, pure nickel had very low catalytic activity, and it could not complete the reaction. Activity of the Ru_1Ni_1/AC was found higher than the sum of the activities of Ru/AC and Ni/AC, this is how it can be seen the addition of nickel accelerated the reaction. This higher activity means there is a synergetic effect between ruthenium and nickel. Stoichiometry can control

the particle size, shape of nanoparticles, phase, structure and catalyst-support interaction [157–159].

Table 6.3 Used amounts for determining the stoichiometry.

Code	Stoichiometry	Ru(mg)	Ru (mmol)	Ni(mg)	Ni(mmol)	AC (mg)
RNAC1	Ru_1Ni_0	2	0,0198	0	0	98
RNAC2	$Ru_1Ni_{0,3}$	2	0,0198	0,348	0,0059	97,65
RNAC3	$Ru_1Ni_{0,5}$	2	0,0198	0,581	0,0099	97,42
RNAC4	$Ru_1Ni_{0,75}$	2	0,0198	0,871	0,0148	97,13
RNAC5	Ru_1Ni_1	2	0,0198	1,161	0,0198	96,84
RNAC6	$Ru_1Ni_{1,5}$	2	0,0198	1,742	0,0297	96,26
RNAC7	Ru_1Ni_2	2	0,0198	2,323	0,0396	95,68
RNAC11	Ru_1Ni_4	2	0,0198	4,646	0,0792	93,35
RNAC15	Ru_1Ni_6	2	0,0198	6,969	0,1187	91,03
RNAC19	Ru_1Ni_8	2	0,0198	9,292	0,1583	88,71
RNAC23	Ru_1Ni_{10}	2	0,0198	11,614	0,1979	86,39
RNAC24	Ru_1Ni_{12}	2	0,0198	13,937	0,2375	84,06
RNAC25	Ru_0Ni_1	0	0	10	0,1704	90

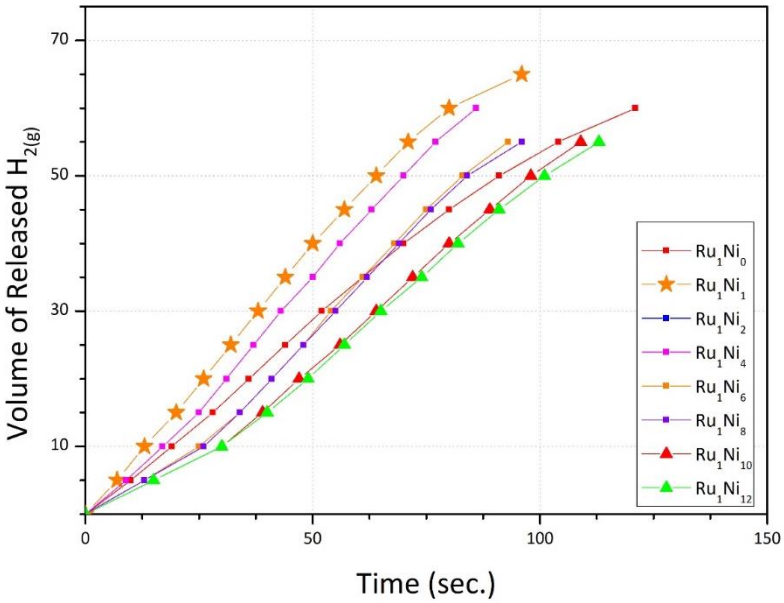

Figure 6.8: Activity test results of different stoichiometries (all samples are supported on AC).

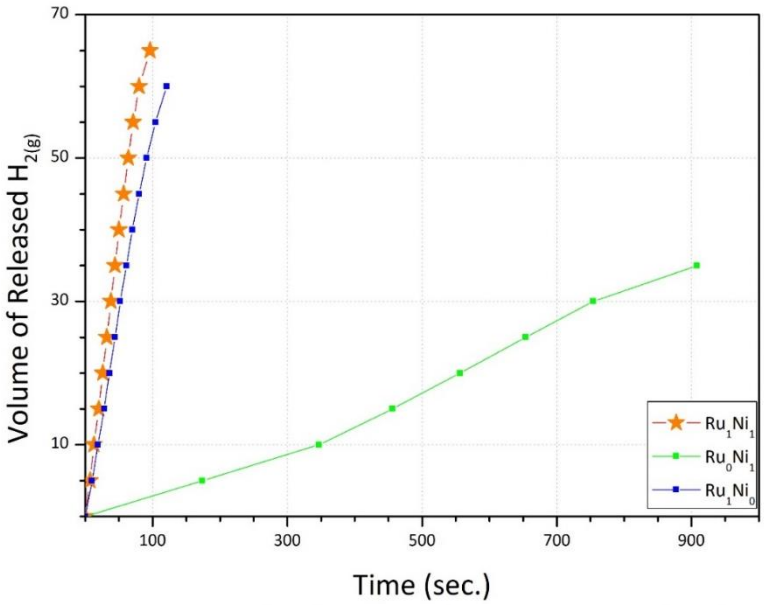

Figure 6.9: Activity test results of different stoichiometries Ru_1Ni_0, Ru_1Ni_1, Ru_0Ni_1 (all samples are supported on AC).

6.1.5. Impact of Metal Loading on Catalytic Activity

After determining of the stoichiometry of catalysts (the selected stoichiometry is hereinafter named as RNAC), new set of catalysts were prepared from 2 wt.% up to 12 wt.% metal loadings to choose the impact of metal loading of catalysts. The catalytic tests were practiced for 1 mmol of AB catalyzed by 0.8 mg Ru equivalent catalysts. Synthesized catalysts and amounts of used material (in mmol and mg) were given in Table 6.4.

Table 6.4: Used amounts for determining the catalyst loading.

Loading (wt.%)	Ru (mmol)	Ru (mg)	Ni (mmol)	Ni (mg)	AC (mg)
2	0,0125	1,265	0,013	0,735	98
4	0,0250	2,531	0,025	1,470	96
6	0,0376	3,796	0,038	2,204	94
8	0,0501	5,061	0,050	2,939	92
10	0,0626	6,326	0,063	3,674	90
12	0,0751	7,592	0,075	4,409	88

Figure 6.10. shows that, 2 wt.% Ru_1Ni_1/AC catalyst loading had highest activity among all catalysts. Without any TEM images it might only be a speculation but, blocking of the pores of support material due to higher metal loading, can explain the activity loss by increased loading. Another possibility can be big particle sizes. It can be thought that there was a surface area loss according to unit mass of metal. Thus, all components of the catalyst were determined by metal loading analysis. 2 wt.% Ru_1Ni_1/AC bimetallic nanocatalyst was determined as most active catalyst of this study. Additionally, when compared to 1 wt.% and 2 wt.% Ru_1Ni_1/AC catalysts, the latter provided higher activity (Figure 6.11).

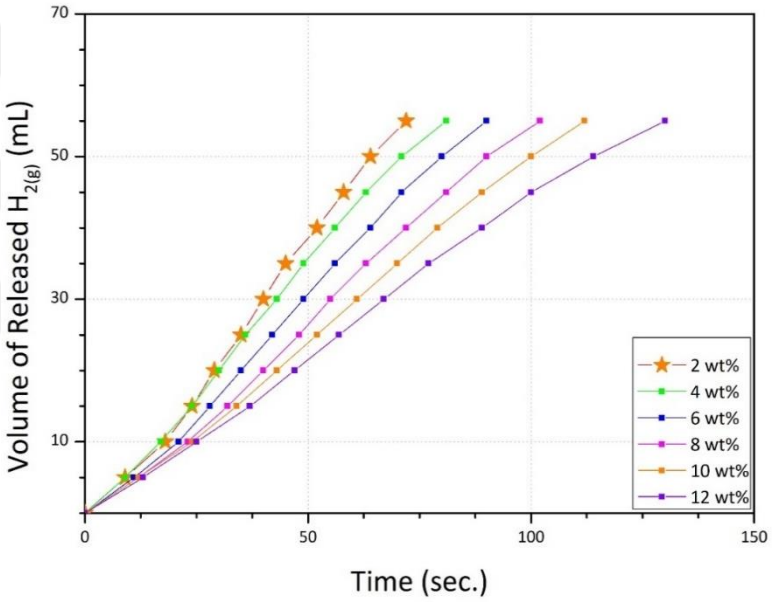

Figure 6.10: Activity test results according to different catalyst loadings (Ru_1Ni_1/AC catalyst).

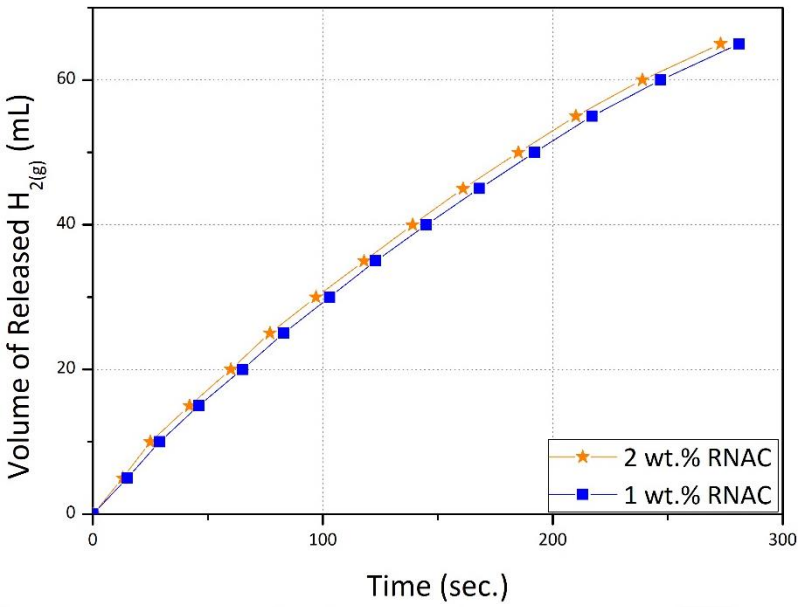

Figure 6.11: Catalytic activity comparison results for 2 wt.% and 1wt.% loaded catalysts.

6.1.6. Impact of Solvent used in Catalyst Synthesis on Catalytic Activity

Methanol, ethanol, distilled water and nitrogen purged distilled water were used to examine the effects of synthesis solvents on catalytic activity. There is a well-known rule in chemistry as “like dissolves like”. The metal precursors which used in this study have polar molecules (ionic metal salts), so polarities of the solvents affect the solvation of metal precursors and affect the reduced amounts of catalysts on supports. As a result, the catalytic activity is affected by solvents. Polarities of ethanol, methanol and, water are 0.654, 0.762 and, 1.000, respectively [158]. As expected, catalyst which synthesized in aqueous media showed better catalytic activity, whereas catalyst synthesized in ethanol shows better activity than those synthesized in methanol in contrast to the polarity values. Due to capillary effect, an amount of precursor stock solutions which dissolved in methanol were smeared to the inner walls of the petri dishes, instead of support. This smearing behavior causes active material loss or unsupported material formation. As it can be seen in Figure 6.12 catalysts synthesized in distilled water and N_2-purged distilled water show almost same catalytic activity, ethanol and methanol follow them respectively.

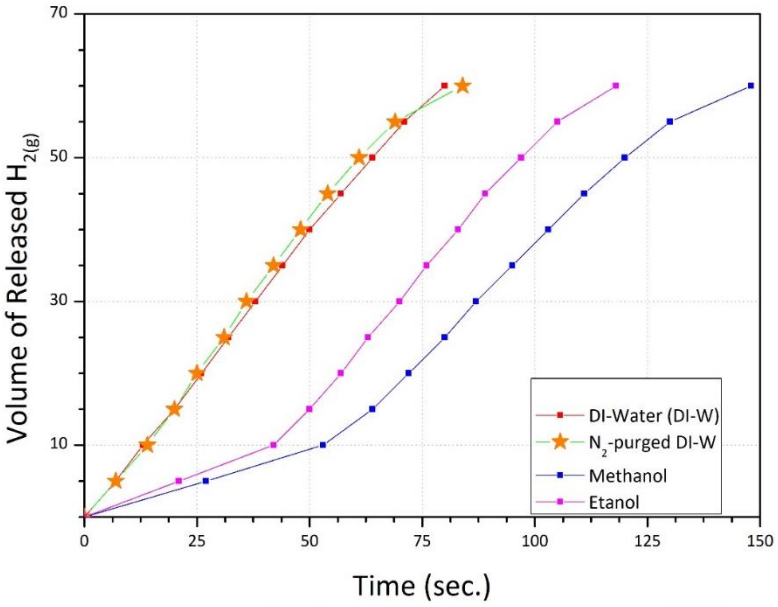

Figure 6.12: Activity test results of catalysts which synthesized in different solvents.

6.2. Catalytic Activity Optimization Tests

6.2.1. Optimization of Ru:AB Molar Ratio

Ru:AB ratio differences are not about the structure of catalyst, it's about the hydrolysis reaction media (post-synthesized). These tests were realized for giving some hints to device design. In despite it is not about structure of catalyst, activities changed according to ratios. 0.002 Ru:AB molar ratio gives highest catalytic activity, turnover frequency of 0.002 ratio is highest one in contrast with the slow hydrogen releasing rate due to the low metal ratio. Relatively higher amount of AB complexes will meet lower catalyst amount. This gives a chance to use higher active area of catalysts, naturally turnover frequency increases while Ru:AB ratio decrease (except 0.006 ratio). Figure 6.13 and Figure 6.14 shows the hydrogen releasing by reaction time and TOF values by Ru:AB molar ratios respectively.

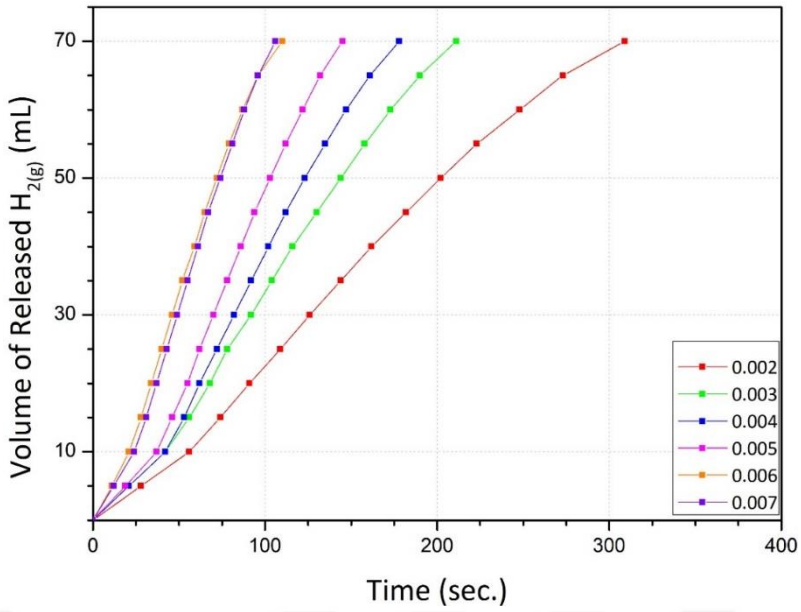

Figure 6.13: Activity test results of different Ru:AB ratios.

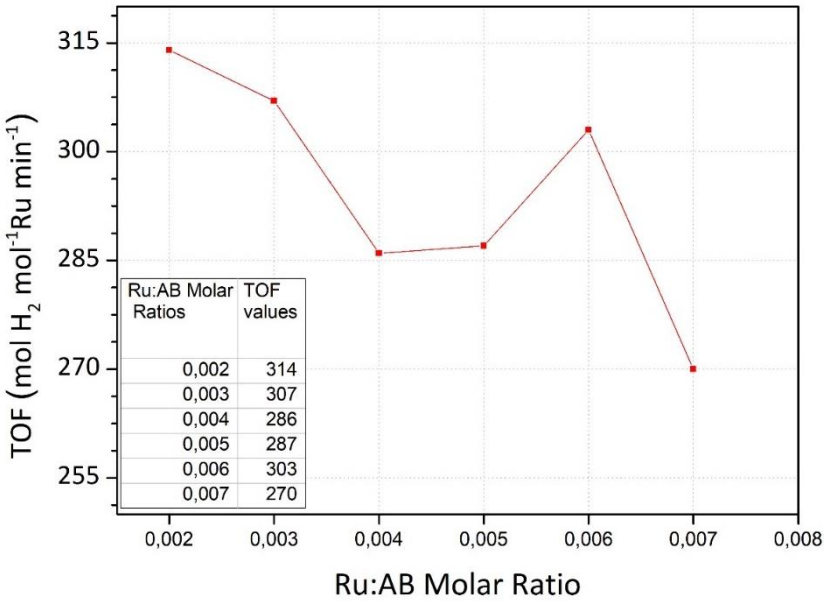

Figure 6.14: TOF value changing according to Ru:AB molar ratios.

6.2.2. Optimization of Ruthenium Molarity

Molarity affects the volume of the media and density of substances increases while molarity increases. It provides higher contact probability of substances in unit volume, and it increases the reaction rate. On the other hand, viscosity of the solution increases when molarity increases due to being in the same media with ammonia borane. Because of increasing of viscosity, the solution cannot penetrate the narrow pores, it means even if the catalyst has high surface area it cannot be used effectively.

At some point viscosity dominates the contact probability and the activity starts to reduce by increasing of molarity. While Figure 6.15 shows the hydrogen releasing rate according to reaction time, Figure 6.16 shows the changing of TOF values by changing the molarity. As it can be seen on the figure, TOF values were increased up to 0.5 mM Ru.

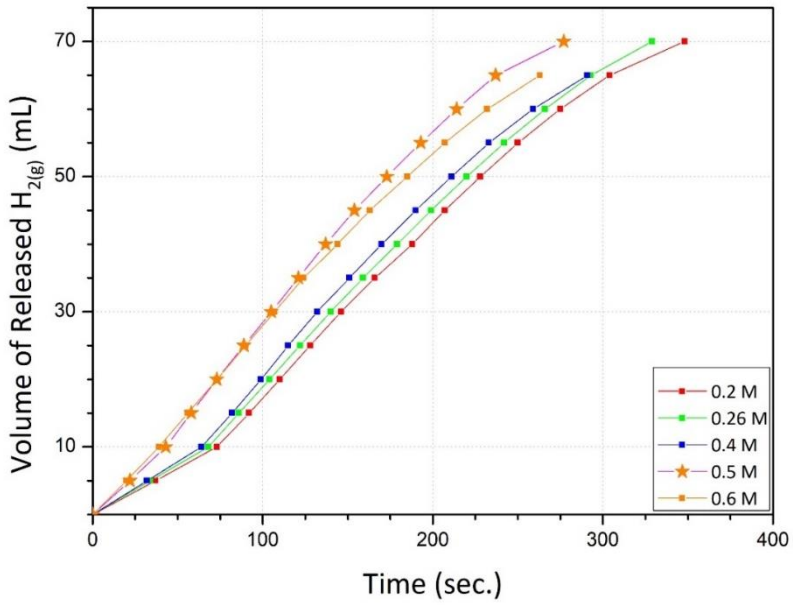

Figure 6.15: Activity test results of different ruthenium molarities.

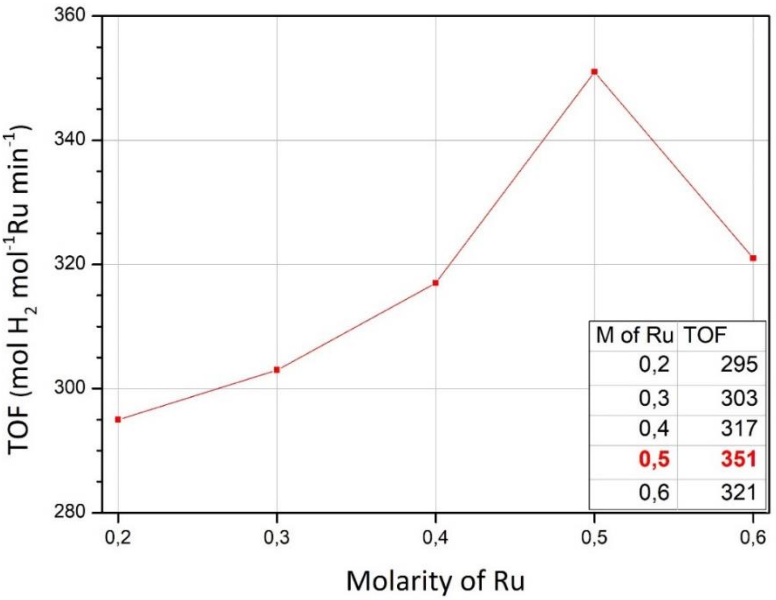

Figure 6.16: TOF values of different ruthenium molarities.

6.3. Calculation of Activation Energy

While explaining what catalysis is, it was mentioned that they change the reaction mechanism and reduced the activation energy by this way. Activation energy is an energy barrier (or cumulative energy difference) between the reactants and the products. Activation energy can be calculated from Arrhenius Equation which is formulated as:

$$k = A\ x\ e^{(-\frac{E_a}{RT})} \tag{6.8}$$

Where, "k" is the rate constant, "A" is frequency factor, "e" is Euler's number, "E_a" is activation energy, "R" is universal gas constant and "T" is temperature. After taking the natural logarithm of both sides of the equation, Arrhenius Equation takes the form of

$$lnk = lnA - (\frac{Ea}{R}\ x\ \frac{1}{T}) \tag{6.9}$$

It can be seen from the Figure 6.17 that the Arrhenius Equation is well-coincide formula with effect of temperature on the catalytic activity. There is an exponential-like increase in TOF values according to temperatures. $\frac{-Ea}{R}$ is given by the slope of ln (TOF)-(1/T) graph in Figure 6.18. The relation between the slope and the activation energy is $m = -\frac{Ea}{R}$,so when gas constant multiplied by slope, activation energy is obtained in the unit of (J/mol). Activation energy is calculated as 60.8 ±1.6 kJ/mol for Ru-Ni/AC catalyzed dehydrogenation of ammonia borane reaction. Although this value is lower than some catalysts given in the literature [123,166–169], catalysts with lower activation energy are also present [98,111,126,170,171]. However, it has a higher turnover frequency value compared to carbon supported ruthenium-based catalysts given in literature [107,122,123,125].

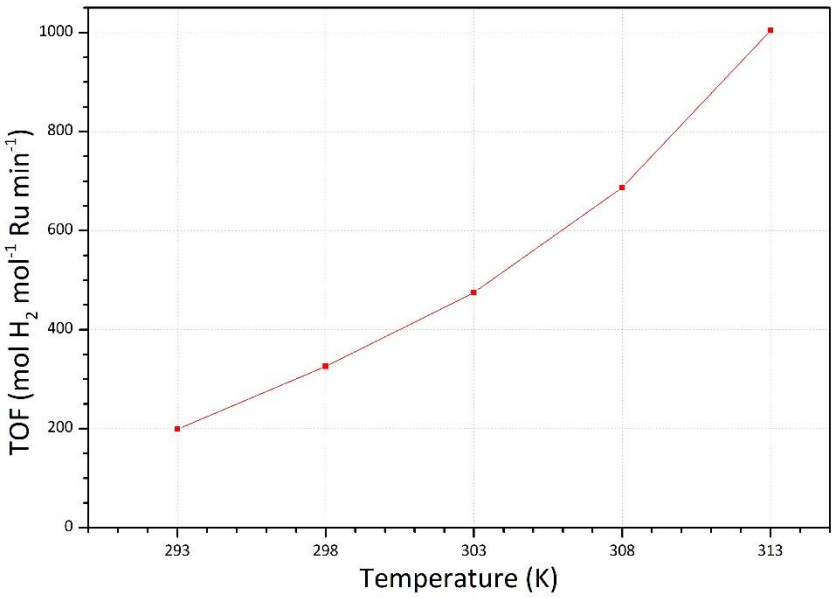

Figure 6.17: TOF value changing according to temperature.

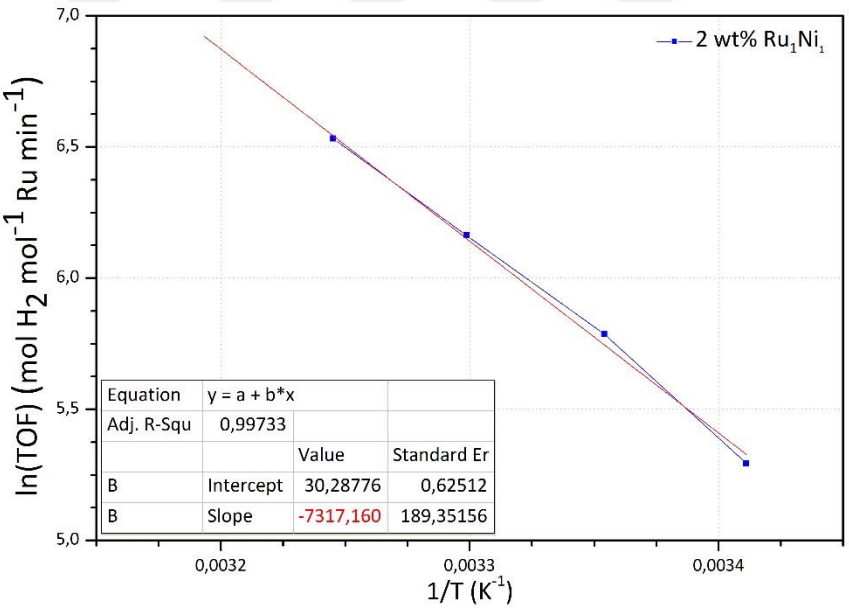

Figure 6.18: Arrhenius plot of 2 wt.% Ru_1Ni_1/AC catalyst.

6.4. Durability Tests

Durability tests were performed to estimate the lifetime of the catalyst. Hydrogen generation rates for four sequence of durability test was given in Figure 6.19. Reducing on the TOF value during the durability test was shown in Figure 6.20, after four test catalyst can save 73% of its first activity. Consequently, even after the fourth trial, it was found to have a higher TOF value than monometallic Ru/AC. This

reduction in hydrogen production rates is related to the change in catalyst structure. Although not completely reliable due to the high noise level in the XPS spectra, almost 50% of Ni leached out from the catalyst while preserving Ru.

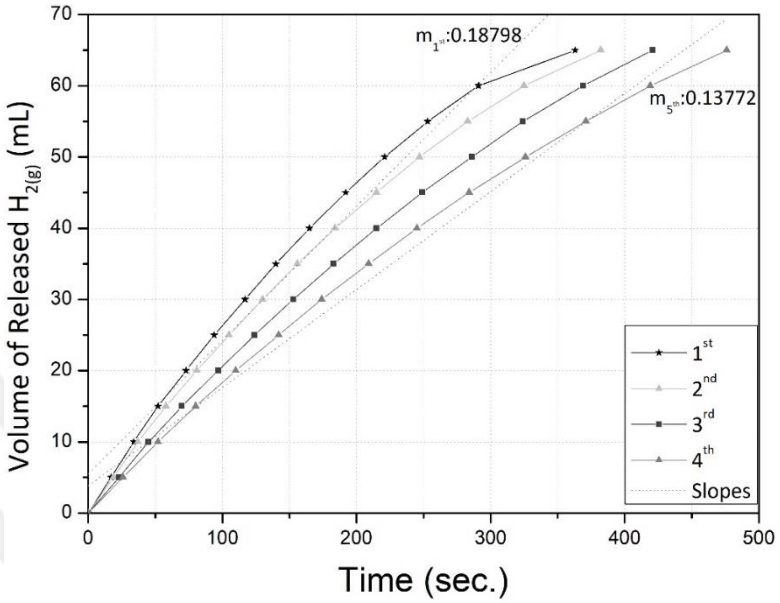

Figure 6.19: Change on the H_2 releasing rate during the durability tests.

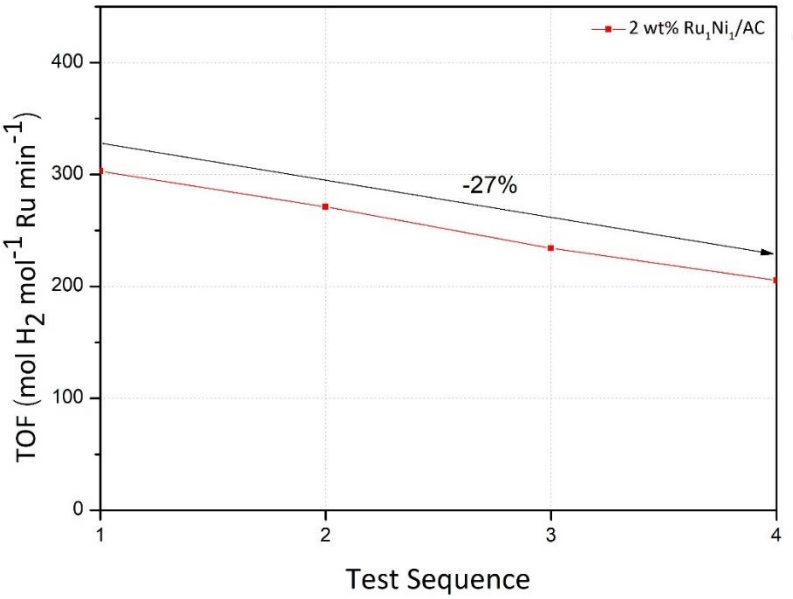

Figure 6.20: Changings on TOF values during the durability test.

6.5. Characterization of Catalysts

Ru_1Ni_1/AC synthesized in DI-water via Route B was determined as the most effective catalyst. This catalyst is characterized in next sections by SEM-EDS, XRD and XPS.

6.5.1. Scanning Electron Microscopy and Energy Dispersive X-Ray Analysis of Catalysts

EDS measurements were done by 4 different samples and 3 different magnification according to conductivity of the samples (Figure 6.14). The intensity scale was kept stable at 85k for each sample to see the intensity change according to NaOH exposure time. Samples got more insulator related with the NaOH exposure time and the peak intensities starts decreasing while conductivity decreasing. To overcome this drawback, EDX measurements observed from different magnifications.

It was obtained from EDX data that for all samples Ru:Ni atomic ratios are same but (metal loading):(total catalyst system) ratios change related to reaction media and washing agent. The peak with the energy of 2.12 keV belongs to Au M radiation and, the source of gold is thin film coating before SEM process to obtain good electronical conductivity on the sample surface. On the other hand, the peak with the energy of 1.739 keV belongs to Si Kα and, it is sourced from the catalyst support material (AC) and the adhesive agent of the carbon tape which is used for SEM imaging, this is the reason not to see significant changes on the Si peaks. It seems like there is a contradiction between the XRD and EDX data, but structure of carbon tape can explain this situation. To illuminate the structure of adhesive carbon tape, the XPS data plot of it is given in 0. According to EDX results, mole ratio of Ru: Ni is almost unity for all RNAC_NN catalysts.

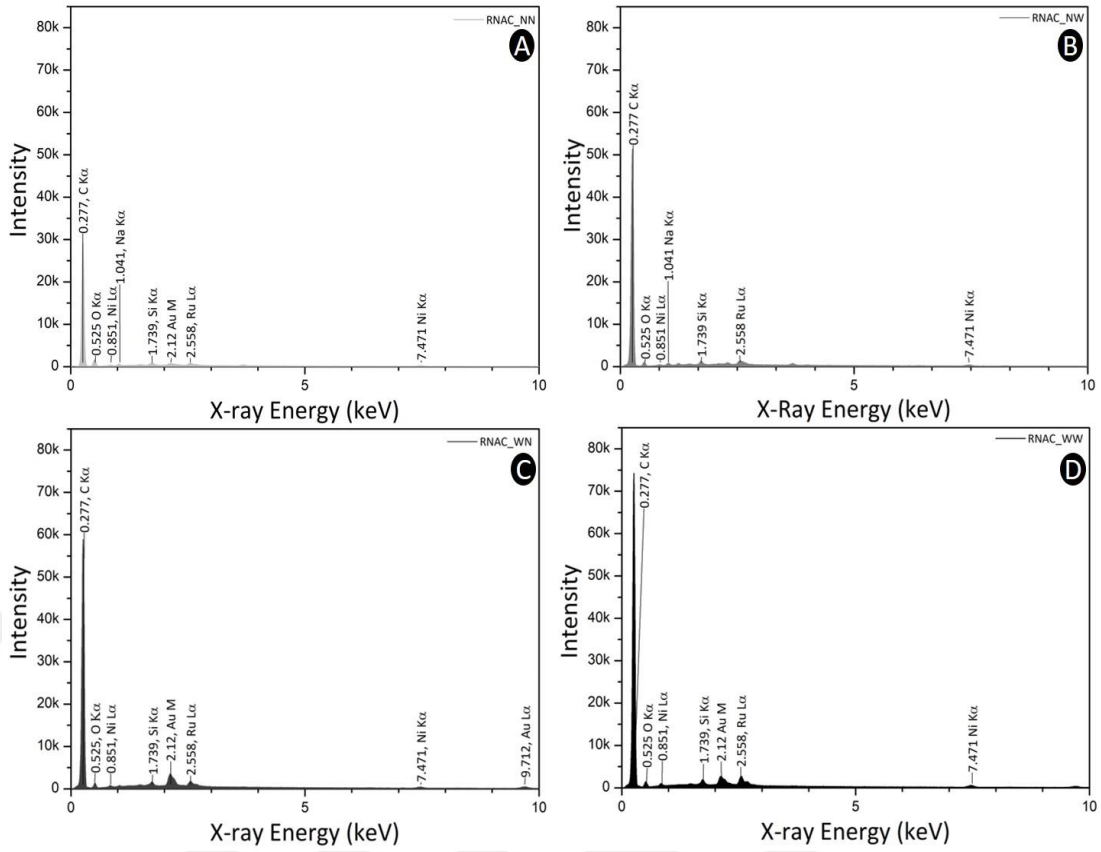

Figure 6.21: EDS measurements of A) RNAC_NN (500X), B) RNAC_NW (1000X), C) RNAC_WN (2000X) and D) RNAC_WW (2000X).

SEM micrographs were taken for the same samples with the EDX, in addition there four micrographs of AC (Figure 6.22) with four different magnifications. It can be seen from the SEM micrographs that there are no differences between the micrographs of AC (Figure 6.22.), and the micrographs of A) RNAC_NN, B) RNAC_NW, C) RNAC_WN, D) RNAC_WW (letters in brackets are corresponding the samples which mentioned in Figure 6.23, Figure 6.24, Figure 6.25 and, Figure 6.26.) The micrographs were given together for all samples and they classified by magnifications to compare them easily. Seeing no differences between the micrographs is due to the porous nature of AC, the metal precursor entered the pores and reduced there. The other possibility for not seeing the metal particles on the support surface is the small particle sizes of metal nanoparticles.

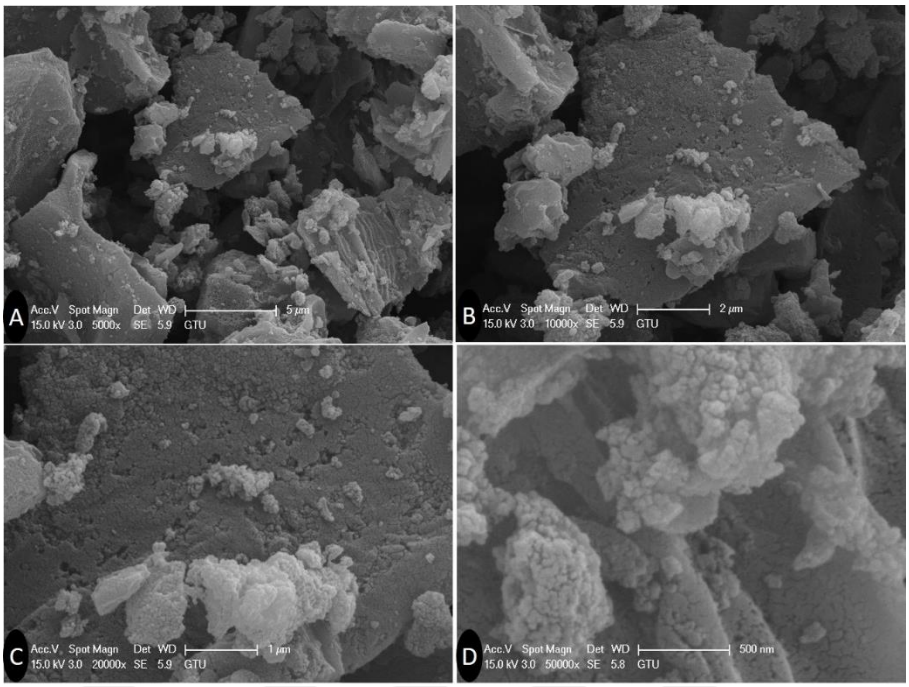

Figure 6.22: SEM micrographs of AC, used in this study, A)5000X, B)10000X, C)20000X and D)50000X magnifications.

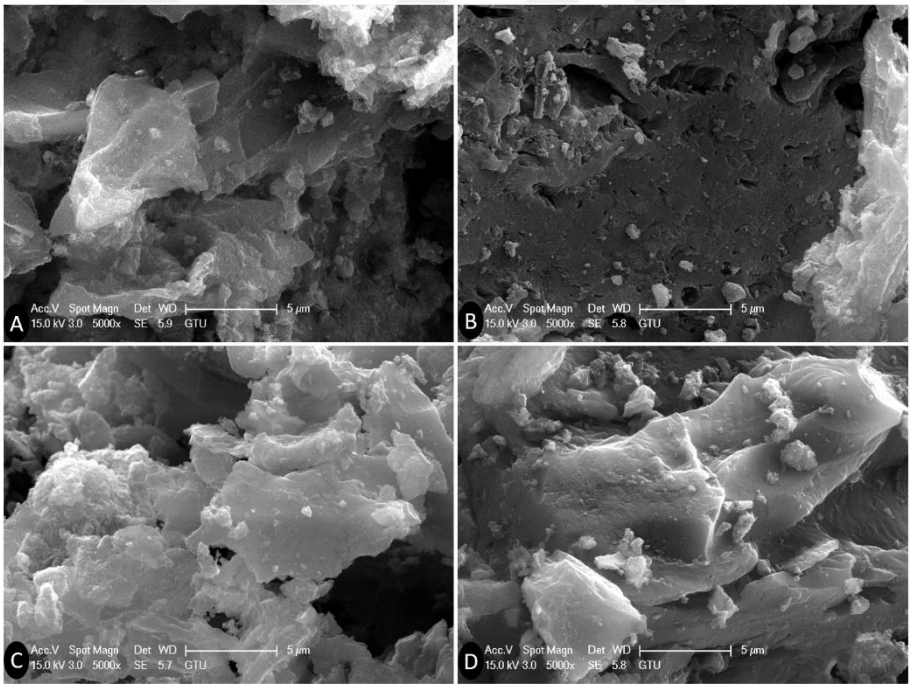

Figure 6.23: 5000X (scale: 5 µm) magnified SEM micrographs of A) RNAC_NN, B) RNAC_NW, C) RNAC_WN and RNAC_WW.

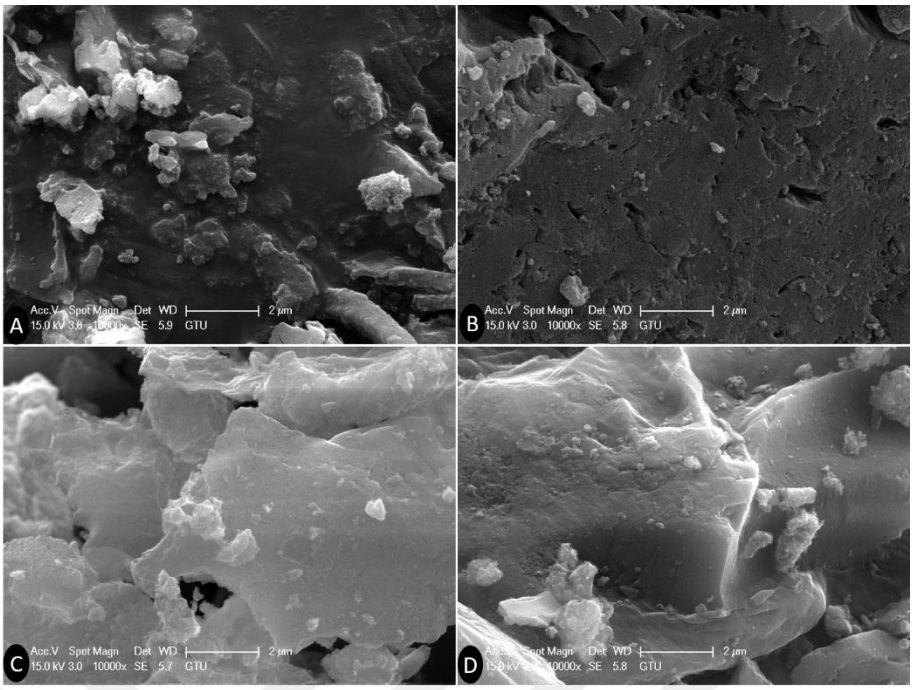

Figure 6.24: 10000X (scale: 2 µm) magnified SEM micrographs of A) RNAC_NN, B) RNAC_NW, C) RNAC_WN and RNAC_WW.

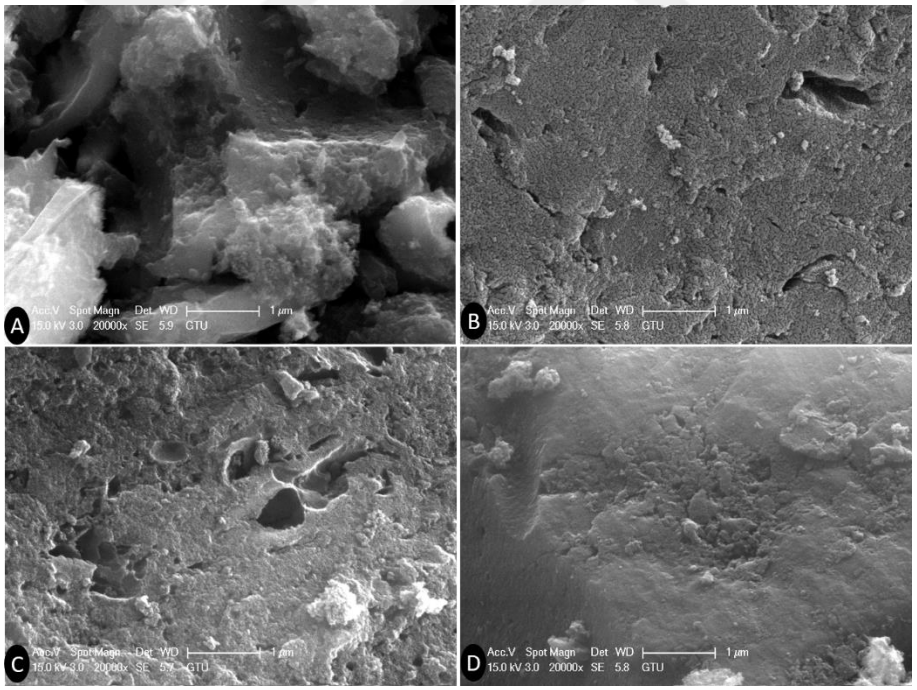

Figure 6.25: 20000X (scale: 1µm) magnified SEM micrographs of A) RNAC_NN, B) RNAC_NW, C) RNAC_WN and D) RNAC_WW.

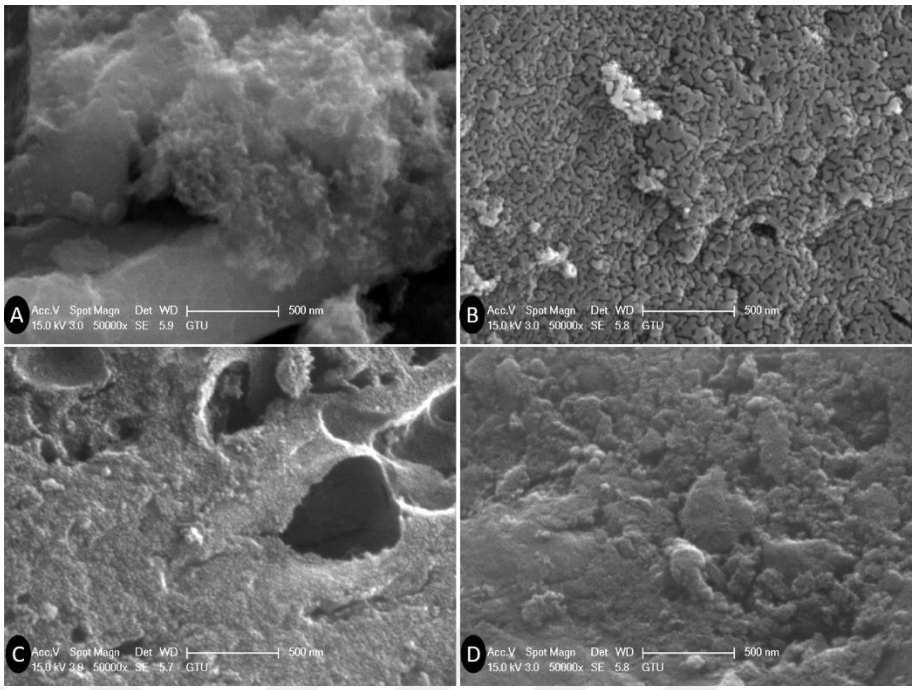

Figure 6.26: 50000X (scale: 500nm) magnified SEM micrographs of A) RNAC_NN, B) RNAC_NW, C) RNAC_WN, and D) RNAC_WW.

The micrograph "A" in Figure 6.26 looks blurrier than the others and this blurriness is also related with the decreasing in conductivity of the material. Even if there is a gold coating on the material surface the inner changes (i.e. conductivity) can cause hardly definable changes.

6.5.2. X-Ray Powder Diffraction Characterization of Catalysts

It can be easily seen from the comparison of x-ray diffraction patterns (Figure 6.27) that the peak around 2Θ=20.8° change dramatically according to pH of the synthesis media which is adjusted by concentration of NaOH (0.1 M NaOH or DI-water), and the washing agent (0.1 M NaOH or DI-water). Additionally, another change is on the peaks about 2Θ=28.2°. Its behavior also changes according to reaction media and washing agent. The peak 2Θ~=20.8° belongs to SiO_2 and there is a portion for silicate under the peak of 2Θ=26.6° (2Θ=26.6° belongs to carbon (003), (004) and, graphite 3R (006) faces).

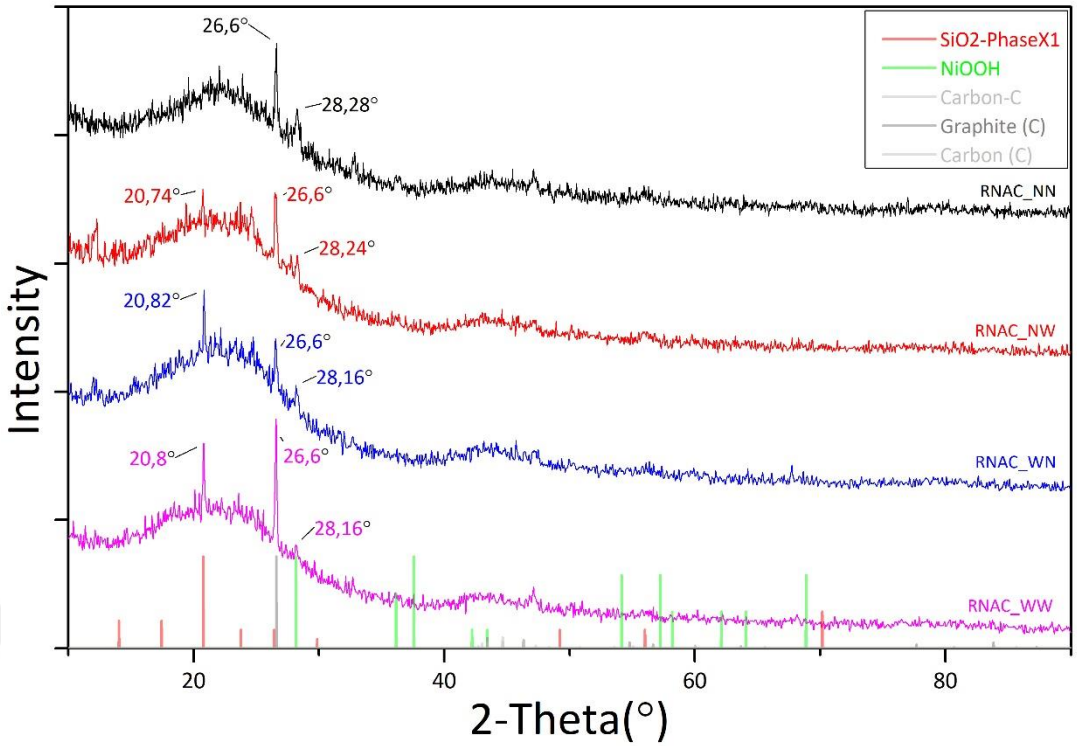

Figure 6.27: The XRD patterns of RNAC_WW, RNAC _WN, RNAC _NW, RNAC _NN (from bottom to top respectively).

NaOH has a reaction with silicate, the reaction was given below (Eq. 6.1):

$$2NaOH + SiO_2 \rightarrow Na_2SiO_3 + H_2O \qquad (6.1)$$

Sodium silicate (Na_2SiO_3) is soluble in water, therefore silicate which exists in AC was transformed to sodium silicate and removed by washing with DI-water. This is the reason for decreasing of the peak intensity of 2Θ~=20.8°. On the other hand, etching of silicate by NaOH, caused a change on the intensity of the peak 2Θ=26.6° (the strongest XRD peak for carbon). The interaction time of NaOH with SiO_2 was about 40 hours for the samples which was synthesized in 0.1 M NaOH solution and about 30 minutes for the samples which washed with 0.1 M NaOH.

The peak at 2Θ=28.2° belongs to NiOOH (111) face, it has lower intensity due to low metal catalyst loading. It was produced even if synthesis media and washing agent is DI-water, because OH^- and H_3O^+ ions exist in DI-water, OH^- bonds can occur by this way. By the increasing of the $[OH^-]$ (by using NaOH) intensity of the NiOOH increased. The formation of NiOOH is sensitive to existence of aqueous NaOH, but the step seems like unimportant. The difference between etching of silicate and

formation of NiOOH is the rate of the reaction. Samples could react with NaOH for 20 minutes during washing procedure, but they have longer time when synthesis media was 0.1 M NaOH. The order of magnitude of the interaction time (t_i) for NaOH and SiO_2 according to samples $t_{RNAC\_WW} < t_{RNAC\_WN} < t_{RNAC\_NW} < t_{RNAC\_NN}$ and, there is a reverse correlation between interaction time and the peak intensity of 2Θ=20.8°. Order of magnitude for the peak intensity according to samples is $I_{RNAC\_WW} > I_{RNAC\_WN} > I_{RNAC\_NW} > I_{RNAC\_NN}$.

From this point it can be claimed that this hydroxyl layer is a thin layer or because of being nanoparticles the surface easily hydroxylated and, the intensity of the peak didn't show any significant change depending to time. The crystal size calculations were obtained from XRD data and by using Scherrer Equation (Eq. 6.2):

$$D = \frac{K\lambda}{\beta * cos\Theta} \tag{6.2}$$

where;

- D: Crystalline size (Å)
- K: 0.9 (Scherrer Constant-unitless)
- λ: 1.5406 (Å)
- β: Full width half maximum (FWHM- radian)
- Θ: Peak angle, two theta (radian)

It can be clearly seen from the analysis of NiOOH that crystallite size of this species is dramatically sensitive to synthesis method/media (Table 6.5).

Table 6.5: XRD Analysis of NiOOH.

Sample	Crystalline Size (Å)	β (radian)	Θ (radian)	λ (Å)	K	d(Å)
RNAC-WW	22.8	0,063	0,246	1.5406	0.9	3,17
RNAC-WN	33	0,043	0,246	1.5406	0.9	3,17
RNAC-NW	42.5	0,034	0,246	1.5406	0.9	3,17
RNAC-NN	39.7	0,036	0,246	1.5406	0.9	3,16

The analysis on plane separation of silicate d-spacing in Table 6.6 showed that the lattice parameters of samples got widener during etching process. The plane separation parameters (d) were calculated by the Bragg's Law (Eq. 6.3).

$$n\lambda = 2d\ x\ sin\Theta \tag{6.3}$$

Table 6.6: XRD Analysis of SiO_2.

Sample	Θ(radian)	λ (Å)	d(Å)
RNAC-WW	0,363	1.5406	2,169
RNAC-WN	0,363	1.5406	2,167
RNAC-NW	0,361	1.5406	2,175

On the other hand, neither peak shift nor widening, only decreasing on the intensity occurred for carbon peak. The decreasing of carbon peak can be related with the etching and removing of silicate, due to peak overlapping of SiO_2 and carbon at ~26.6°. There is no peak observable for any species of ruthenium and any species of nickel out of NiOOH for XRD. It is guessed and hoped that other species behave like NiOOH. By this way catalytic activities of the prepared samples can get related with their crystalline sizes. If the particle size is bigger than the crystal size and enough big to harbor more than one crystal, the density of grain boundaries will increase. Since the catalytic activity is related with the surface free energy and the auxiliary sources of SFE are surface defects/ discontinuities (i.e. grain boundaries, dislocations, edges, sides), increasing the density of the grain boundaries on the surface would also increase the SFE. As long as the energy of the grain boundaries is sufficient to

allow the desorption of the (by)products of the catalytic reactions, increasing the density of grain boundaries at the surface will increase the catalytic activity[159,160].

The calculations on the size had done from XRD data due to lack of TEM measurement and the device does not work at least for 1 year. Because of this crystalline size of NiOOH was calculated from the XRD data instead of TEM.

6.5.3. Material Characterization by X-Ray Photoelectron Spectroscopy

XPS spectra of fresh and spent Ru_1Ni_1/AC, most active nanocatalyst synthesized in this study by Route B, given below and, they named as RNAC_WW_fresh and RNAC_WW_spent respectively. The spectra were shifted for -0.512 eV for RNAC_WW_fresh sample and, -0.514 eV for RNAC_WW_spent sample according to fermi edge fitting.

XPS fitting procedure for ruthenium was fulfilled on Ru_{3p} peaks instead of Ru_{3d} due to the C_{1s} and Ru_{3d} overlapping. Two peaks, which has the energy of 462.6 and 465.2 eV which are assigned to Ru^0 and RuO_x/Ru respectively were obtained from Ru_{3p} region of RNAC_WW_fresh sample (Figure 6.29). For nickel, three main peaks were observed with binding energies of 854.8 eV, 855.7 eV, 856.9 eV which belongs to Ni^0, NiO, NiOOH [161–165] respectively and, 861.7 eV belongs to satellite peak (Figure 6.28). Ni_{2p} window shifted to higher binding energy values for 1 eV and, 0.4 eV positive shift is observed for Ru_{3p} window [166,167]. This shift can prove the interaction between Ru, Ni and C. To investigate the total interaction between the species the XPS data of Ru, Ni, C and O must be delicately analyzed. Due to overlapping of Ru_{3d} and C_{1s} spectra, carbon bonds should be investigated via an auxiliary characterization technique.

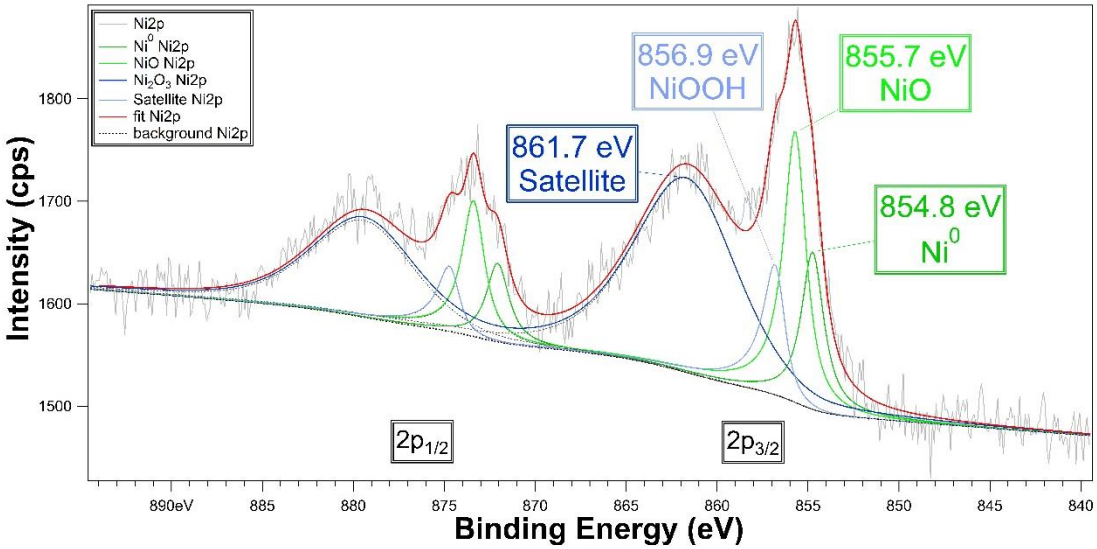

Figure 6.28: X-ray photoelectron spectra of Ni_{2p} in RNAC_WW_fresh sample.

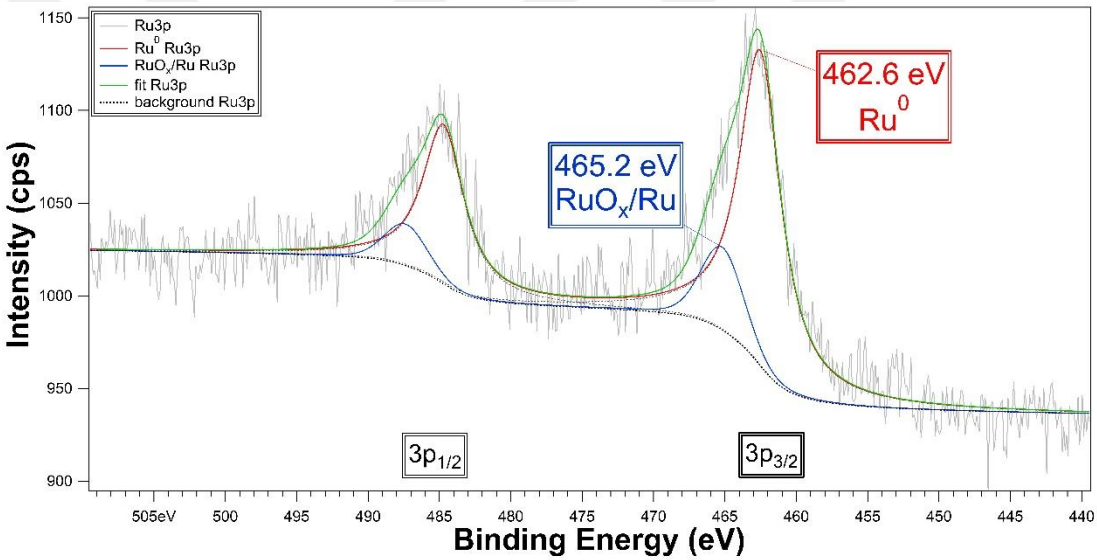

Figure 6.29: X-ray photoelectron spectra of Ru_{3p} in RNAC_WW_fresh sample.

It is estimated that NiOOH formation occurs due to the combination of ionic nature of the water (OH^-, H_3O^+), and the dissolved oxygen in the water. Existence of dissolved oxygen during the reduction and particle growth may cause oxidation of Ni particles. This may be a reason why oxidized ruthenium was seen in XPS and XRD. Ruthenium needs a relatively high temperature and, partial oxygen pressure to get oxidized, but in the case of the synthesis method used in this study, the presence of dissolved oxygen in the water during the reduction causes the oxidizing agent and metal to meet when metal particles have metastable particle sizes. The aging process is used to produce $Ni(OH)_2$ at room temperature and they formed from Ni

nanoparticles by waiting in DI-water for a determined amount of time [168]. The formation reaction of NiOOH from $Ni(OH)_2$ was given below.

$$2Ni(OH)_2 + NaClO \rightarrow 2NiOOH + NaCl + H_2O \quad (6.4)$$

When it is divided to two part (partial anode and partial cathode), the reaction can be described as

$$2Ni(OH)_2 + 2(OH^-) \rightarrow 2NiOOH + 2e^- + 2H_2O \quad (6.5)$$

$$NaClO_4 + H_2O + 2e^- \rightarrow NaCl + 2OH^- \quad (6.6)$$

In this case, AC can behave like a ClO^- source instead of $NaClO_4$. By the help of ionic nature of the water NiOOH formation could occur without any OH^- source addition. AC, especially in granulized form (GAC), used as filtration material to remove chloride ions and the other unwanted species from water[169]. Chloride ions, originated from metal precursors, are able to get adsorbed to the carbon surface. These are the reasons to formation of NiOOH.

According to the calculations obtained from the XPS data of the as-prepared (fresh) and tested (spent) Ru_1-Ni_1/AC the stoichiometric ratio of the Ru:Ni observed by given formula:

$$\frac{\left[\frac{I_{Ru}}{ASF_{Ru}}\right]}{\left[\left(\frac{I_{Ru}}{ASF_{Ru}}\right)+\left(\frac{I_{Ni}}{ASF_{Ni}}\right)\right]} \quad (6.7)$$

- I: Peak intensity (area-obtained from the XPS fitting)
- ASF: Atomic sensitivity factor (RSF: Relative sensitivity factor -in some reference guides-)

The results were summarized in the Table 6.7.

Table 6.7: XPS fitting results of $Ru_{3p\ 3/2}$ and $Ni_{2p\ 3/2}$ for RNAC_WW_fresh and RNAC_WW_tested samples.

Sample	$I_{Ru(3p\ 3/2)}$	$I_{Ni(2p\ 3/2)}$	$ASF_{Ru(3p\ 3/2)}$	$ASF_{Ni(2p\ 3/2)}$	Ru:(Ru+Ni)
$RNAC_{fresh}$	1093.66	2859.84	1.3	3.0	0.469
$RNAC_{spent}$	1117.34	1216.87	1.3	3.0	0.679

The ASF is not a required parameter to calculate the RuO_x/Ru ratio, because the results will be obtained from the intensity for same element. The calculated results were presented in Table 6.8.

Table 6.8: $Ru_{3p\ 3/2}$ fitting results for RNAC_WW_fresh and RNAC_WW_spent samples and changing on [Ru^0/(Ru^0+RuO_x)] ratio.

Sample	$I_{Ru(3p\ 3/2)}$	$I_{RuOx(3p\ 3/2)}$	$Ru/(Ru+RuO_x)$
$RNAC_{fresh}$	909.57	184.09	0.832
$RNAC_{spent}$	974.15	143.19	0.872

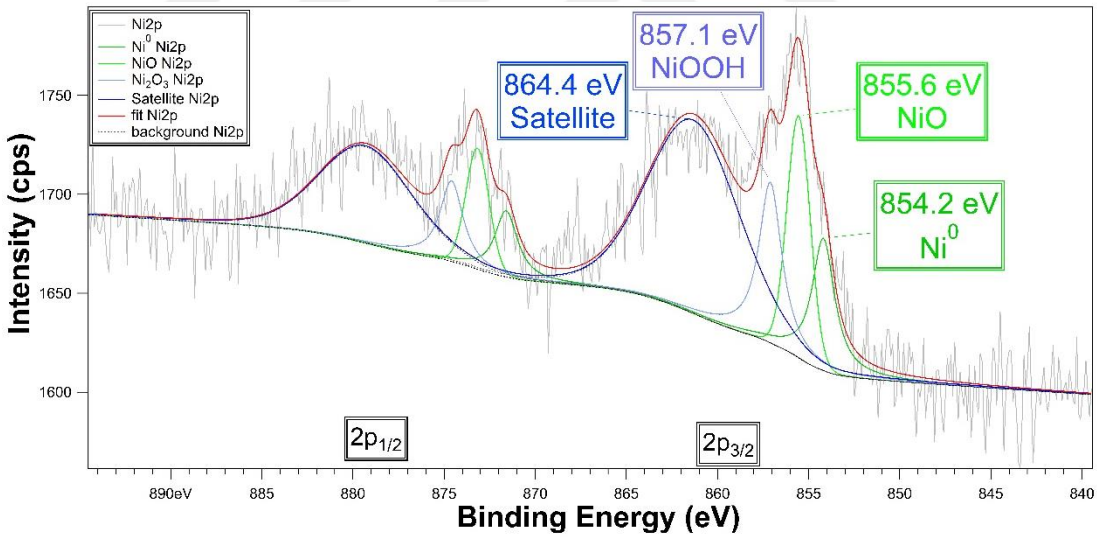

Figure 6.30: X-ray photoelectron spectra of Ni_{2p} in RNAC_WW_spent sample.

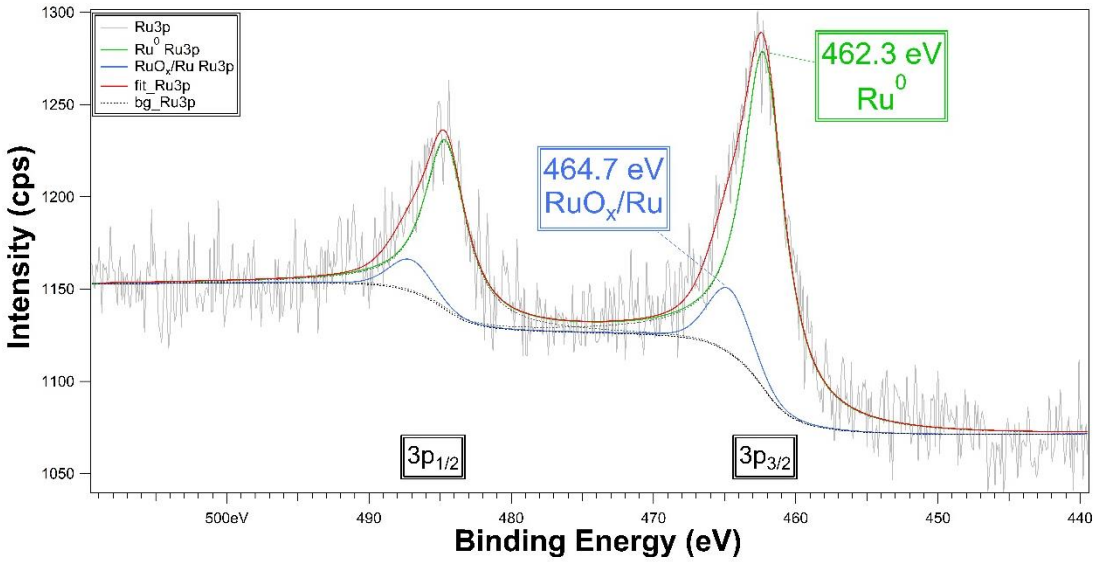

Figure 6.31: X-ray photoelectron spectra of Ru_{3p} in RNAC_WW_spent sample.

As it can be seen from the results of the calculations, after first test, different amounts of ruthenium and nickel removed from the catalyst system. It may be observed from the differences between the data of fresh and tested catalysts about 57% of nickel got lost and, it is hard to say that there is a core-shell structure for the metals or, even if there is a core-shell structure, it's not a preferable Ni: core/ Ru: shell structure. This can be an evidence for being a synergetic effect between Ru and Ni. The activity was reduced more than the separated contributions of the lost materials. On the other hand, there is no significant change for the Ru_{3p} but there are some little changes, which may be originated from the changes on the Ni-based species.

By analyzing the XPS data for RNAC_WW_spent catalyst 462.3 eV and 464.7 eV binding energies observed, which assigned to Ru^0 and RuO_x/Ru respectively with little shift. Ni^0, NiO, NiOOH species also observed after first test with the binding energies of 854.2 eV, 855.6 eV and, 857.1 eV respectively.

7. CONCLUSION

Synthesis and characterization of highly active, ruthenium-based bimetallic nanocatalysts for dehydrogenation of ammonia borane were mainly aimed within this study. In addition to this aim, the synthesis of ammonia borane and optimization of working conditions of the catalyst also studied.

Generating energy in an environmentally friendly way is one of the most important issues of our modern societies. Hydrogen is one of the best candidates as an energy carrier by using in fuel cells. Hydrogen has storage and transportation problems. Even if it can be stored in high-pressure vessels, they are not safe for mobile applications and not mass and volume-effective. Among hydrogen storage materials ammonia borane has higher mass effective storage capacity (19.6 wt.%), environmentally benignity, stability in ambient conditions.

Noble metals are frequently used as heterogeneous catalysts for dehydrogenation of ammonia borane, they have higher activity than non-noble-transition metals however their high prices are a drawback for the usage of them. The main idea of the catalyst technologies to produce cost-effective catalysts by either using non-noble transition metals or improving the catalytic activities of the noble-metal-based catalysts in different ways. Catalyst science tries to illuminate the mechanisms of catalytic reactions, parameters that affect the catalytic activity and controlling the parameters.

Monometallic and multi-metallic catalyst systems are investigated to improve the activities. Examples for monometallic and multi-metallic systems were listed under Title3.3.5 in Table 3.1 and Table 3.2. They supported on different supports.

In this case, thirteen different materials used as support materials and tested. The most effective ones among them are carbon black, titania, AC respectively. The reason to choose AC was the combination of low price, easy attainability, modifiable surface properties and rare usage in academic researches.

The TOF values for $RuNi_4$ catalysts which supported on different materials were given in the Table 7.1. Those catalysts were synthesized by following Route C.

Table 7.1: TOF values of $RuNi_4$ supported on different materials.

Support Material	TOF
Alumina-Silicate	53
Silicate	87
Hematite	45
MCM48	68
Activated Carbon	128
Carbon Black	197
Zirconia	45
Alumina	90
Titania	133
MWCNT	76
CNF	74

Two types of AC were tested after choosing it as a support material. Surface and intrinsic properties of AC is highly dependent on the raw materials, activation agents, post-activation treatments. The ACs tested within this study were used without any post-treatment out of separation of hydrophobic parts of AC by filtration. The Table 7.2 gives the TOF values according to different AC types.

Table 7.2: TOF values of $RuNi_4$ supported on different ACs.

Carbon Type	TOF
Alfa Aesar (Treated)	97
Alfa Aesar (Untreated)	186
Sigma Aldrich (Untreated)	124

Here the treated AC was boiled in NH_3 before synthesis to add new radical groups on the surface to get a totally hydrophilic surface. However, untreated, only acetone-washed AC supported catalysts showed the best catalytic activity among them.

Four different synthesis method used to synthesize Ru_1Ni_1/AC catalysts and the most effective one found as Route B. TOF values according to synthesis methods were discussed in section 6.1.6. Route B offers more time for the adsorption of the metal

ions to the surface of the support, when the supported precursor was redistributed in 10-15 mL of water for the reduction reaction, byproducts was randomly distributed in the suspension and they can be easily removed from the system by washing. In contrast with Route B, supported catalyst precursor meet much more concentrated reducing agent solution and this affects the particle size.

Ru_1Ni_1/AC had the highest catalytic activity among the other twelve catalysts and, 2 wt.% loaded one synthesized and tested afterward, reached the highest TOF value among all other loadings. Changing in the activity due to the stoichiometry means that there is a synergetic effect between Ru and Ni. Seeing this synergy was one of the (by)wishes of this study.

It was seen that reduction reaction solvent is also important. Methanol, ethanol, DI-water and N_2-purged DI-water was chosen as solvents to see their effects. The effects of the solvents can be shown in Table 7.3.

Table 7.3: Changes on TOF value by changing the solvents.

Solvent	**TOF**
DI-Water	255
N_2-purged DI-water	267
Ethanol	170
Methanol	136

The Ru_1Ni_1/AC catalyst synthesized in N_2-purged DI-water showed the highest catalytic activity among the others. This activity change is originated from oxidation of Ni and Ru via dissolved oxygen in water, it was inhibited by purging the water, on the other hand, the byproduct of the $NaBH_4$ dehydrogenation and metal-ion reduction reaction $NaBO_2$ (sodium metaborate) is insoluble in ethanol because of this an amount of $NaBO_2$ couldn't remove from the surface and the same reason is valid for methanol as well.

After completion of determining the parameters of the catalyst, (support, stoichiometry, loading, solvent, synthesis method), optimization tests performed on Ru:AB ratio and Ru molarity. Six different ratios were tested and 0.002 Ru:AB ratio was found as the most active ratio and 0.5 mM Ru had the highest activity.

DI-water was the best washing agent and basic reduction reaction media cause decreasing in the catalytic activity. The Best combination for reaction media/washing agent was DI-water/ DI-water doublet. pH of the reaction media was adjusted to basic region by NaOH and the effect of NaOH usage was seen on the XRD pattern. The effect was decreasing of the peak intensity which belongs to silicate and increasing on the NiOOH peak.

The formation of NiOOH was seen both characterization methods of XRD and XPS. There was high noise level on XPS measurements, notwithstanding NiOOH, Ru/RuO_x compounds detected from fitting procedures. XPS measurements were performed for RNAC_WW fresh and tested samples and it was seen that an amount of Ni was removed from the catalyst during the test, in addition there wasn't seen any loss of ruthenium, but an increasement on the amount of metallic ruthenium, and decreasing on oxide phase was observed. This means that Ru works in metallic form during the catalysis process, then its surface oxidized-back due to the dissolved oxygen in reaction media.

Very small crystalline sizes were obtained from the XRD calculations on NiOOH pattern and an exponential-like relation was seen between the crystalline size and the TOF. It is well-known that grain boundaries contribute to excess surface free energy which has a big role on catalysis. Small crystalline sizes have a good impact on the activity.

SEM micrographs show no differences due to two main possibility. One is very small particle sizes and the other one can be reduction of the particles in the pores.

As a future work this study should be improved by supporting with TEM images and impact of density of the grain boundaries can be investigated by this way. Addition to TEM images, ICP-MS measurements can give the effectiveness of the synthesis methods.

REFERENCES

[1] Erias A., Karaka C., Corinna G., James C., Mekalia P., Jantunen P., Prajwal B., Samal B., Valenzuela J.M., World Energy Resources 2016, 2016.

[2] Breinbauer A., Plaku G., (2008), "Introduction", Donauraum, 48 (3), 199–204.

[3] Weiß M., Witzenberger B., Grafiken-Wie sehr Fliegen dem Klima schadet-Wissen-Süddeutsche.de > Grafiken-Wie sehr Fliegen dem Klima schadet Wie sehr Fliegen dem Klima schadet, 2017.

[4] BP, Statistical Review of World Energy: Electricity, 2019. https://www.bp.com/en/global/corporate/energy-economics/statistical-review-of-world-energy/electricity.html.

[5] BP Energy Economics, 2018 Energy Outlook, 2018.

[6] Canadell P., Sharifi A., Carbon Budget 2018, 2018. https://www.globalcarbonproject.org/carbonbudget/.

[7] Carbon dioxide information analysis center, (2015), "Fossil-Fuel CO2 Emissions", 13/04/2015,. http://cdiac.ornl.gov/trends/emis/meth_reg.html (erişim 04 Ocak 2019).

[8] Gomes G.L., (2018), "Elements in the atomism theory, according to Aristotle", HYPNOS, (41), 146–165.

[9] "Aristotle-The Greek Elements",. http://chemed.chem.purdue.edu/genchem/history/aristotle.html (erişim 04 Ocak 2019).

[10] Bennaceur K., Clark B., Orr F.M., Ramakrishnan T.S., Roulet C., Stout E., Hydrogen: A future energy carrier?, in: Oilfield Review, 2005, 30–41.

[11] Web 1, (2019), Chastain B., "Jan Baptista van Helmont | Belgian scientist | Britannica.com",. https://www.britannica.com/biography/Jan-Baptista-van-Helmont (erişim 04 Ocak 2019).

[12] Banchetti-Robino M.P., (2016), "Van Helmont's hybrid ontology and its influence on the chemical interpretation of spirit and ferment", Foundations of Chemistry, 18 (2), 103–112.

[13] Clericuzio A., (1993), "From van helmont to boyle. A study of the transmission of Helmontian chemical and medical theories in seventeenth-century

England", The British Journal for the History of Science, 26 (3), 303–334.

[14] Web 2, (2019), "The history of hydrogen | Linde",. https://whyhydrogen.linde.com/basics/the-history-of-hydrogen/ (erişim 06 Ocak 2019).

[15] Web 3, (2019), Tez Z., (2015), "Çağdaş kimyanın babası: Antoine Laurent Lavoisier | Bilim ve Gelecek", Bilim ve Gelecek,. https://bilimvegelecek.com.tr/index.php/2015/03/01/cagdas-kimyanin-babasi-antoine-laurent-lavoisier/ (erişim 04 Ocak 2019).

[16] Noyes W.A., (1895), "A Short History of Chemistry", Science, 1 (17), 469.

[17] Janek J., (2019), "The Birth of the Rational Chemical Nomenclature", Chemicke Listy, 113 (7), 438–440.

[18] Klein U., (2015), "A Revolution that never happened", Studies in History and Philosophy of Science, 49, 80–90.

[19] Lehman C., (2016), "Searching for the nature of the diamond : Guyton de Morveau, the successor of Macquer and Lavoisier", Annales Historiques de la Revolution Francaise, (383), 81+.

[20] Branca M., Dichiarante V., Esterhuysen C., Szell P.M.J., (2017), "Highlights from the Faraday Discussion: Halogen Bonding in Supramolecular and Solid State Chemistry", Chemical Communications, 53 (85), 11615–11621.

[21] Fleckner U., (2014), "Respiration and Inspiration. Jacques-Louis Davids Effigy of the Chemist Antoine-Laurent Lavoisier and his Wife Marie-Anne", Zeitschrift fur Kunstgeschichte, 77 (4), 545–564.

[22] Web 4, (2019), Crosland M.P., "Louis Bernard Guyton de Morveau | French chemist and educator | Britannica.com",. https://www.britannica.com/biography/Louis-Bernard-Guyton-de-Morveau (erişim 04 Ocak 2019).

[23] Rodolphe T., Delaveau P., Méthode de nomenclature chimique, 2006.

[24] Web 5, (2019), "William Nicholson | English chemist and inventor | Britannica.com",. https://www.britannica.com/biography/William-Nicholson-English-chemist-and-inventor (erişim 07 Ocak 2019).

[25] Cole R.J., (1952), "Sir Anthony Carlisle, F.R.S. (1768–1840)", Annals of Science, 8 (3), 255–270.

[26] Web 6, (2009), Jonas J., "The history of hydrogen | AltEnergyMag",. https://www.altenergymag.com/article/2009/04/the-history-of-

hydrogen/555/ (erişim 07 Ocak 2019).

[27] (1949), "J. W. Dobereiner (1780–1849)", Nature, 163 (4142), 434–435.

[28] Williams W.D., (1999), "Döbereiner's Hydrogen Lighter", Bulletin for the History of Chemistry, 24, 66–68.

[29] Appleby A.J., (1990), "From Sir William Grove to today: fuel cells and the future", Journal of Power Sources, 29 (1–2), 3–11.

[30] Grove W.R., (1839), " XXIV. On voltaic series and the combination of gases by platinum ", The London, Edinburgh, and Dublin Philosophical Magazine and Journal of Science, 14 (86–87), 127–130.

[31] Web 7, (2019), Usselman M.C., "William Hyde Wollaston | British scientist | Britannica.com",. https://www.britannica.com/biography/William-Hyde-Wollaston (erişim 14 Ocak 2019).

[32] Wisniak J., (2013), "Thomas Graham. I. Contributions to thermodynamics, chemistry, and the occlusion of gases", Educacion Quimica, 24 (3), 316–325.

[33] Web 8, (2019), "Thomas Graham | Scottish chemist | Britannica.com",. https://www.britannica.com/biography/Thomas-Graham (erişim 17 Ocak 2019).

[34] Verne J., L'ile Mystériouse II, 5th ed., Ithaki, 1874.

[35] Web 9, (2019), Evans A.B., "Jules Verne | Biography & Facts | Britannica.com",. https://www.britannica.com/biography/Jules-Verne (erişim 27 Ocak 2019).

[36] Web 10, (2019), "Sir James Dewar | British scientist | Britannica.com",. https://www.britannica.com/biography/James-Dewar (erişim 17 Ocak 2019).

[37] Rowlinson J.S., James Dewar and His Route to the Liquefaction of Hydrogen, in: K. Gavroglu (Ed.), History of Artificial Cold, Scientific, Technological and Cultural Issues, 2014, 53–64.

[38] Web 11, (2019), "History of thermos",. https://www.thermos.com/history (erişim 17 Ocak 2019).

[39] Web 12, (2017), "Fritz Haber | Science History Institute", Sci. Hist.,. https://www.sciencehistory.org/historical-profile/fritz-haber (erişim 17 Ocak 2019).

[40] Web 13, (2019), Jensen W.B., "Fritz Haber | Biography & Facts | Britannica.com",. https://www.britannica.com/biography/Fritz-Haber (erişim

17 Ocak 2019).

[41] Web 14, (2019), The Nobel Foundation, (1966), "Fritz Haber - Biographical",. https://www.nobelprize.org/prizes/chemistry/1918/haber/biographical/ (erişim 17 Ocak 2019).

[42] Web 15, (2019), Tufan T., "Haber: Milyonları doyurdu, milyonları öldürdü - Tarkan Tufan",. https://www.gazeteduvar.com.tr/dunya-forum/2018/04/15/dunya-forum-fritz-haber-milyonlari-doyurdu-milyonlari-oldurdu/ (erişim 17 Ocak 2019).

[43] Web 16, (2019), Altaras D., "1918 Nobel Kimya Ödülü sahibi Fritz Haber'in öteki öyküsü | Şalom Gazetesi",. http://www.salom.com.tr/arsiv/haber-105807-1918_nobel_kimya_odulu_sahibi_fritz_haberin_oteki_oykusu.html (erişim 17 Ocak 2019).

[44] Rohrbach-Lochner F., von Borstel G., (2019), "Fritz and Clara Haber: united in peace - divided in war. Instruction for Multi-Perspective, Interdisciplinary Lessons About an Outstanding Couple of Chemists at the Beginning of the 20th Century", CHEMKON, 26 (7), 301–306.

[45] Schummer J., (2018), "Ethics of Chemical Weapons Research: Poison Gas in World War One", HYLE, 24 (1, SI), 5–28.

[46] McCracken G., Stott P., (2013), "The Hydrogen Bomb", Fusion, 59–66.

[47] Web 17, (2014), Veziroglu T.N., "Welcome to the International Association for Hydrogen Energy", Int. Assoc. Hydrog. Energy,. http://www.iahe.org/history.asp (erişim 18 Ocak 2019).

[48] Web 18, (2015), Hidrojen Teknolojileri Derneği Kuruldu, 2015. www.uhtek2015.org (erişim 18 Ocak 2019).

[49] Anonymous, Our changing planet, in: Eos, Transactions American Geophysical Union, Prentice-Hall, 1989, 50.

[50] Nikolaidis P., Poullikkas A., (2017), "A comparative overview of hydrogen production processes", Renewable and Sustainable Energy Reviews, 67, 597–611.

[51] Ersöz A., (2008), "Investigation of hydrocarbon reforming processes for micro-cogeneration systems", International Journal of Hydrogen Energy, 33 (23), 7084–7094.

[52] Katheria S., Deo G., Kunzru D., (2019), "Rh-Ni/$MgAl_2O_4$ catalyst for steam reforming of methane: Effect of Rh doping, calcination temperature and its application on metal monoliths", Applied Catalysis A: General, 570 (August

2018), 308–318.

[53] Gac W., Greluk M., Słowik G., Millot Y., Valentin L., et al., (2018), "Effects of dealumination on the performance of Ni-containing BEA catalysts in bioethanol steam reforming", Applied Catalysis B: Environmental, 237 (February), 94–109.

[54] Arslan Bozdag A., Deniz Kaynar A.D., Dogu T., Sezgi N.A., (2019), "Development of ceria and tungsten promoted nickel/alumina catalysts for steam reforming of diesel", Chemical Engineering Journal, 377, 1–10.

[55] Balthasar W., (1984), "Hydrogen production and technology: today, tomorrow and beyond", International Journal of Hydrogen Energy, 9 (8), 649–668.

[56] Kim Y., Kim Y., Yeo S., Kim K., Jung-Eun Koh K., Seo J. E., Shin S. J., Choi D. K. Yoon C. W., Nam S. W., (2013), "Development of a continuous hydrogen generator fueled by ammonia borane for portable fuel cell applications", Journal of Power Sources, 229, 170–178.

[57] Web 19, (2014), Shiklomanov I., "How much water is there on Earth, from the USGS Water Science School", USGS Water Sci. Sch., 1. https://water.usgs.gov/edu/earthhowmuch.html%0Ahttps://water.usgs.gov/edu/earthhowmuch.html%0Ahttp://water.usgs.gov/edu/earthhowmuch.html (erişim 03 Şubat 2019).

[58] Sherif S.A., Barbir F., Veziroglu T.N., (2003), "Principles of hydrogen energy production, storage and utilization", Journal of Scientific and Industrial Research, 62 (1), 46–63.

[59] Acar C., Dincer I., (2014), "Comparative assessment of hydrogen production methods from renewable and non-renewable sources", International Journal of Hydrogen Energy, 39 (1), 1–12.

[60] Habibollahzade A., Gholamian E., Behzadi A., (2019), "Multi-objective optimization and comparative performance analysis of hybrid biomass-based solid oxide fuel cell/solid oxide electrolyzer cell/gas turbine using different gasification agents", Applied Energy, 233–234 (September 2018), 985–1002.

[61] International Energy Agency, (2006), "Hydrogen Production and Storage. R&D Priorities and Gaps", Hydrogen Implementing Agreement, 13, 392–392.

[62] Dincer I., Acar C., (2017), "Innovation in hydrogen production", International Journal of Hydrogen Energy, 42 (22), 14843–14864.

[63] Conte M., Di Mario F., Iacobazzi A., Mattucci A., Moreno A., Ronchetti M., (2009), "Hydrogen as future energy carrier: The ENEA point of view on technology and application prospects", Energies, 2 (1), 150–179.

[64] Ahmed M., Dincer I., (2019), "A review on photoelectrochemical hydrogen production systems: Challenges and future directions", International Journal of Hydrogen Energy, 44 (5), 2474–2507.

[65] Nasir Uddin M., Daud W.M.A.W., Abbas H.F., (2013), "Potential hydrogen and non-condensable gases production from biomass pyrolysis: Insights into the process variables", Renewable and Sustainable Energy Reviews, 27, 204–224.

[66] Hallenbeck P.C., (2004), "Fundamentals and limiting processes of biological hydrogen production", Biohydrogen III: Renewable Energy System by Biological Solar Energy Conversion, 27, 1185–1193.

[67] Das D., Veziroğlu T.N., (2001), "Hydrogen production by biological processes: A survey of literature", International Journal of Hydrogen Energy, 26 (1), 13–28.

[68] Pugazhendhi A., Shobana S., Nguyen D.D., Banu J.R., Sivagurunathan P., Chang S. W., Ponnusamy V.K., Kumar G., (2019), "Application of nanotechnology (nanoparticles) in dark fermentative hydrogen production", International Journal of Hydrogen Energy, 44 (3), 1431–1440.

[69] Nagarajan D., Lee D.J., Kondo A., Chang J.S., (2017), "Recent insights into biohydrogen production by microalgae – From biophotolysis to dark fermentation", Bioresource Technology, 227, 373–387.

[70] Maddock B.D., Hydrogen as Future Energy Carrier, in: Green Energy and Technology, 2011, 33–70.

[71] Web 20, (2016), H2tools, "Hydrogen Pipelines | Hydrogen Tools",. https://h2tools.org/hyarc/hydrogen-data/hydrogen-pipelines (erişim 23 Şubat 2019).

[72] Adolf J., Balzer H.C., Louis J., Schabla U., Fischedick M., Arnold K., Energy of the Future? Sustainable Mobility through Fuel Cells and H2, Hamburg, 2017.

[73] Barthelemy H., Weber M., Barbier F., (2017), "Hydrogen storage: Recent improvements and industrial perspectives", International Journal of Hydrogen Energy, 42 (11), 7254–7262.

[74] Niaz S., Manzoor T., Pandith A.H., (2015), "Hydrogen storage: Materials, methods and perspectives", Renewable and Sustainable Energy Reviews, 50, 457–469.

[75] Durbin D.J., Malardier-Jugroot C., (2013), "Review of hydrogen storage techniques for on board vehicle applications", International Journal of Hydrogen Energy, 38 (34), 14595–14617.

[76] Zhang F., Zhao P., Niu M., Maddy J., (2016), "The survey of key technologies in hydrogen energy storage", International Journal of Hydrogen Energy, 41 (33), 14535–14552.

[77] Kelly M.T., (2011), "Perspective on the storage of hydrogen: Past and future", Structure and Bonding, 141, 169–201.

[78] Liu Z., Zhang K., Wu Y., Xi H., (2018), "New functionalized IRMOF-10 with strong affinity for methanol: A simulation study", Applied Surface Science, 440, 351–358.

[79] Côté A.P., Benin A.I., Ockwig N.W., O'Keeffe M., Matzger A.J., Yaghi O. M., (2005), "Chemistry: Porous, crystalline, covalent organic frameworks", Science, 310 (5751), 1166–1170.

[80] Klontzas E., Tylianakis E., Froudakis G.E., (2010), "Designing 3D COFs with enhanced hydrogen storage capacity", Nano Letters, 10 (2), 452–454.

[81] El-Kaderi H. M., Hunt J. R., Mendoza-Cortés L., Côté A. P., Taylor R. E., O'Keeffe M., Yaghi O. M., (2007), "Designed Synthesis of 3D Covalent", Science (80-.)., 13 (April), 268–273.

[82] Web 21, (2019), "Glass Capillary Arrays | PHOTONIS",. https://www.photonis.com/product/glass-capillary-arrays (erişim 11 Mart 2019).

[83] Klerke A., Christensen C.H., Nørskov J.K., Vegge T., (2008), "Ammonia for hydrogen storage: Challenges and opportunities", Journal of Materials Chemistry, 18 (20), 2304–2310.

[84] Pattabathula Venkat R.J., (2016), "Introduction to Ammonia Production", CEP Magazine, (2), 69–75.

[85] Ye X., Wang Y., Hopkins R.C., Adams M.W.W., Evans B.R., Mielenz J. R., Zhang Y. H. P., (2009), "Spontaneous high-yield production of hydrogen from cellulosic materials and water catalyzed by enzyme cocktails", ChemSusChem, 2 (2), 149–152.

[86] Kim J. E., Zhang Y. H. P., "Use of carbohydrates for hydrogen storage", in: Compendium of Hydrogen Energy, (2016), 219–241.

[87] Zhou L., (2005), "Progress and problems in hydrogen storage methods", Renewable and Sustainable Energy Reviews, 9 (4), 395–408.

[88] Jain I.P., Jain P., Jain A., (2010), "Novel hydrogen storage materials: A review of lightweight complex hydridespuye", Journal of Alloys and Compounds, 503

(2), 303–339.

[89] Sakintuna B., Lamari-Darkrim F., Hirscher M., (2007), "Metal hydride materials for solid hydrogen storage: A review", International Journal of Hydrogen Energy, 32 (9), 1121–1140.

[90] Özkar S., Zahmakiran M., (2005), "Hydrogen generation from hydrolysis of sodium borohydride using Ru(0) nanoclusters as catalyst", Journal of Alloys and Compounds, 404–406 (Special Issue), 728–731.

[91] Özdemir E., (2015), "Enhanced catalytic activity of Co-B/glassy carbon and Co-B/graphite catalysts for hydrolysis of sodium borohydride", International Journal of Hydrogen Energy, 40 (40), 14045–14051.

[92] Rakap M., (2015), "Hydrolysis of Sodium Borohydride and Ammonia Borane for Hydrogen Generation Using Highly Efficient Poly(N-Vinyl-2-Pyrrolidone)-Stabilized Ru-Pd Nanoparticles as Catalysts", International Journal of Green Energy, 12 (12), 1288–1300.

[93] Wee J.H., (2006), "A comparison of sodium borohydride as a fuel for proton exchange membrane fuel cells and for direct borohydride fuel cells", Journal Power Sources, 155 (2), 329–339.

[94] Duman S., Özkar S., (2018), "Ceria supported manganese(0) nanoparticle catalysts for hydrogen generation from the hydrolysis of sodium borohydride", International Journal of Hydrogen Energy, 43 (32), 15262–15274.

[95] Demirci U.B., Miele P., (2014), "Cobalt-based catalysts for the hydrolysis of $NaBH_4$ and NH_3BH_3", Physical Chemistry Chemical Physics, 16 (15), 6872–6885.

[96] Stephens F.H., Pons V., Tom Baker R., (2007), "Ammonia–borane: The hydrogen source par excellence?", Journal of the Chemical Society. Dalton Transactions, (25), 2613–2626.

[97] Zhang L., Zhou L., Yang K., Gao D., Huang C., et al., (2016), "Pd-Ni nanoparticles supported on MIL-101 as high-performance catalysts for hydrogen generation from ammonia borane", Journal of Alloys Compounds, 677, 87–95.

[98] Shang N., Zhou X., Feng C., Gao S., Wu Q., et al., (2017), "Synergetic catalysis of Ni–Pd nanoparticles supported on biomass-derived carbon spheres for hydrogen production from ammonia borane at room temperature", International Journal of Hydrogen Energy, 42 (9), 5733–5740.

[99] Akbayrak S., Kaya M., Volkan M., Özkar S., (2014), "Palladium(0) nanoparticles supported on silica-coated cobalt ferrite: A highly active, magnetically isolable and reusable catalyst for hydrolytic dehydrogenation of ammonia borane", Applied Catalysis B: Environmental, 147, 387–393.

[100] Yuan M., Cui Z., Yang J., Cui X., Tian M., Xu D., Ma J., Dong Z., (2017), "Ultrafine platinum nanoparticles modified on cotton derived carbon fibers as a highly efficient catalyst for hydrogen evolution from ammonia borane", International Journal of Hydrogen Energy, 42 (49), 29244–29253.

[101] Basu S., Brockman A., Gagare P., Zheng Y., Ramachandran P. V., Delgass W. N., Gore J. P., (2009), "Chemical kinetics of Ru-catalyzed ammonia borane hydrolysis", Journal of Power Sources, 188 (1), 238–243.

[102] Fang Y., Li J.L., Togo T., Jin F.Y., Xiao Z.F., Liu L. J., Drake H., Lian X. Z., Zhou H. C., (2018), "Ultra-Small Face-Centered-Cubic Ru Nanoparticles Confined within a Porous Coordination Cage for Dehydrogenation", Chem, 4 (3), 555–563.

[103] Akbayrak S., Tanyildizi S., Morkan I., Özkar S., (2014), "Ruthenium(0) nanoparticles supported on nanotitania as highly active and reusable catalyst in hydrogen generation from the hydrolysis of ammonia borane", International Journal of Hydrogen Energy, 39 (18), 9628–9637.

[104] Rakap M., (2015), "PVP-stabilized Ru-Rh nanoparticles as highly efficient catalysts for hydrogen generation from hydrolysis of ammonia borane", Journal of Alloys and Compounds, 649, 1025–1030.

[105] Yao Q., Lu Z.H., Jia Y., Chen X., Liu X., (2015), "In situ facile synthesis of Rh nanoparticles supported on carbon nanotubes as highly active catalysts for H 2 generation from NH_3BH_3 hydrolysis", International Journal of Hydrogen Energy, 40 (5), 2207–2215.

[106] Liu Y., Guan H., Zhang J., Zhao Y., Yang J.H., Zhang B., (2018), "Polydopamine-coated halloysite nanotubes supported AgPd nanoalloy: An efficient catalyst for hydrolysis of ammonia borane", International Journal of Hydrogen Energy, 43 (5), 2754–2762.

[107] Liang H., Chen G., Desinan S., Rosei R., Rosei F., Ma D., (2012), "In situ facile synthesis of ruthenium nanocluster catalyst supported on carbon black for hydrogen generation from the hydrolysis of ammonia-borane", International Journal of Hydrogen Energy, 37 (23), 17921–17927.

[108] Aijaz A., Karkamkar A., Choi Y.J., Tsumori N., Rönnebro E., Autrey T., Shioyama H., Xu Q., (2012), "Immobilizing highly catalytically active Pt nanoparticles inside the pores of metal-organic framework: A double solvents approach", Journal of the American Chemical Society, 134 (34), 13926–13929.

[109] Hu M., Wang H., Wang Y., Zhang Y., Wu J., Xu B., Gao D., Bi J., Fan G., (2017), "Alumina nanofiber-stabilized ruthenium nanoparticles: Highly efficient catalytic materials for hydrogen evolution from ammonia borane hydrolysis", International Journal of Hydrogen Energy, 42 (38), 24142–24149.

[110] Ma Y., Li X., Zhang Y., Chen L., Wu J., Gao D., Bi J., Fan G., (2017), "Ruthenium nanoparticles supported on TiO2 (B) nanotubes: Effective catalysts in hydrogen evolution from the hydrolysis of ammonia borane", Journal of Alloys and Compounds, 708, 270–277.

[111] Chen J., Lu Z.H., Wang Y., Chen X., Zhang L., (2015), "Magnetically recyclable Ag/SiO_2-$CoFe_2O_4$ nanocomposite as a highly active and reusable catalyst for H2 production", International Journal of Hydrogen Energy, 40 (14), 4777–4785.

[112] Tonbul Y., Akbayrak S., Özkar S., (2018), "Nanozirconia supported ruthenium(0) nanoparticles: Highly active and reusable catalyst in hydrolytic dehydrogenation of ammonia borane", Journal of Colloid and Interface Science, 513, 287–294.

[113] Kalkan E.B., Akbayrak S., Özkar S., (2017), "Ruthenium(0) nanoparticles supported on nanohafnia: A highly active and long-lived catalyst in hydrolytic dehydrogenation of ammonia borane", Molecular Catalysis, 430, 29–35.

[114] Kaya M., Zahmakiran M., Özkar S., Volkan M., (2012), "Copper(0) nanoparticles supported on silica-coated cobalt ferrite magnetic particles: Cost effective catalyst in the hydrolysis of ammonia-borane with an exceptional reusability performance", ACS Applied Materials and Interfaces, 4 (8), 3866–3873.

[115] Zhang J., Chen C., Yan W., Duan F., Zhang B., Gao Z., Qin Y., (2016), "Ni nanoparticles supported on CNTs with excellent activity produced by atomic layer deposition for hydrogen generation from the hydrolysis of ammonia borane", Catalysis Science and Technology, 6 (7), 2112–2119.

[116] Yang L., Cao N., Du C., Dai H., Hu K., Luo W., Cheng G., (2014), "Graphene supported cobalt(0) nanoparticles for hydrolysis of ammonia borane", Materials Letters, 115, 113–116.

[117] Wu Y., Wu X., Liu Q., Huang C., Qiu X., (2017), "Magnetically recyclable Ni@h-BN composites for efficient hydrolysis of ammonia borane", International Journal of Hydrogen Energy, 42 (25), 16003–16011.

[118] Yan J.M., Zhang X.B., Han S., Shioyama H., Xu Q., (2008), "Iron-nanoparticle-catalyzed hydrolytic dehydrogenation of ammonia borane for chemical hydrogen storage", Angewandte Chemie - International Edition, 47 (12), 2287–2289.

[119] Yang Y., Lu Z.H., Hu Y., Zhang Z., Shi W., Chen X., Wang T., (2014), "Facile in situ synthesis of copper nanoparticles supported on reduced graphene oxide for hydrolytic dehydrogenation of ammonia borane", RSC Advances, 4 (27), 13749–13752.

[120] Yang K., Yao Q.L., Lu Z.H., Kang Z.B., Chen X.S., (2017), "Facile synthesis of CuMo nanoparticles as highly active and cost-effective catalysts for the hydrolysis of ammonia borane", Wuli Huaxue Xuebao/ Acta Physico - Chimica Sinica, 33 (5), 993–1000.

[121] Ke D., Wang J., Zhang H., Li Y., Zhang L., Zhao X., Han S., (2017), "Fabrication of Pt–Co NPs supported on nanoporous graphene as high-efficient catalyst for hydrolytic dehydrogenation of ammonia borane", International Journal of Hydrogen Energy, 42 (43), 26617–26625.

[122] Cao N., Su J., Luo W., Cheng G., (2014), "Graphene supported Ru@Co core-shell nanoparticles as efficient catalysts for hydrogen generation from hydrolysis of ammonia borane and methylamine borane", Catalysis Communications, 43, 47–51.

[123] Cao N., Su J., Luo W., Cheng G., (2014), "Hydrolytic dehydrogenation of ammonia borane and methylamine borane catalyzed by graphene supported Ru@Ni core-shell nanoparticles", International Journal of Hydrogen Energy, 39 (1), 426–435.

[124] Ge Y., Shah Z.H., Lin X.J., Lu R., Liao Z., Zhang S., (2017), "Highly efficient Pt decorated CoCu bimetallic nanoparticles protected in silica for hydrogen production from ammonia-borane", ACS Sustainable Chemistry and Engineering, 5 (2), 1675–1684.

[125] Cao N., Hu K., Luo W., Cheng G., (2014), "RuCu nanoparticles supported on graphene: A highly efficient catalyst for hydrolysis of ammonia borane", Journal of Alloys and Compounds, 590, 241–246.

[126] Chen G., Desinan S., Nechache R., Rosei R., Rosei F., Ma D., (2011), "Bifunctional catalytic/magnetic Ni@Ru core-shell nanoparticles", Chemical Communications, 47 (22), 6308–6310.

[127] Sun D., Mazumder V., Metin Ö., Sun S., (2011), "Catalytic hydrolysis of ammonia borane via cobalt palladium nanoparticles", ACS Nano, 5 (8), 6458–6464.

[128] Møller K.T., Jensen T.R., Akiba E., Li H. W., (2017), "Hydrogen - A sustainable energy carrier", Progress in Natural Science: Materials International, 27 (1), 34–40.

[129] Haynes A., Concepts of Modern Catalysis and Kinetics, 2005.

[130] Zheng A., Deng F., Liu S. B., "Acidity Characterization of Solid Acid Catalysts by Solid-State 31P NMR of Adsorbed Phosphorus-Containing Probe Molecules", 1st ed., Elsevier, 2014.

[131] Zhang X., Zhao J., Song Z., Liu W., Zhao H., Zhao M., Xing Y., Ma Z., Du H., (2020), "The catalytic oxidation performance of toluene over the Ce-Mn-Ox catalysts: Effect of synthetic routes", Journal of Colloid and Interface Science, 562, 170–181.

[132] Pritchard J.C., He Q., Ntainjua E.N., Piccinini M., Edwards J.K., Herzing A. A., Carley A. F., Moulijn J. A., Kiely C. J., Hutchings G. J., (2010), "The effect of catalyst preparation method on the performance of supported Au-Pd catalysts for the direct synthesis of hydrogen peroxide", Green Chemistry, 12 (5), 915–921.

[133] Schwarz J.A., Contescu C., Contescu A., (1995), "Methods for Preparation of Catalytic Materials", Chemical Reviews, 95 (3), 477–510.

[134] Wen Y., Tang X., Li J., Hao J., Wei L., Tang X., (2009), "Impact of synthesis method on catalytic performance of MnO_x-SnO_2 for controlling formaldehyde emission", Catalysis Communications, 10 (8), 1157–1160.

[135] Rodriguez-Reinoso F., Silvestre-Albero J., "Activated Carbon and Adsorption", in: Reference Module in Materials Science and Materials Engineering, Elsevier, 2016.

[136] Yeganeh M.M., Kaghazchi T., Soleimani M., (2006), "Effect of raw materials on properties of activated carbons", Chemical Engineering and Technology, 29 (10), 1247–1251.

[137] Huang C.P., Stumm W., (1972), "The specific surface area of γ-Al_2O_3", Surface Science, 32 (2), 287–296.

[138] Tschapek M., Wasowski C., Torres Sanchez R.M., (1976), "The p.z.c. and i.e.p. of γ-Al_2O_3 and TiO_2", Journal of Electroanalytical Chemistry, 74 (2), 167–176.

[139] Raj K.J.A., Ramaswamy A. V., Viswanathan B., (2009), "Surface area, pore size, and particle size engineering of titania with seeding technique and phosphate modification", Journal of Physical Chemistry C, 113 (31), 13750–13757.

[140] Chatman S., Zarzycki P., Rosso K.M., (2013), "Surface potentials of (001), (012), (113) hematite (α-Fe_2O_3) crystal faces in aqueous solution", Physical Chemistry Chemical Physics, 15 (33), 13911–13921.

[141] Garcia D., Picasso G., Hidalgo P., Peres H.E.M., Sun K. R., Gonçalves J. M., (2017), "Sensors based on Ag-loaded hematite (α-Fe2O3) nanoparticles for methyl mercaptan detection at room temperature", Analytical Chemistry Research, 12, 74–81.

[142] Christy A.A., (2008), "Quantitative determination of surface area of silica gel particles by near infrared spectroscopy and chemometrics", Colloids and

Surfaces A: Physicochemical and Engineering Aspects, 322 (1–3), 248–252.

[143] Kim J., Lawler D.F., (2005), "Characteristics of Zeta Potential Distribution in Silica Particles", Bulletin of the Korean Chemical Society, 26 (7), 1083–1089.

[144] Li W., Lu X., Xu K., Qu J., Qiang Z., (2015), "Cerium incorporated MCM-48 (Ce-MCM-48) as a catalyst to inhibit bromate formation during ozonation of bromide-containing water: Efficacy and mechanism", Water Research, 86, 2–8.

[145] Kruk M., Jaroniec M., Ryoo R., Kim M. J., (2007), "Characterization of High-Quality MCM-48 and SBA-1 Mesoporous Silicas Michal", Chemistry of Materials, 2991 (09), 60467.

[146] Chuah G.K., Jaenicke S., S.A. C., Chan K.S., (1996), "The influence of preparation conditions on the surface area of zirconia", Applied Catalysis A: General, 145, 267–284.

[147] Muhammad S., Hussain S.T., Waseem M., Naeem A., Hussain J., Tariq J. M., (2012), "Surface charge properties of zirconium dioxide", Iranian Journal of Science and Technology, Transaction A: Science, 36 (4), 481–486.

[148] Rodriguez-Reinoso F., Silvestre-Albero J., (2016), "Activated Carbon and Adsorption", Reference Module in Materials Science and Materials Engineering, (April 2015), 1–14.

[149] Mianowski A., Owczarek M., Marecka A., (2007), "Surface area of activated carbon determined by the iodine adsorption number", Energy Sources, Part A: Recovery, Utilization and Environmental Effects, 29 (9), 839–850.

[150] Vasiliev L.L., Larisa K., Kulakov A.G., Mishkinis D., (2007), " Activated Carbon and Hydrogen Adsorption Storage", Hydrogen Materials Science and Chemistry of Carbon Nanomaterials, (January), 1-19.

[151] Smith W.R., Thornhill F.S., Bray R.I., (1942), "Surface Area and Properties of Carbon Black", Rubber Chemistry and Technology, 15 (1), 206–215.

[152] Borah D., Satokawa S., Kato S., Kojima T., (2008), "Surface-modified carbon black for As(V) removal", Journal of Colloid and Interface Science, 319 (1), 53–62.

[153] Wang J., Zhang Z., Zhang Q., Liu J., Ma J., (2018), "Preparation and adsorption application of carbon nanofibers with large specific surface area", Journal of Materials Science, 53 (24), 16466–16475.

[154] Zhu J., Zhao T., Kvande I., Chen D., Zhou X., Yuan W., (2008), "Carbon nanofiber-supported Pd catalysts for heck reaction: Effects of support

interaction", Cuihua Xuebao / Chinese Journal of Catalysis, 29 (11), 1145–1151.

[155] Birch E. M., Ruda-Eberenz T. A., Chai M., Andrews R., Hatfield R. L., (2016), " Properties that Influence the Specific Surface Areas of Carbon Nanotubes and Nanofibers ", The Annals of Occupational Hygiene, 118 (24), 6072–6078.

[156] Lee S., Zhang Z., Wang X., Pfefferle L.D., Haller G.L., (2011), "Characterization of multi-walled carbon nanotubes catalyst supports by point of zero charge", Catalysis Today, 164 (1), 68–73.

[157] ShamsiJazeyi H., Kaghazchi T., (2010), "Investigation of nitric acid treatment of activated carbon for enhanced aqueous mercury removal", Journal of Industrial and Engineering Chemistry, 16 (5), 852–858.

[158] Web 22, (2019), Murov S., "Solvent Polarity Table - Miller's Home",. https://sites.google.com/site/miller00828/in/solvent-polarity-table (erişim 15 Ocak 2020).

[159] Feng X., Jiang K., Fan S., Kanan M.W., (2015), "Grain-Boundary-Dependent CO_2 Electroreduction Activity", Journal of the American Chemical Society, 137 (14), 4606–4609.

[160] Petró J., Polyánszky É., Csürös Z., (1974), "Relationship between the activity and the excess free surface energy of noble metal catalysts", Journal of Catalysis, 35 (2), 289–296.

[161] Zhao J., Ren X., Han Q., Fan D., Sun X., Kuang X., Wei Q., Wu D., (2018), "Ultra-thin wrinkled NiOOH–$NiCr_2O_4$ nanosheets on Ni foam: an advanced catalytic electrode for oxygen evolution reaction", Chemical Communications, 54 (39), 4987–4990.

[162] Li C.P., Proctor A., Hercules D.M., (1984), "Curve Fitting Analysis of ESCA Ni 2p Spectra of Nickel-Oxygen Compounds and Ni/Al_2O_3 Catalysts", Applied Spectroscopy, 38 (6), 880–886.

[163] Kishi K., (1988), "Adsorption of ethylenediamine on clean and oxygen covered Fe/Ni(100) surfaces studied by XPS", Journal of Electron Spectroscopy and Related Phenomena, 46 (1), 237–247.

[164] Salvati L., Makovsky L.E., Stencel J.M., Brown F.R., Hercules D.M., (1981), "Surface spectroscopic study of tungsten-alumina catalysts using x-ray photoelectron, ion scattering, and Raman spectroscopies", The Journal of Physical Chemistry, 85 (24), 3700–3707.

[165] Lian K.K., (1995), "Investigation of a 'Two-State' Tafel Phenomenon for the Oxygen Evolution Reaction on an Amorphous Ni-Co Alloy", Journal of The Electrochemical Society, 142 (12), 4309.

[166] Shen J.Y., Adnot A., Kaliaguine S., (1991), "An ESCA study of the interaction of oxygen with the surface of ruthenium", Applied Surface Science, 51 (1–2), 47–60.

[167] Folkesson B., Bjorøy M., Pappas J., Skaarup S., Aaltonen R., Swahn C. G., (1973), "ESCA Studies on the Charge Distribution in Some Dinitrogen Complexes of Rhenium, Iridium, Ruthenium, and Osmium.", Acta Chemica Scandinavica, 27, 287–302.

[168] Wang S., Wang Z., Wang Y., Chen J., Chen Z., Chen Y., Fu J., (2019), "Environmentally friendly room temperature synthesis of hierarchical porous α-$Ni(OH)_2$ nanosheets for supercapacitor and catalysis applications", Green Chemistry, 21 (21), 5960–5968.

[169] Dybing E., Krogh T., Drinking water and health, 1994.

[170] Klooster W.T., Koetzle T.F., Siegbahn P.E.M., Richardson T.B., Crabtree R.H., (1999), "Study of the N−H···H−B Dihydrogen Bond Including the Crystal Structure of BH_3NH_3 by Neutron Diffraction", Journal of the American Chemical Society, 121 (27), 6337–6343.

BIOGRAPHY

Ceyhun Yıldırım was born in 1987, as first child of Ekrem and Fatma couple and also the big brother of Erdost, in Istanbul. He graduated from Gebze Technical University Material Science and Engineering Department and he was studying on hydroxyapatite-based biomaterials during his undergraduate thesis. During this thesis study which you read; he was a Master of Science Student at Institute of Nanotechnology in Gebze Technical University. Ceyhun is a member of Hydrogen Technology Research Laboratory and Surface Physics Laboratory.

APPENDICES

Appendix A: Ruthenium-Nickel phase diagram

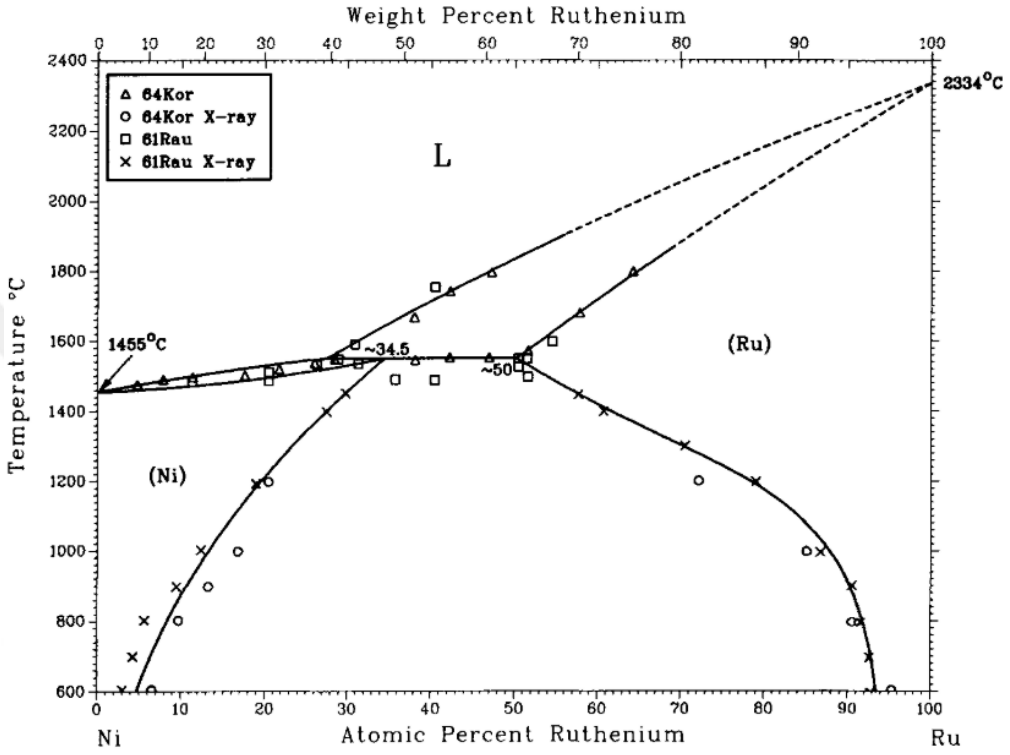

Figure A.1: Ruthenium-Nickel phase diagram.

Appendix B: X-Ray Photoelectron Spectra of Adhesive Carbon Tape

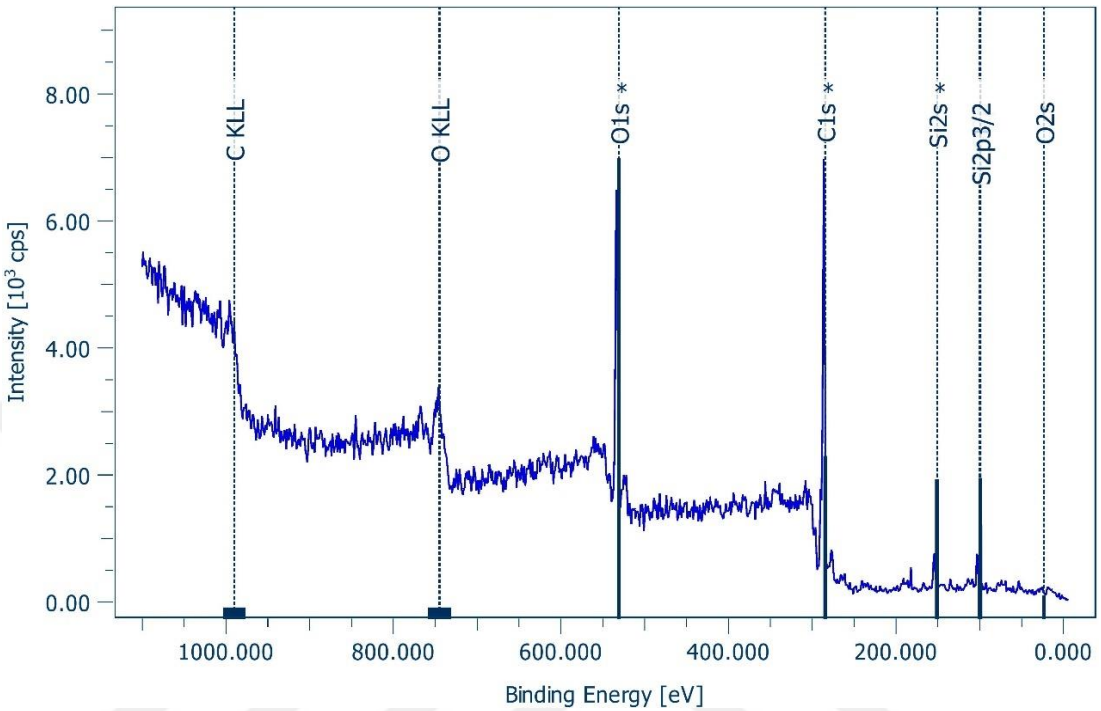

Figure A.2: X-ray photoelectron spectra of adhesive carbon tape (purchased from Agar Scientific).

Figure A.2. shows the x-ray photoelectron spectra of adhesive conductive carbon tape (ACCT) used for powder holder for XPS, SEM and EDX. It is seen from the spectra that ACCT consists Si in addition to C and O. There is only survey scan, C and O window scans in the database of Surface Physics Laboratory for ACCT, but it is enough to see it consists Si. About 4 eV peak shift detected for main peaks of Si $2p_{3/2}$ and Si 2s and their binding energies are about 103 and 154 eV, these peaks are related with the SiO_2.

Appendix C: Crystal Structure Views of AB from Three Different Directions

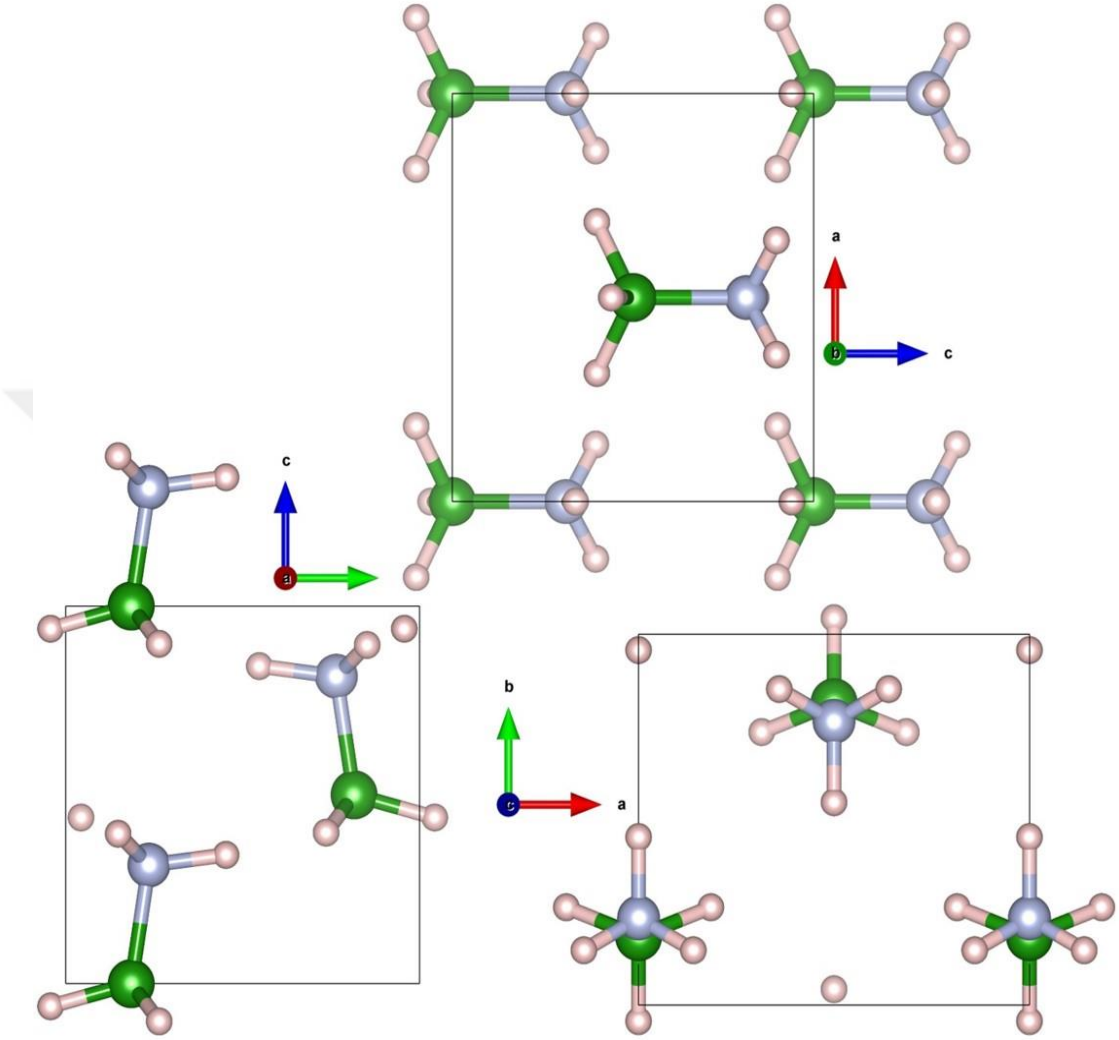

Figure A.3: AB crystal structure view from x-direction (left-bottom), y-direction (top), z-direction (right-bottom).

The structure was drawn on Vesta 3.4.7 by using the crystal information file (.cif) in the supporting information of the article [170].